REPORT

Additional Model Testing of Cyclic Axial Loading on Piles for Jacket Foundations

FINAL REPORT

BOEM Contract Number 140M0118C002

DOC.NO. 18-1076-02-R
REV.NO. 3 / 2020-08-20

NORWEGIAN GEOTECHNICAL INSTITUTE
NGI.NO/HOUSTON

Project

Project title:	Additional Model Testing of Cyclic Axial Loading on Piles for Jacket Foundations
Document title:	Final Report
Document no.:	18-1076-02-R
Date:	2019-11-20
Revision no. /rev. date:	3 / 2020-08-20

Client

Client:	Bureau of Ocean Energy Management
Client contact person:	Dan O'Connell
Contract reference:	140M0118C002

for NGI

Project manager:	Amir Rahim/Andrew Deeks
Prepared by:	ARa, ADE, ASB, TEK, AH, JS
Reviewed by:	Andrew Deeks

Summary

This study presents field tests carried out on model piles embedded in sand in order to study the effect of cyclic loading and aging on pile capacity and stiffness. The study aims to provide better understanding of piles subjected to cyclic axial loading that are used in the wind industry. Sites at the University of Rhode Island (URI) and University of Texas at Austin (UT) were selected to carry out axial cyclic tests of piles in sand. The driven steel piles were open-ended, 110 mm in diameter and embedded about 4 m into the ground. Testing included:

1. monotonic tension tests
2. cyclic low-frequency (LF) 0.125 Hz tension tests (~ 1-way)
    a. followed by monotonic tensile pull-out
3. cyclic high-frequency (HF) 40 Hz compression tests (~ 1-way)
    a. followed by monotonic tensile pull-out

Monotonic tensile load tests were performed to determine the side friction capacity. Some piles were loaded cyclically and then loaded to failure monotonically.

The tests were conducted few days after pile installation and up to five months after installation in order to evaluate the effect of aging on strength and stiffness.

Applied ~one-way load cycles (~10,000 in tension, or ~150,000 in compression), were not detrimental to short (~7-10 day) or long (~100 day) term capacity in this case, even for maximum load levels almost equal (up to 80 or 90%) to the subsequent axial capacity.

Under low frequency loading the pile head stiffness was 2 to 4 times higher than under maintained load. This is hypothesized to be a soil rate of loading (viscosity) effect.

As design methods are typically calibrated for 7 to 10 day capacity, this indicates there is significant safety margin for driven piles against cyclic loading. However, this might differ for other installation types, e.g. jacked piles.

For one test pile (URI-P4) post installation cycles potentially accelerated long term aging, initiating an enhanced creep type 'aging' capacity. Post installation cycles may have increased / accelerated other pile capacities, but this could not be determined reliably.

The safety to cyclic loads is contingent on reliable design (7 to 10 day) capacity assessment that would include effects from friction fatigue during driving. In that context:

- URI and UT piles showed low capacity relative to a selected CPTU design method (UWA-05).
- It may be that the pile interface has affected these results.
    - These piles reflect typical design materials (steel), but due to pipe sizes, the provided finish was relatively smooth and un-rusted. Hence the interface friction angle and dilation induced at the interface on loading was low,
    - In contrast, field scale piles typically have a rough finish and hence dilate on loading after cyclic compaction (although the compacted state due to installation could me more or less dense than a smooth pile).

The data collected in this study is not sufficient to develop a holistic design approach, rather indicates further work is required.

Further field scale testing is recommended to investigate, and clarify for design if the findings of resilience to post-installation cyclic loads can be relied upon to investigate:

- Additional in-situ site characterisation to reduce interpretation variability
- Pipe roughness
    - Do rougher piles activate cyclic degradation proactively?
- End condition
    - Does the stress regime induced by installation of piles with a different area ratio (e.g., thinner wall, closed ended) change the aging and cyclic response?
- Diameter
    - Are large piles less susceptible due to lower confining stiffness?
- Cycles for installation (e.g. jacked c.f. driven)
    - Are piles installed with low cycle more susceptible to future degradation?
- Maintained load over time
    - Can strength gains with time be relied upon if a pile had been subject to maintained working load throughout its life?

This final report has been reviewed by the BOEM and approved for publication. Approval does not signify that the contents necessarily reflect the views and policies of the BOEM, nor does mention of the trade names or commercial products constitute endorsement or recommendation for use.

This study was funded by the Bureau of Ocean Energy Management (BOEM), U.S. Department of the Interior, Washington, D.C., under Contract 140M0118C002. It was supplemented with support from the National Science Foundation (CMMI 1636217 and CMMI-1520808).

Contents

Tables

Figures

Appendix

Review and reference page

List of symbols and terms used

BOEM	Bureau of Ocean Energy Management
BSEE	Bureau of Safety and Environmental Enforcement
CNS	Constant Normal Stiffness
CPT	Cone Penetration Test
CPTU	CPT with piezocone water pressure measurement
D	Pile diameter
e_o	Initial voids ratio
f_s	Cone sleeve friction
ft	Foot or feet
G_{max}	initial shear modulus
HF	high frequency
I_P	plasticity index
ID	Pile inner diameter
k_v	vertical permeability coefficients
k_h	horizontal permeability coefficients
K_o	coefficient of earth pressure at rest (= $\sigma'_{h0}/\sigma'_{v0}$)
K	Stiffness
K_{static}	Static stiffness
LF	low frequency
LVDT	linear variable differential transformer
m	Mass
m	meter
mbgl	Meters below ground level
N_c	Bearing capacity factor
NGI	Norwegian Geotechnical Institute
OCR	Over Consolidation Ratio
OD	Pile outer diameter
PSL	Pile stick-up length
p_0'	in situ vertical effective stress (=σ'_{v0})
q_t	cone penetration resistance corrected for pore water pressure effects
Q_{axial}	Axial pile load
Q_{cycli}	Axial cyclic load
Q_{min}	Minimum axial load
R	Pile radius
SCPT	Seismic CPT
SM	Silty sand
SP	Poorly graded sand
SP-SM	poorly graded SAND with silt

SW-SM	well-graded SAND with silt
$s_u = c_u$	undrained (undisturbed) shear strength of soil
s_{uC}	static triaxial compression undrained shear strength
s_{uD}	static DSS undrained shear strength
s_{uE}	static triaxial extension undrained shear strength
TL	Pile total length
URI	University of Rhode Island
USCS	Unified Soil Classification System
UT	University of Texas at Austin
V_s	shear wave velocity
y	Lateral soil spring deflection
y_c	Ultimate lateral pile deflection
ZFL	Zero friction length
α	Soil-pile adhesion factor
γ'	submerged unit weight of soil
ε_c or ε_{50}	Strain at half of maximum undrained deviator stress from compression test
ν	Poisson's ratio
σ	stress
σ'_{v0}	in situ vertical effective stress (= p_0')
σ'_{h0}	in situ horizontal effective stress
ϕ'	effective angle of internal friction

1 Introduction

1.1 General

This research *"Additional Model Testing of Cyclic Axial Loading on Piles for Jacket Foundations"* aims to further the understanding of jacket foundation pile behavior in sand under long term cyclic axial loading and to assess aging effects.

This final report has been reviewed by the BOEM and approved for publication. Approval does not signify that the contents necessarily reflect the views and policies of the BOEM, nor does mention of the trade names or commercial products constitute endorsement or recommendation for use.

This study was funded by the Bureau of Ocean Energy Management (BOEM), U.S. Department of the Interior, Washington, D.C., under Contract 140M0118C002. It was supplemented with support from the National Science Foundation (CMMI 1636217 and CMMI-1520808).

The problem setting is illustrated on Figure 1-1.

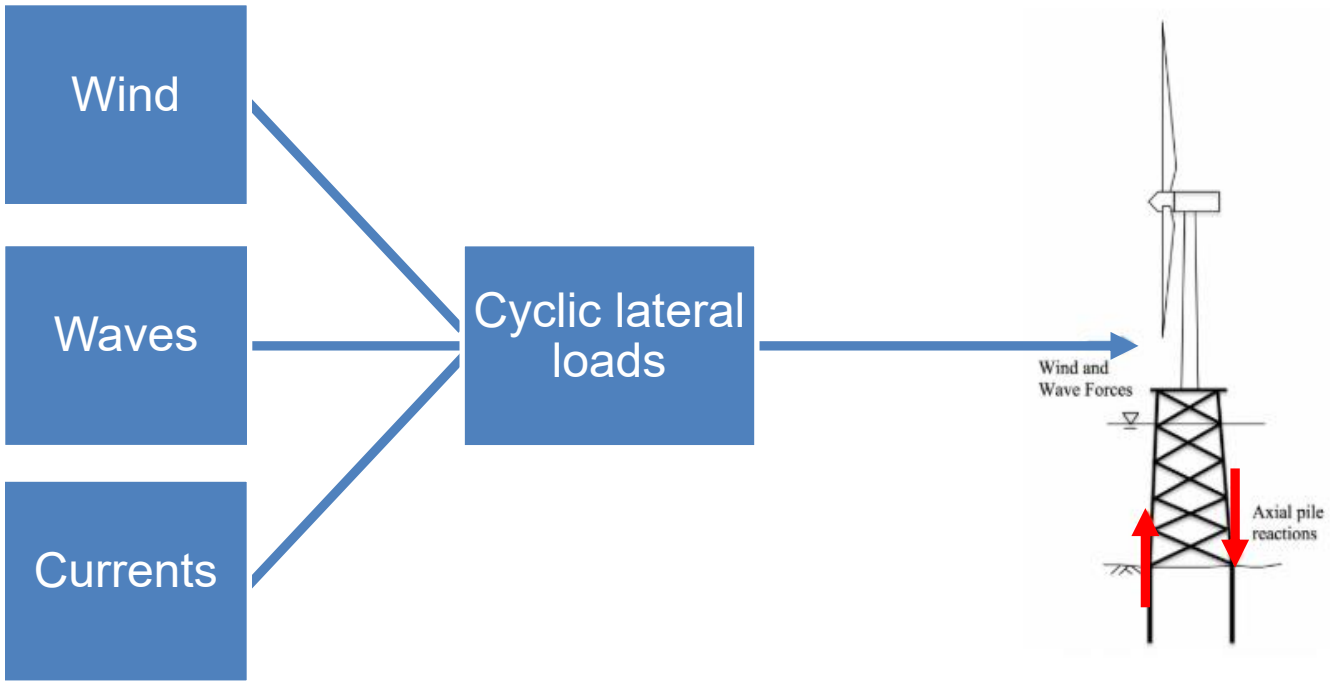

Figure 1-1 Settings

The first objective is illustrated in Figure 1-2 where the loading is broken down into a cyclic component and a time related (aging) component.

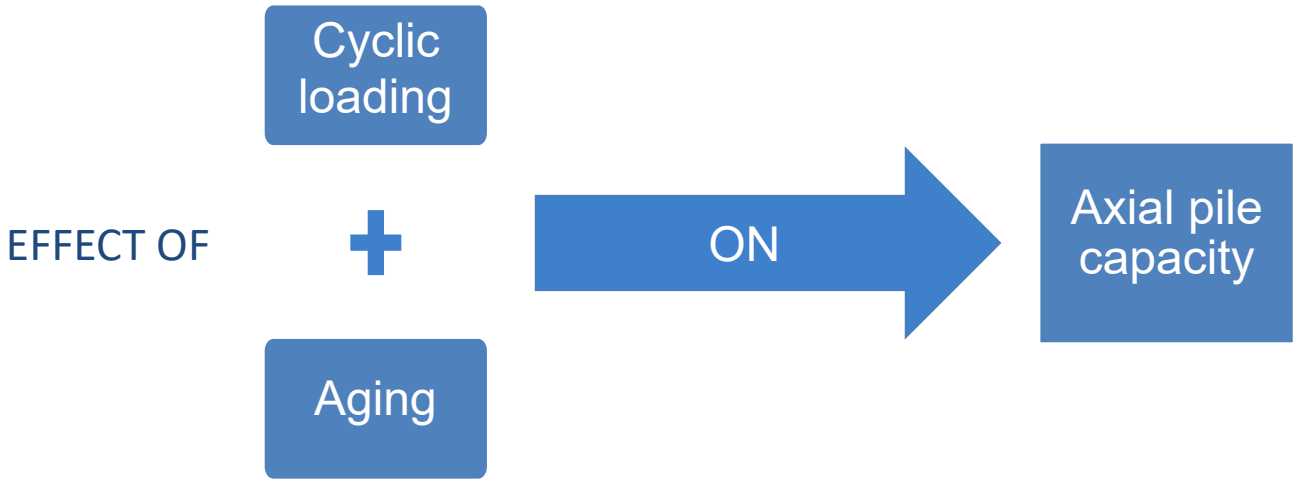

Figure 1-2 Objectives I

Objective I is further broken down to specific loading methods with low frequency cyclic loads attributed to wind and wave, while high frequency loads are attributed to the turbine blade rotation. This is shown in Figure 1-3.

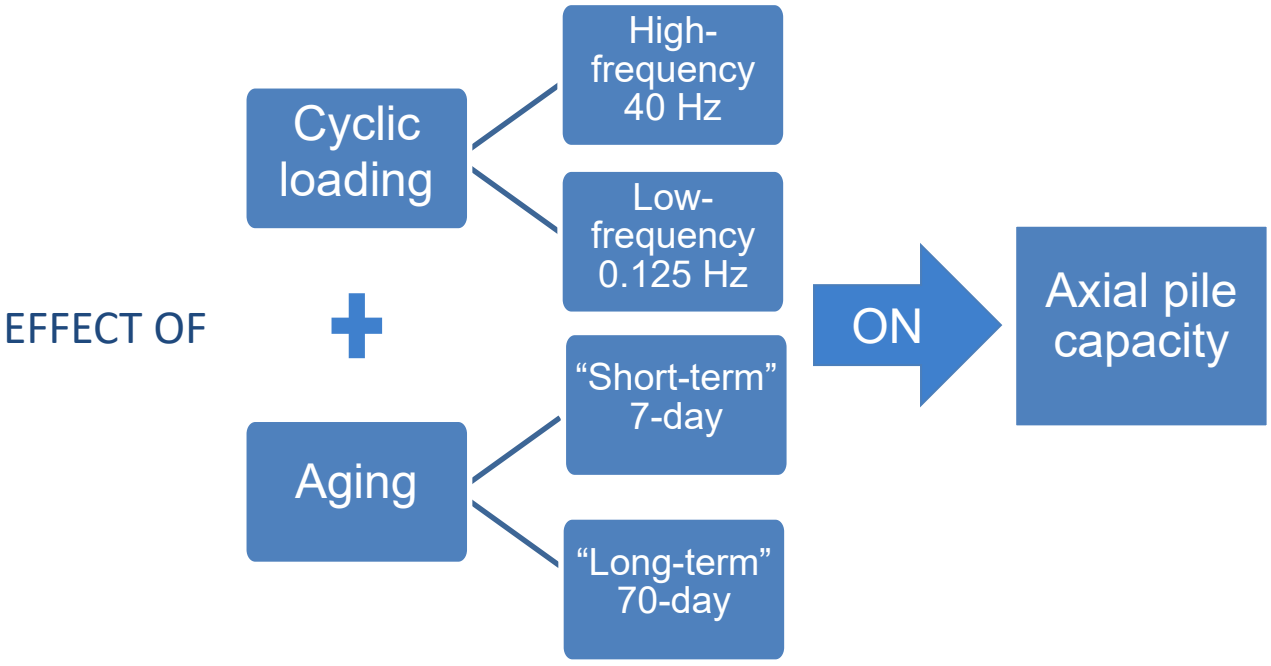

Figure 1-3 Objectives II

Axial cyclic pile testing in sand was carried out at field test sites at the University of Rhode Island (URI) and the University of Texas at Austin (UT) and the project was managed by the Norwegian Geotechnical Institute (NGI).

The approach used intermediate scale 1-G tests of piles in sand. The test program was targeted to investigate two mechanisms that influence pile capacity in sand, specifically, (i) the variation of pile capacity with time (pile capacity typically increases with time), commonly referred to as aging, and (ii) that pile capacity may degrade with cyclic loading, commonly referred to as cyclic degradation. This model testing is complemented by in-situ tests and soil element tests on soil recovered from the test sites to enable design insight. The governing forces for pile subjected to static and cyclic axial loading are illustrated on Figure 1-4.

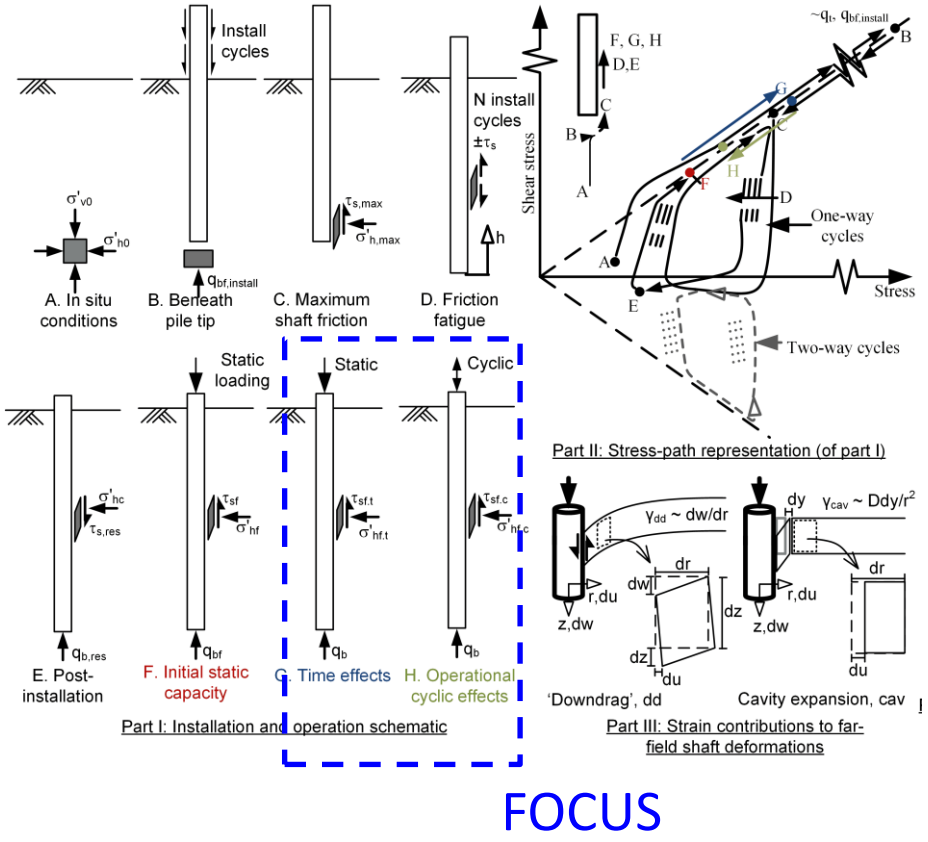

Figure 1-4 Illustration of governing forces for pile under axial static and cyclic loading, modified after White & Deeks 2007.

Two sites consisting primarily of sandy soils were identified for testing. These are the University of Texas at Austin (UT) Hornsby Bend site in Austin, Texas and the University of Rhode Island (URI) Davisville site in North Kingstown, Rhode Island. These two sites were selected as it is thought that they are representative of the sandy soils that might be expected offshore along the U.S. east coast. The test piles had outer diameter of 110 mm and were driven to a target depth of about 4 m in sand. The piles were loaded axially under monotonic and cyclic conditions in tension (URI & UT) and compression (UT).

The testing was performed by the following geotechnical team:

- University of Rhode Island
  - Timothy Keefe tek123@uri.edu – Former graduate student
  - Prof. Aaron Bradshaw abrads@uri.edu – Main contact
  - Prof. Christopher Baxter cbaxter@uri.edu
  - Javier Fernandez- Former graduate student
- University of Texas
  - Ahmed Mustafa Hussien ahussien@utexas.edu – Graduate student
  - Prof. Robert Gilbert bob_gilbert@mail.utexas.edu
  - Farnyuh Menq fymenq@utexas.edu – Main contact

Additionally, the project was coordinated by the following staff from the Norwegian Geotechnical Institute in Oslo and Houston:

- Amir Rahim amir.rahim@ngi.no – NGI Houston
- Andrew Deeks andrew.deeks@ngi.no – NGI Oslo

The team was assisted by technical expert, James Schneider:
james.schneider04@gmail.com

This report supersedes the following three past references issued to BOEM:

- NGI (2019a)
  Field Work Plan -Additional Model Testing of Cyclic Axial Loading on Piles for Jacket Foundations
  NGI Technical Note 18-1076-02, Rev 0, 2019-03-20

- NGI (2019b)
  In-situ characterization -Additional Model Testing of Cyclic Axial Loading on Piles for Jacket Foundations
  NGI Technical Note 18-1076-03, Rev 0, 2019-06-24

1.2 Scope of work

The scope of work for this project included site characterization, element testing, intermediate scale 1-G model pile testing, analyses of results for the aforementioned tests, and recommendations based on the test results.

One-way cyclic loading ($Q_{axial} \approx Q_{cyclic}$, $Q_{min} = 0$) was performed at various load ratios in the metastable region, as defined by a stability chart. The accumulation of displacements were recorded to assess changes in secant and tangent stiffness. Cyclic loads would be for a pile loaded 7 days after installation and 70 days after installation. Due to the coronavirus shelter-in-place rules imposed by state and university authorities, the UT long-term pile tests were carried out between 149 to 168 after pile installation.

The aged static capacity was determined on a separate reference pile, immediately prior to cyclic loading to capture aging effects.

2 Test sites overview

2.1 URI site

Testing at the University of Rhode Island site occurred on property owned by the University in Davisville, North Kingstown, Rhode Island. An aerial view of the URI site is shown in Figure 2-1

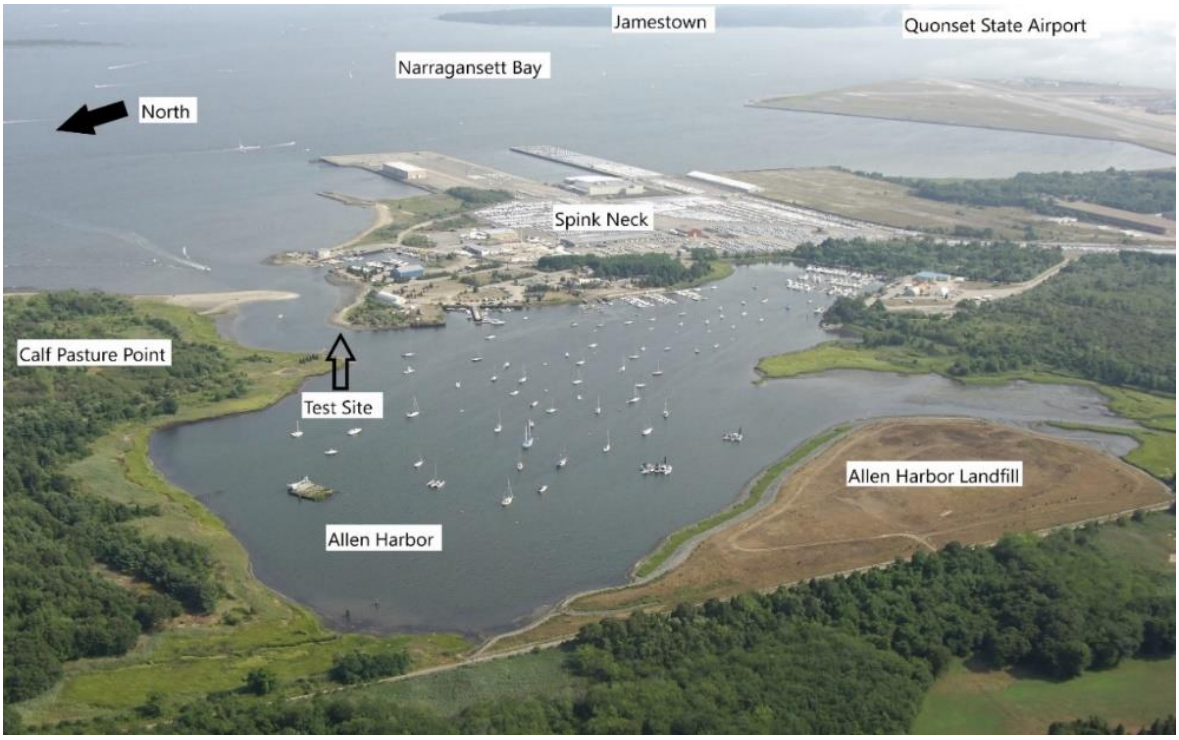

Figure 2-1 Aerial view of the URI site

Figure 2-2 shows the site layout. It features a beach facing a channel from the Narragansett Bay into Allen Harbor, which is tidally influenced.

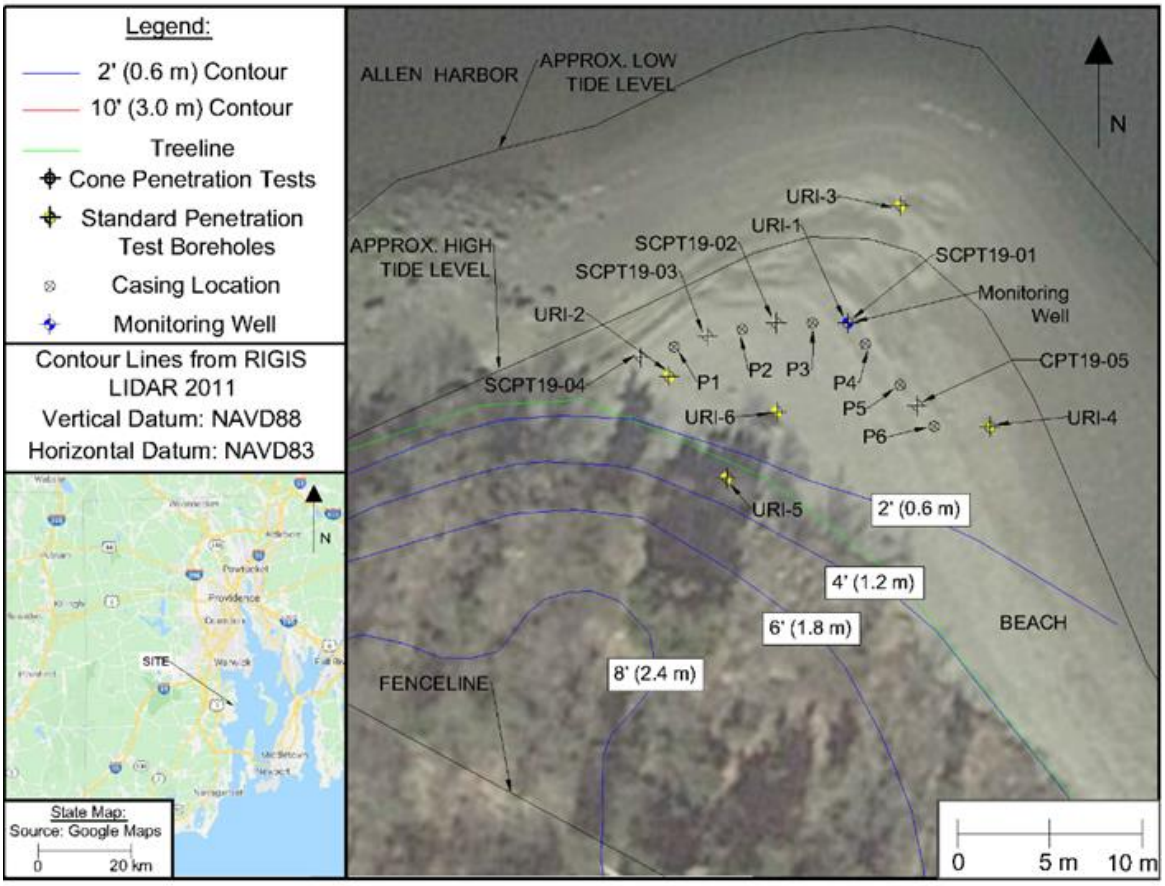

Figure 2-2 Site plan of geotechnical investigations and pile testing at the URI test site

2.1.1 CPT data

Geotechnical borings as well as seismic cone penetration testing (SCPT) were performed at the test site as shown in Figure 2-3. Soil data suggested mainly sandy soils based on the soil behavior index. Negative pore pressures observed during penetration were associated with higher silt content strata.

Soil index classification based on Robertson (2010) is detailed in Table 2-1

Table 2-1 Soil index classification I_c based on Robertson (2010)

Zone	Soil Behavior Type	I_c
1	*Sensitive, fine grained*	N/A
2	*Organic soils – clay*	> 3.6
3	*Clays – silty clay to clay*	2.95 – 3.6
4	*Silt mixtures – clayey silt to silty clay*	2.60 – 2.95
5	*Sand mixtures – silty sand to sandy silt*	2.05 – 2.6
6	*Sands – clean sand to silty sand*	1.31 – 2.05
7	*Gravelly sand to dense sand*	< 1.31
8	*Very stiff sand to clayey sand**	N/A
9	*Very stiff, fine grained**	N/A

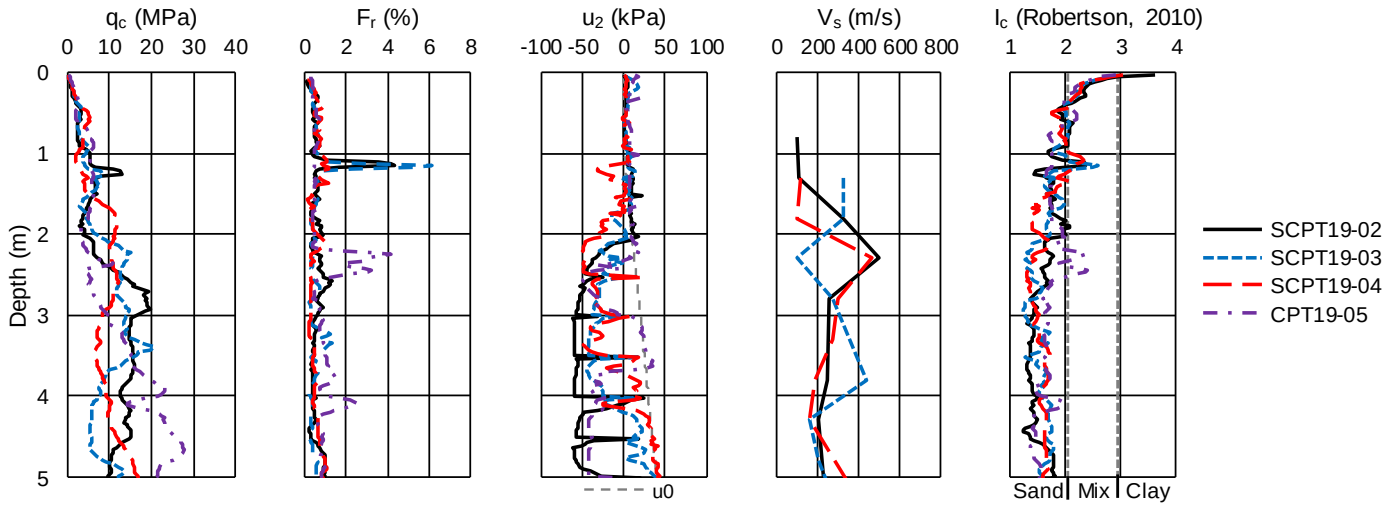

Figure 2-3 Results of SCPT testing performed at the URI Davisville site

Based on sieve tests, the soils in the upper 5 meters were found to consist of medium to dense poorly graded sand, silty sand, and mixes of both (USCS: SP, SM, SP-SM, respectively). The fines content was less than 17% in all samples.

Relative density estimations from CPT correlations using the Jamiolkowski, et. al (2003) method indicate values ranging from 50 to 75% from a depth of 0 to 2 meters and 75 to 100% to a depth of 5 meters. The soils had zero carbonate content. Relative density interpretation for the five CPT sites is given in Figure 2-4:

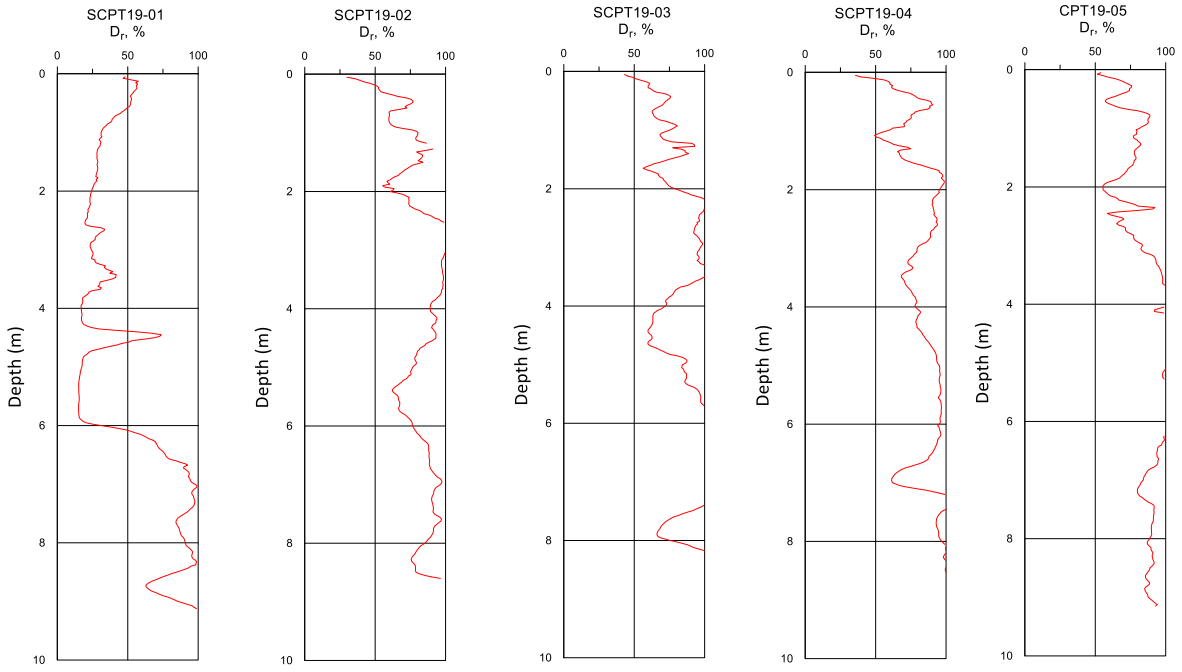

Figure 2-4 Correlation of saturated relative density from CPT data of URI site

It should be noted that SPCT19-01 was inadvertently performed at the same location as geotechnical borehole URI-1. Therefore, the low cone penetration resistance and low relative density for this location is not representative of the site and may be ignored.

2.1.2 URI Pile installation

The test piles at the URI site consisted of W-series casing sections manufactured with AISI Grade 4130 steel and were driven open-ended. The casing sections were 1.52-meters long, with inner and outer diameters of 101.6 and 114.3 mm, respectively (N&N Drilling, 2019). The piles were in a non-rusted condition at installation. Surface profile measurements obtained to quantify the interface conditions on a pile installed at the site for 39 days and subsequently removed indicated average roughness (R_a) values between 0.75 and 1.25 μm above the water table, and 8.95 to 10.55 μm in the intertidal zone where the pile rusted. Values were not obtained from a zone with constant water table exposure.

Six piles were installed just above the mean high tide level, see Figure 2-2 , with a Diedrich D-50 Turbo track rig with a Safe-T Hammer and cathead system. The hammer weight was 1.33 kN and drop height was 0.76 meters. Each pile was installed using three sections of casing resulting in a final embedment of about 4.2 m. Figure 2-5 summarizes the blow counts recorded during installation. At the end of driving, the soil surface inside the piles were measured to be 0.83 to 1.14 m below the ground surface outside the pile.

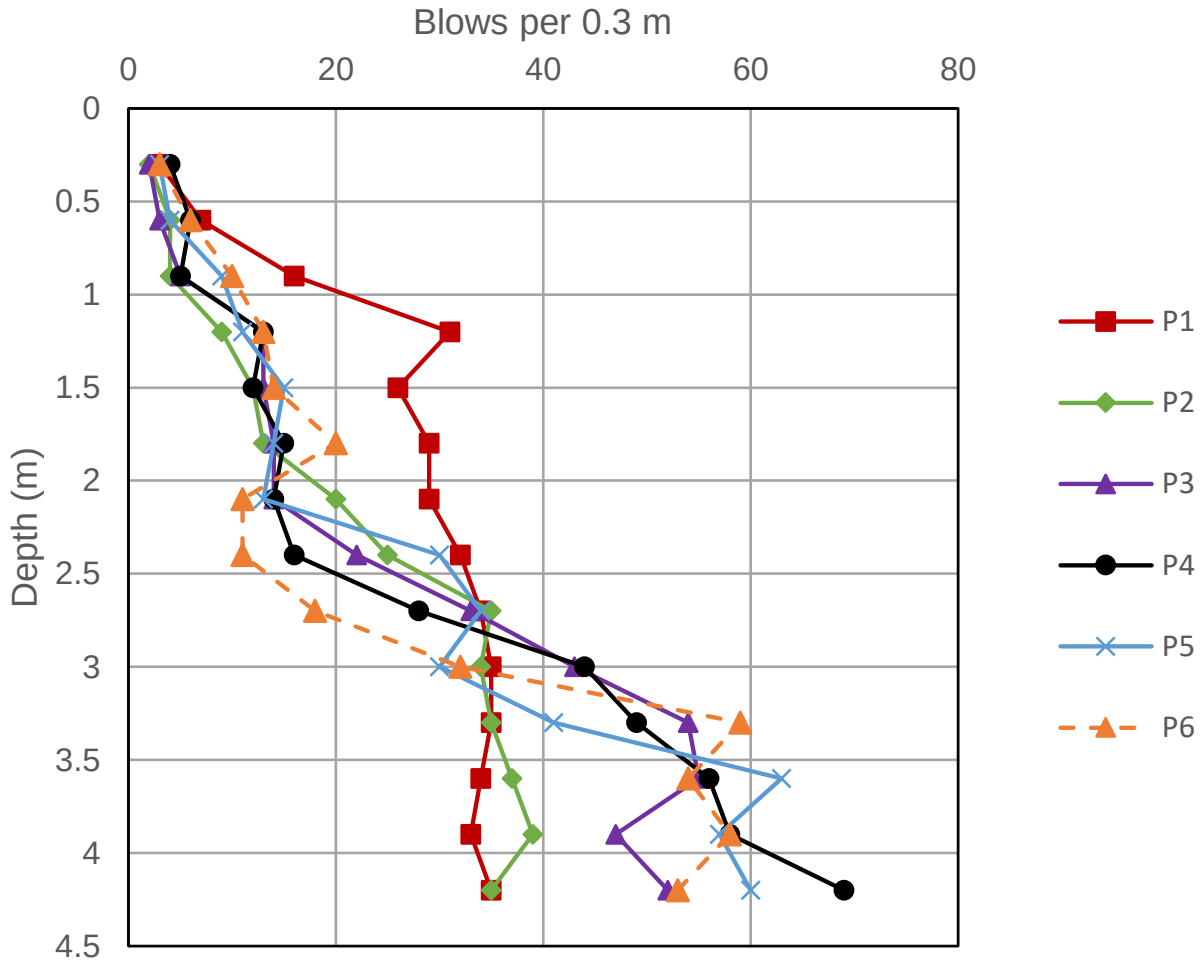

Figure 2-5 Measured pile driving resistance for piles installed at the URI site

Table 2-2 details the total driving resistance for each.

Table 2-2 Total driving resistance for piles installed at URI Davisville site

	Pile 1	Pile 2	Pile 3	Pile 4	Pile 5	Pile 6
Sum of Blows per 0.3 m:	**379**	**304**	**370**	**389**	**384**	**362**

Figure 2-6 shows a photograph of the pile driving equipment.

Figure 2-6 Pile driving at Davisville, URI

Figure 2-7 shows a photograph of all of the driven piles at Davisville, URI.

Figure 2-7 Driven piles at Davisville, URI

Figure 2-8 shows an illustration of one pile casing segment used. Three connected casing sections were installed to reach the final embedment of 4.2 meters for each pile installed.

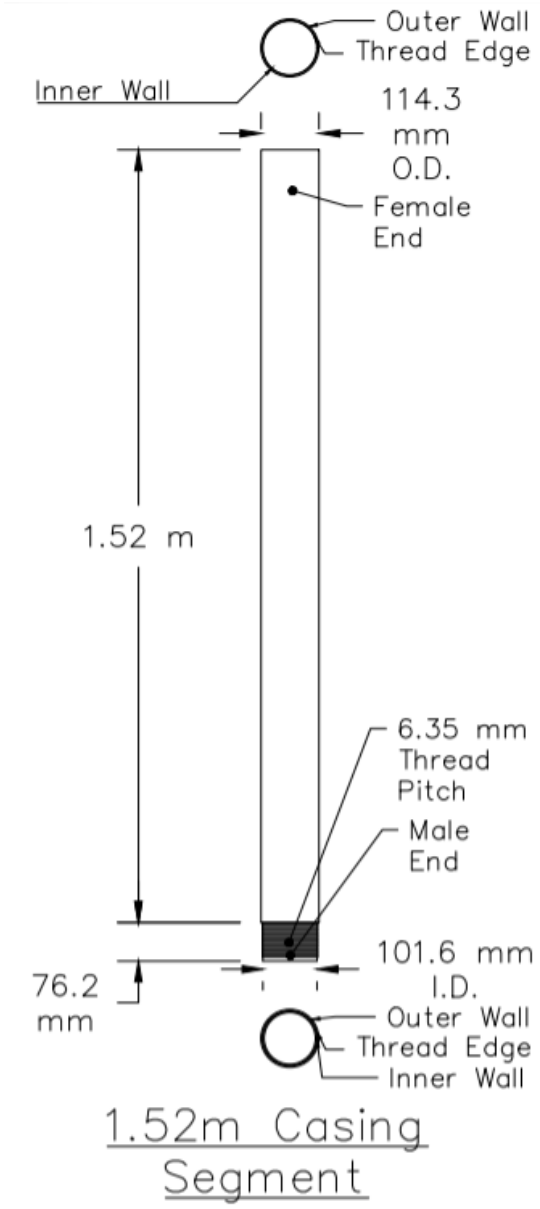

Figure 2-8 Casing segment illustration

2.2 UT site

The UT test site is at the Hornsby Bend Biosolids Management Plant, which is owned and operated by the City of Austin. Figure 2-9 presents the site. Piles were installed across an area that is about 30 m wide.

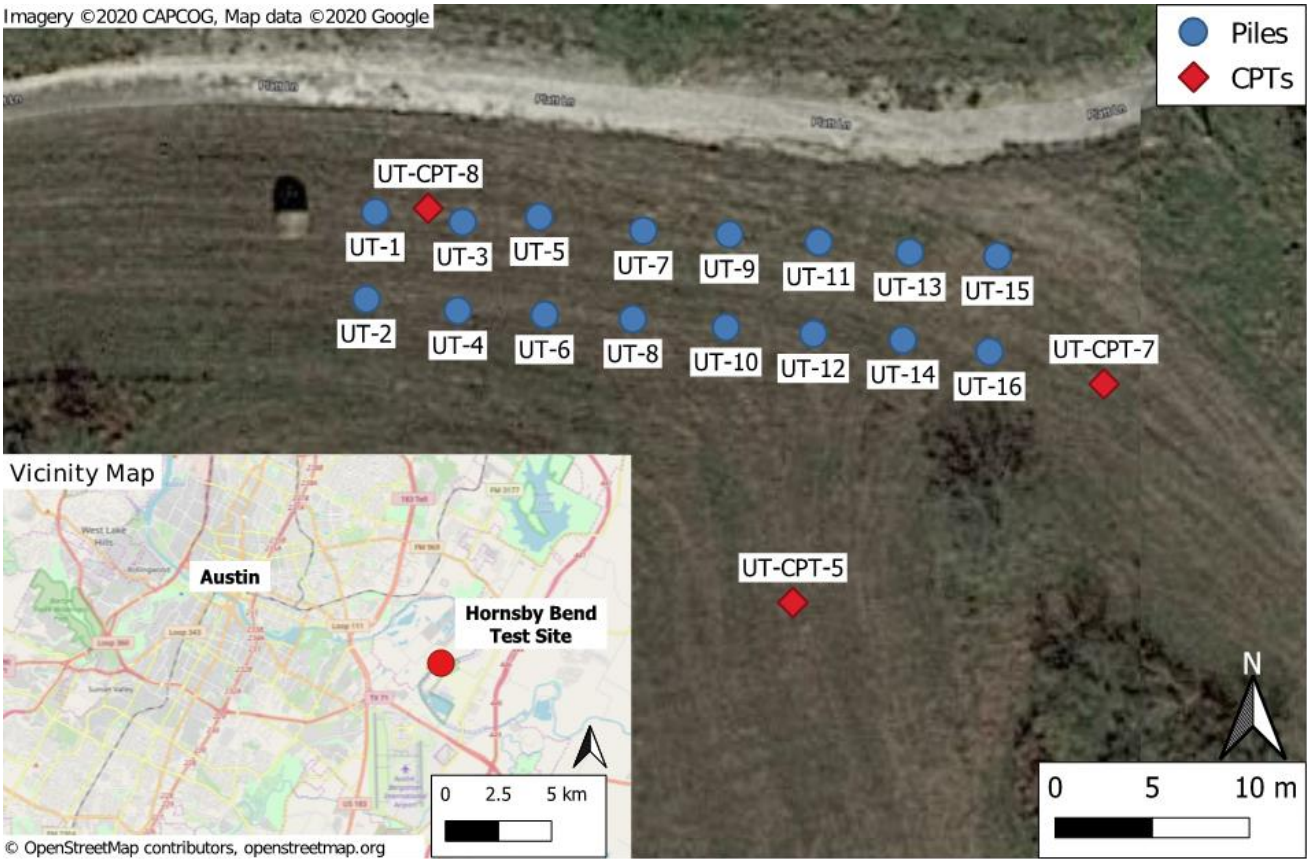

Figure 2-9 Site plan of geotechnical investigations and pile testing at the UT test site

2.2.1 CPT data

Three CPTs, in an approximate 18 meter radius, were performed in a region of the test site with the thickest sand layer, see Figure 2-10.

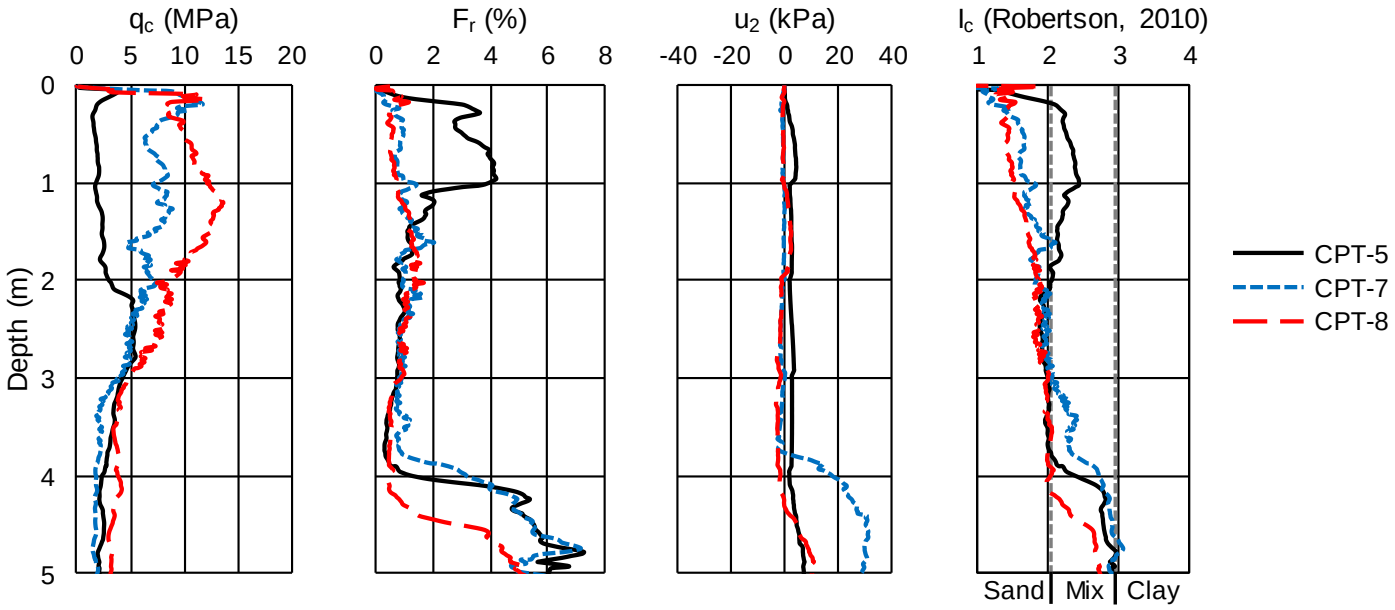

Figure 2-10 Results of CPT testing performed at the UT Hornsby Bend

The soil in the upper 4 meters behaved like sand to sand mixture, with some finer soils observed in the first meter of UT--CPT--5. The groundwater table was not encountered.

Relative density estimations from CPT correlations using the Jamiolkowski, et. al (2003) method indicated values ranging from 80 to 100% from a depth of 0 to 3 meters and 40 to 50% to a depth of 5 meters. Predicted relative density profiles are given in Figure 2-11.

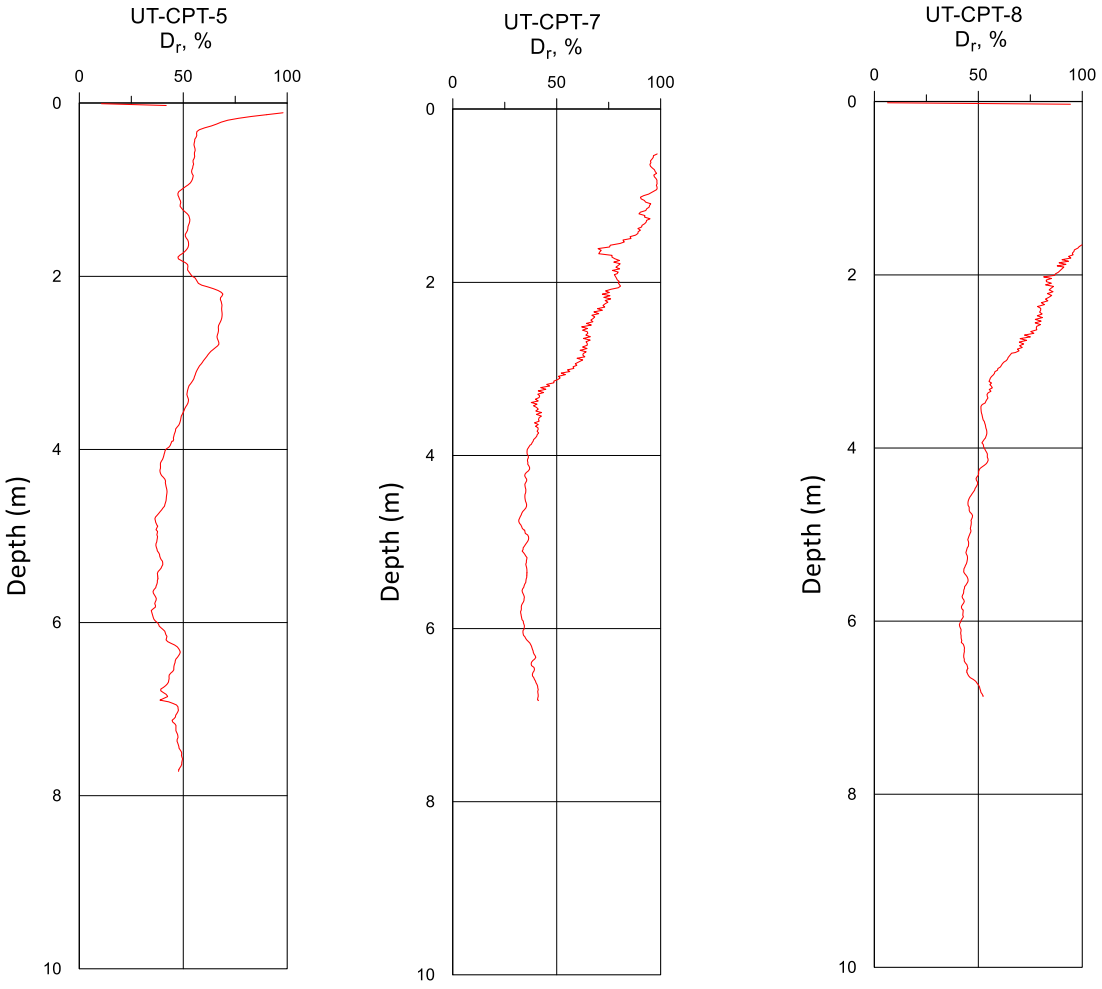

Figure 2-11 Correlation of saturated relative density from CPT data of UT site.

It should be noted that the low relative density of UT-CPT-05 compared to other borings can be related to lateral variability of soil data as UT-CPT-05 is located further away from locations of the test piles. Therefore, data from this boring may be ignored.

2.2.2 Pile installation

The sixteen test piles at the UT site consisted of 4-in A53B schedule 40 ERW steel pipes that were driven open-ended. The pipes have an inner and outer diameter of 102.3 and 114.3 mm, respectively. The piles were in a non-rusted condition at installation. Fourteen piles were 3.96 m long and were driven to a final embedment of 3.66 m. Two shorter piles, UT-1 and UT-15, were 2.44 m long and were driven to a final embedment of 2.13 m.

Piles were installed with a Linkbelt LS 78 crane equipped with a 10.8-kN drop hammer. A 0.75-m drop height was used in the first 2.44 m of driving for the longer piles. Pile driving analysis sensors were then attached and the pile was driven to completion with a 0.3-m drop height, except for UT-9 where the drop height of 0.75 m was used to completion. The driving histories of all the piles are shown in Figure 2-12. After installation, the soil surface inside the piles was measured to be 2.50 to 3.05 m from the ground surface (i.e., implying that they plugged during installation).

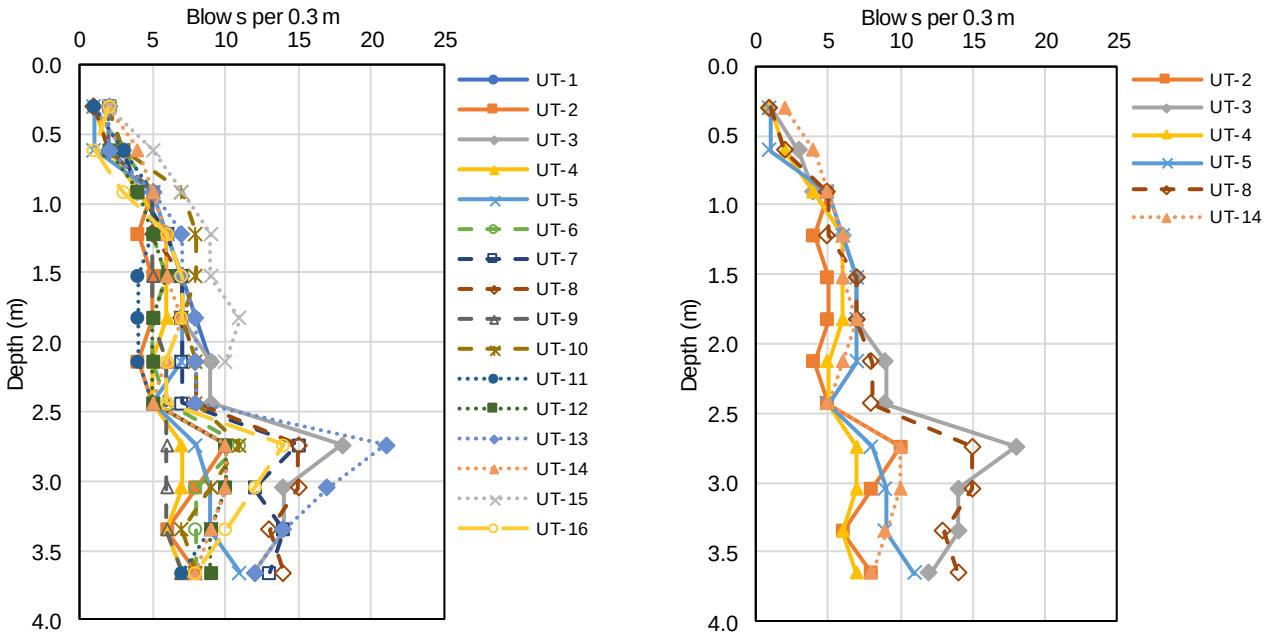

Figure 2-12 Measured pile driving resistance for piles installed at UT site. Hammer drop=0.75m in first 2.4m penetration, 0.3m thereafter

2.3 Pile capacity prediction based on CPT data

Several methods are available for predicting pile capacity from soil data. The UWA-05 method seeks to relate CPT cone tip resistance provided with pile capacity due to the similar strength mechanics involved between piles and CPT tests (Lehane et al., 2007). The UWA-05 method explicitly includes the effects of friction fatigue and shear band dilation.

Predictions were based on pile geometry in addition to CPT data.
The total skin friction is defined by the following equation (Lehane et al., 2007):

$$TSF = \left(\frac{f}{fc}\right) * (\sigma'_{rc} + \Delta\sigma'_{rc}) * tan(\delta_{cv}) \qquad \text{Equation 2.1}$$

Where $\left(\frac{f}{fc}\right)$ = empirical constant that relates tensile resistance to compressive cone tip resistance (unity in the case of compressive loading, 0.75 in the case of tensile loading), σ'_{rc} = radial effective stress after pile installation and equalization, $\Delta\sigma'_{rc}$ = change in radial effective stress due to soil dilation during application of pile loads, and δ_{cv} = constant volume (critical state) interface friction angle of the soil-pile system.

The method also takes into account the small strain shear modulus of the site soil to determine the dilatory change in effective stress. Values can either be input based on shear wave velocity determinations or calculated from the following relation of shear modulus to the uncorrected cone tip resistance:

$$\frac{G}{q_c} = 185(q_{c1n})^{-0.75} \qquad \text{Equation 2.2}$$

Where G=shear modulus, q_c = uncorrected cone tip resistance and q_{c1N} = the normalized cone tip resistance normalized to overburden effective stress

For the depth of penetration of 4.27m, the predicted maximum tension capacity for the URI site is detailed in Table 2-3 for each CPT location.

Table 2-3 UWA-05 predictions for URI site using 4.27m pile embedment

CPT Test	Average Qs	
	lbs	kN
SCPT19-02	13,122.0	58.4
SCPT19-03	11,224.5	49.9
SCPT19-04	10,127.3	45.0
CPT19-05	12,778.3	56.8
Average	11,813.0	52.5

Using the UT site CPT data, pile tension capacity were evaluated by using several published methods. Results are shown in Figure 2-13 using UT-CPT07 and Figure 2-14 using UT-CPT08 data.

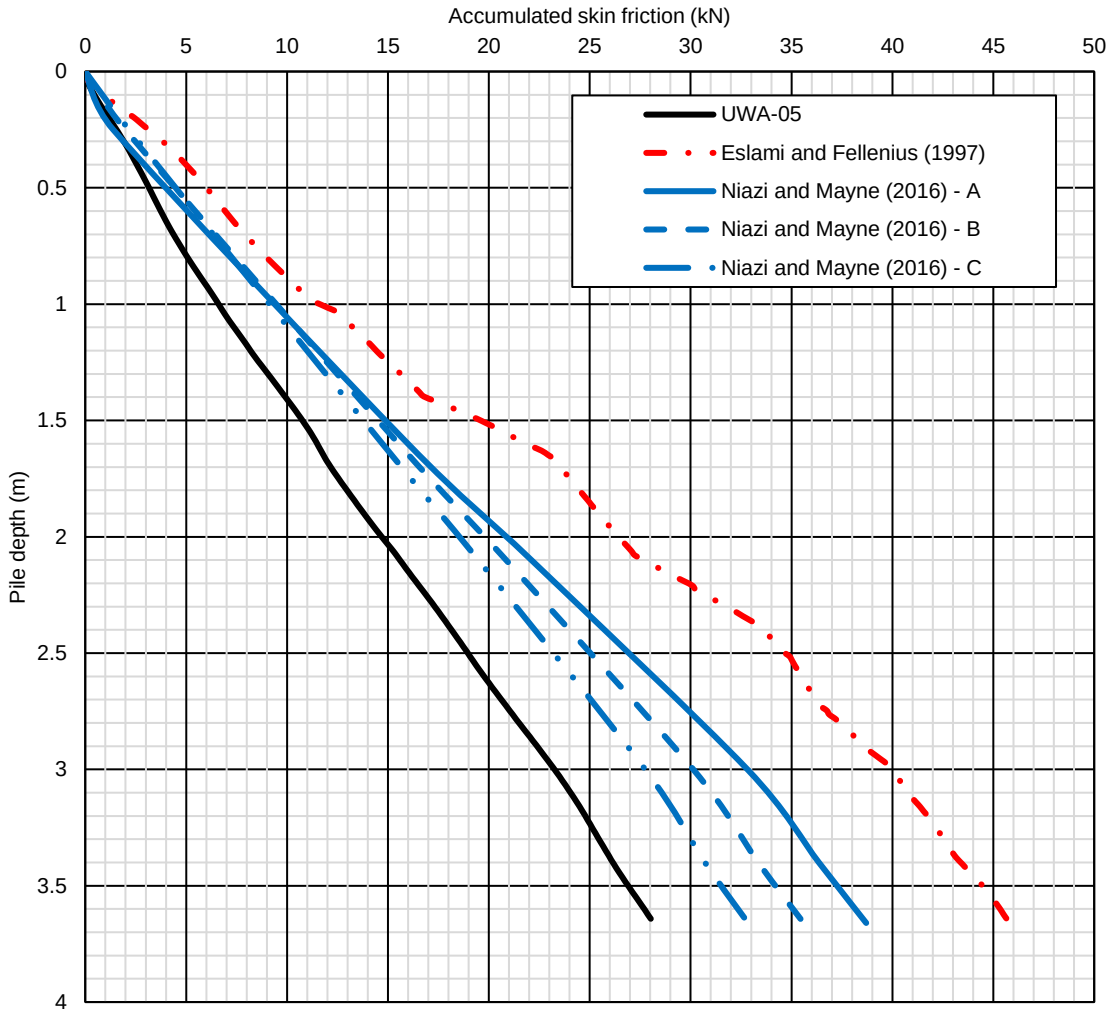

Figure 2-13 UT site predicted pile capacity in tension based on CPT07 data

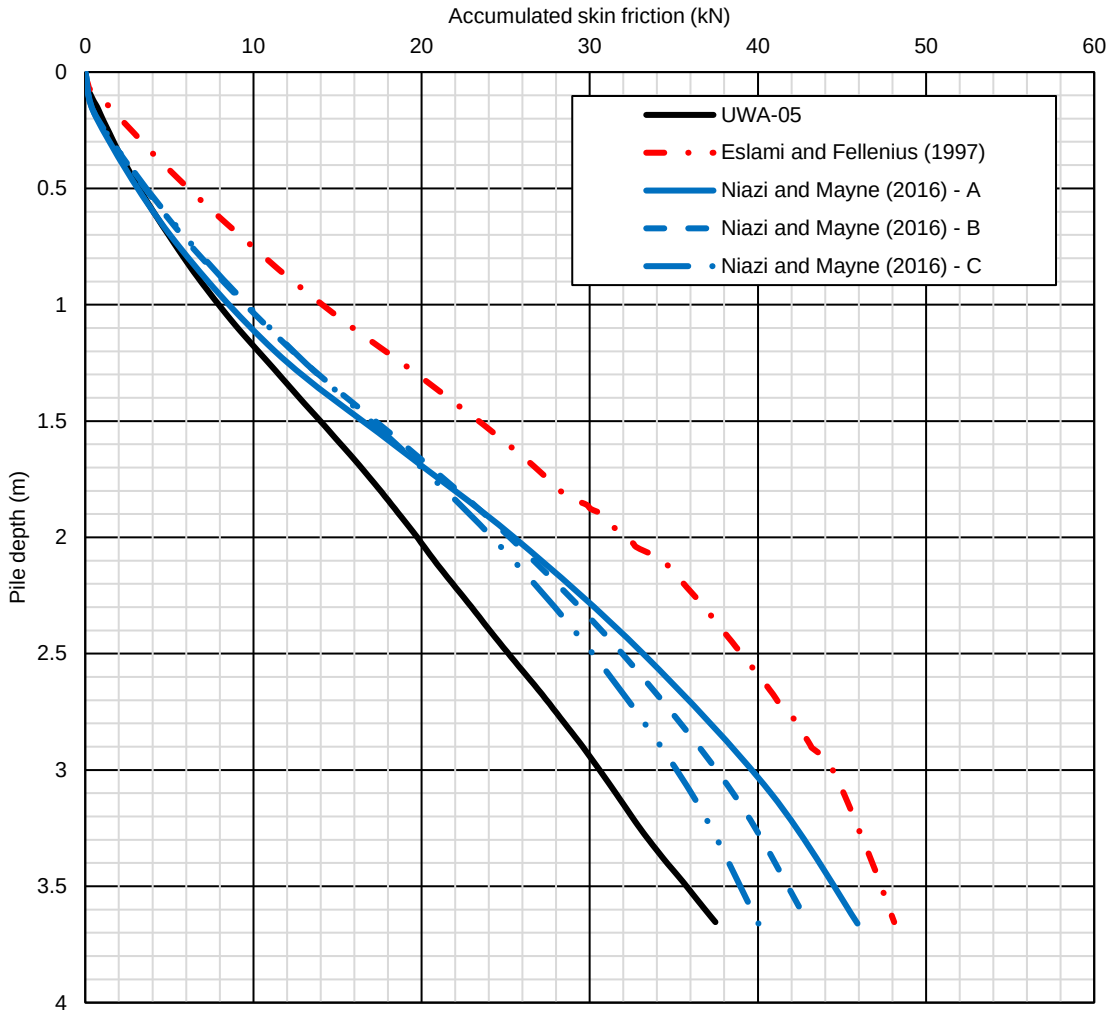

Figure 2-14 UT site predicted pile capacity in tension based on CPT08 data

The CPT based UWA-05 prediction showed a variation of capacity between 37.5 kN at UT-CPT08 on the west side, to 28 kN at UT-CPT07 on the east side. Therefore, the UWA-05 average shaft shear strength discussed in Section 5 is assumed to vary linearly from UT-1 to UT-16. The pile average shaft shear strength is the pile capacity divided by the outer wall surface area.

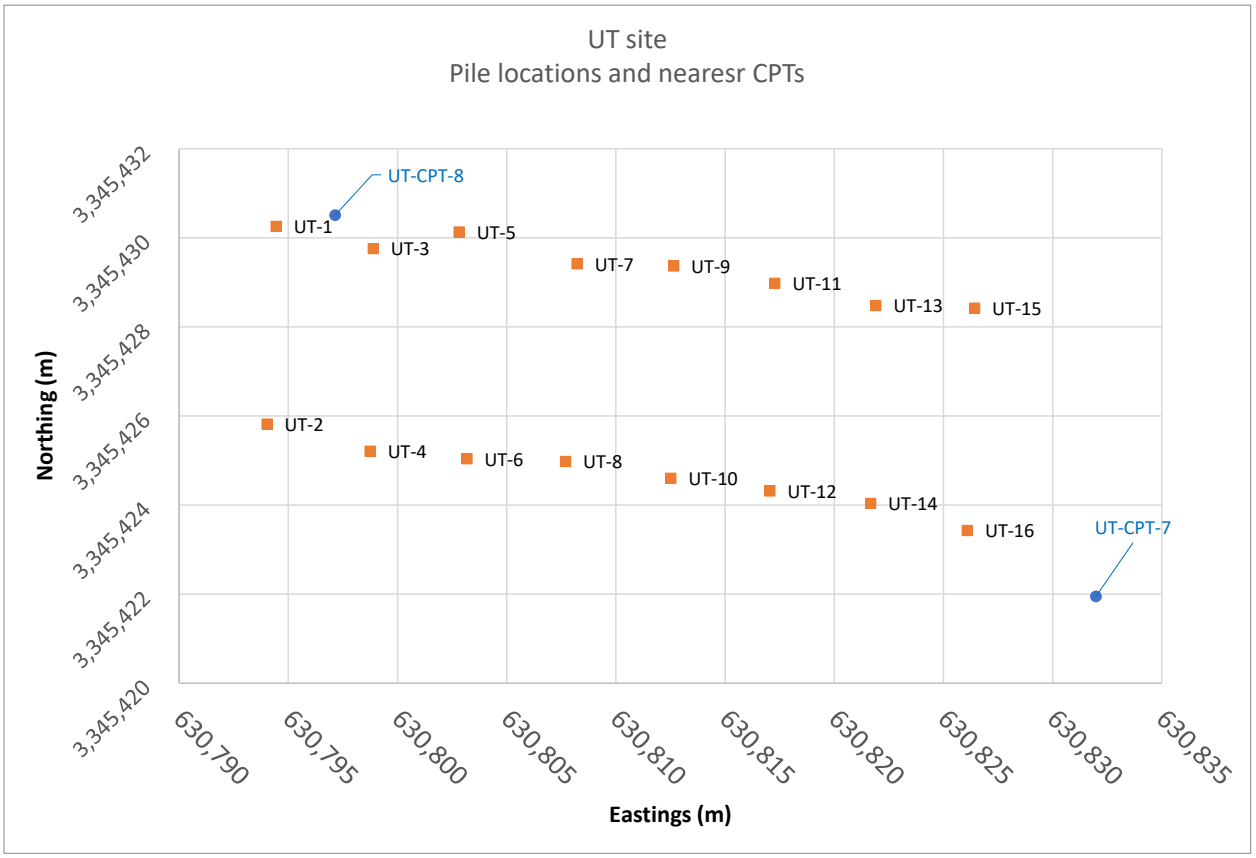

Figure 2-15 UT piles and CPT locations using UTM 14 R coordinate system

3 Laboratory tests

3.1 URI lab tests

3.1.1 Grain size tests

Sieve analyses were performed on recovered soil samples according to ASTM D6913. Soils in the upper 5 m consisted of medium to dense poorly graded sand, silty sand, and mixes of both (USCS: SP, SM, SP-SM, respectively). The fines content was less than 17% in all samples. The diameter corresponding to 50 percent of the total sample mass (D_{50}) ranged from 0.17 to 0.6 mm. See Figure 3-1.

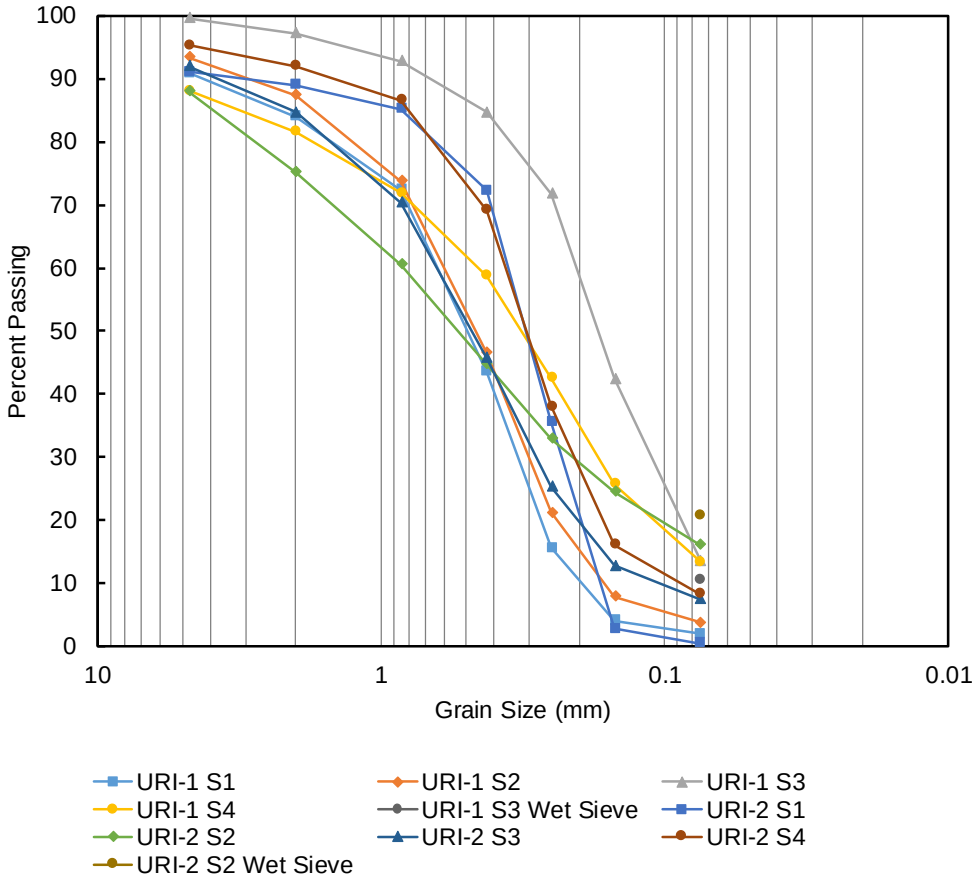

Figure 3-1 Grain size data for soil samples from URI site.

3.1.2 Soil Interface Shear Tests

Eighteen two-way Constant Normal Stiffness (CNS) interface shear tests were conducted by Javier Fernandez Scarioni on soil recovered from the site and reported as part of his master's thesis (Scarioni 2019). Table 3-1 lists the stiffness tests that were carried out.

Table 3-1 Summary of CNS testing on sand samples from the Davisville test site.

Test No.	Sample	Representative Depth (m)	Unit Weight (kN/m^3)	Initial Normal Stress (kPa)	Normal Stiffness (kPa/mm)	Shear Displacement Amplitude (mm)
CNS MONO 1	URI-1 S2	1.4	15.84	25	970	na
CNS CYC 1	URI-1 S2	1.4	15.84	25	970	0.1
CNS CYC 2	URI-1 S2	1.4	15.84	25	970	0.25
CNS CYC 3	URI-1 S2	1.4	15.84	25	970	0.5
CNS MONO 2	URI-1 S2	2.3	15.84	50	1235	na
CNS CYC 4	URI-1 S2	2.3	15.84	50	1235	0.1
CNS CYC 5	URI-1 S2	2.3	15.84	50	1235	0.25
CNS CYC 6	URI-1 S2	2.3	15.84	50	1235	1
CNS MONO 3	URI-1 S4	3.7	15.84	115	1570	na
CNS CYC 7	URI-1 S4	3.7	15.84	115	1570	0.1
CNS CYC 8	URI-1 S4	3.7	15.84	115	1570	0.25
CNS CYC 9	URI-1 S4	3.7	15.84	115	1570	1
CNS CYC 10	URI-1 S2	1.4	17.11	25	970	0.25
CNS CYC 11	URI-1 S2	1.4	-	25	970	0.25
CNS CYC 12	URI-1 S4	2.3	17.11	50	1235	0.25
CNS CYC 13	URI-1 S4	2.3	-	50	1235	0.25
CNS CYC 14	URI-1 S4	3.7	17.11	115	1570	0.25
CNS CYC 15	URI-1 S4	3.7	-	115	1570	0.25

An example test result is presented on Figure 3-2.

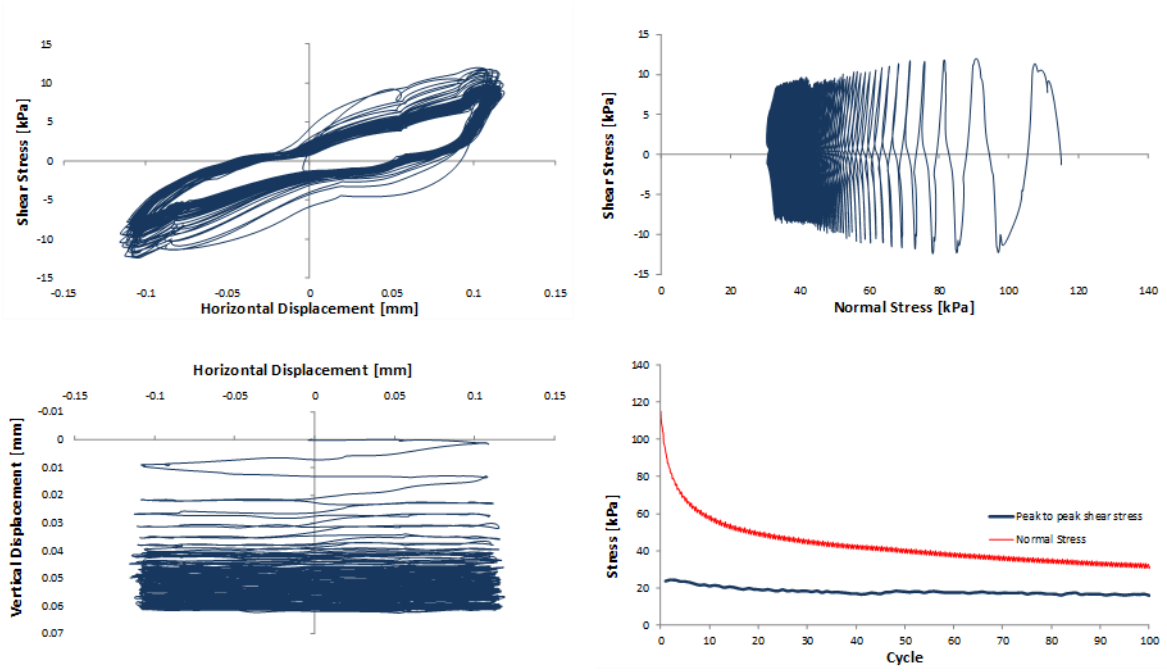

Figure 3-2 Scarioni (2019), CNS test result on Davisville sand.

3.1.3 Carbonate tests

A total of four sandy samples from the URI-2 borehole for depths from zero to 4 m were tested in the NGI Houston laboratory for carbonate content using ASTM D-4373. It was found the samples contained zero carbonate content.

3.2 UT lab testing

3.2.1 Grain size tests

Sieve analyses were performed on recovered soil sample at 1 m depth next to UT-CPT-5 according to ASTM D6913. The fines content was less than 35%. The diameter corresponding to 50 percent of the total sample mass (D_{50}) is 0.145 mm. See Figure 3-3.

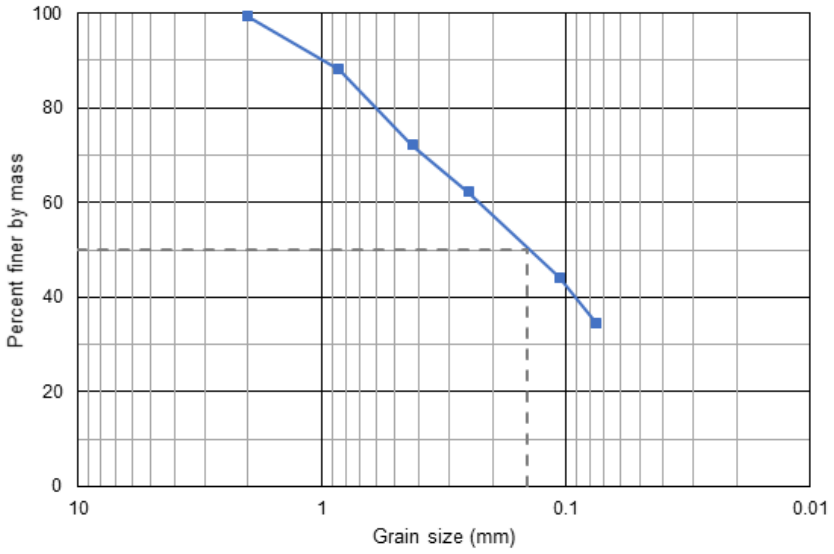

Figure 3-3 Grain size data for soil sample from UT site

4 Pile load testing

4.1 Load testing method

Three types of pile load tests were performed:

1. monotonic tension test: maintained load tension
2. cyclic low-frequency (LF) 0.125 Hz: approximately one-way cyclic tension, followed by monotonic tension
3. cyclic high-frequency (HF) 40 Hz: approximately one-way cyclic compression, followed by monotonic tension

Monotonic tensile load tests were performed to determine the un-cycled side friction capacity as a function of time. The other piles were loaded cyclically and then loaded to failure monotonically. Type 1 and 2 tests were performed and URI and UT. Type 3 tests were only conducted at UT.

The equipment used for a typical monotonic and low-frequency cyclic pile load test setup is shown in Figure 4-1. A portable hydraulic load control system was developed at URI to be able to test the piles under specified monotonic and low-frequency (about 0.125 Hz) cyclic tensile load patterns. The hydraulic equipment consisted of an OTC air-hydraulic pump connected to an Emerson ER5000 hydraulic controller and a SPX Flow Power Team center-hole hydraulic jack. The jack pressures controlled by the ER5000 were pre-programmed using a dedicated laptop computer. The minimum (tensile) pressure that could be applied by the controller was 200 psi (1,379 kPa), and thus a (compressive) stack of deadweight was used to lower the initial pile load.

Figure 4-1 Photograph of a typical pile load test setup at the URI test site

Monotonic loading was performed by applying load increments with a 5-minute hold to assess creep rates. The load increments were increased until pile pullout was observed. Cyclic loads were applied in a sinusoidal manner. An eight-second period was selected to be consistent with the period of ocean wave loading on offshore structures.

Pile head displacements during monotonic and low-frequency cyclic loading were measured using an LVDT mounted to a reference beam. Voltage readings from the pile head load cell and LVDT were recorded and post-processed.

High-frequency cyclic loading was performed only at the UT site using the vertical component of the urban shaker *Thumper*, one of the NHERI@UTexas large-scale mobile shakers described by Stokoe et al. (2017). In all tests, approximately 150,000 vertical cycles were applied in compression at a frequency of about 40 Hz. For most tests, the piles were loaded using the truck mass, see Figure 4-2 a. In one test, the shaker mass was removed and applied directly to the pile for smaller loads, see Figure 4-2 b. On both setups an accelerometer and LVDT were used to measure the pile head displacements during high-frequency cycling, and load was monitored using a pile head load cell.

(a) shaker truck load applied to pile *(b) shaker mass load applied to pile*

Figure 4-2 Photograph of a high-frequency pile loading setup at the UT test site

4.2 Results at URI test site

Table 4-1 lists the pile tests carried out at the URI site.

Table 4-1 Summary of pile tests at URI

Pile number	Aging time	Type of tests
P1	8	Monotonic
P2	7	Monotonic
P2	8	Cyclic-monotonic (LF)
P2	14	Cyclic-monotonic (LF)
P3	71	Monotonic
P4	8	Cyclic-monotonic (LF)
P5	77	Monotonic-cyclic-monotonic (LF)
P6	87	Cyclic-monotonic-cyclic-monotonic (LF)

Table 4-2 summarizes the pile tests results at the URI site. All cyclic tests were carried out with low frequency (LF) of 0.125 Hz. Table 4-3 summarizes the different load parcels applied in cyclic tests; project load definitions as per Figure 4-3.

Table 4-2 List of URI monotonic and cyclic (0.125 Hz) Pile Tests

Pile No.	Test Description	Aging Time	Ult. Post-Cyclic/Mono. Capacity	Net Disp. at Ult. Capacity [1]	Mono. Capacity at 1% Net Pile Diameter Disp. [1]	No. of Cycles	Cyclic Load Ratio [2]	Cyclic Disp.
		Days	kN	mm	kN			mm
P1	Monotonic	8	5.84	0.92	5.64	N/A	N/A	N/A
P2	Monotonic	7	7.01	2.75	5.83	N/A	N/A	N/A
P2	Cyclic-Monotonic	8	5.83	22.74	5.36	300	0.40	0.1
P2	Cyclic-Monotonic	14	6.94	20.80	5.90	1250	0.94	26.45
P3	Monotonic	71	27.66	4.00	27.04	N/A	N/A	N/A
P4	Cyclic-Monotonic	8	23.03	15.30	17.26	10150	0.41	0.84
P5	Monotonic-Cyclic-Monotonic	77	29.2	27.00	27.00	2790	0.80	2.26
P6	Cyclic-Monotonic-Cyclic-Monotonic	87	36.45	0.95	35.64	7650	0.68	1.30*
Notes:	[1] Net disp. is calculated as 1% of pile OD or 1.14 mm in monotonic portion							
	[2] Cyclic load ratio =(Qave + Qcyc)/Qt, where Qcyc & Qave characterize the time averaged maximum cyclic load, Qt = Ultimate post-cyclic monotonic capacity. Peak loads in individual cycles maybe higher (see load-time histories).							
	* Includes initial cyclic loading and secondary cyclic loading displacement (0.40 mm and 0.90 mm, respectively)							

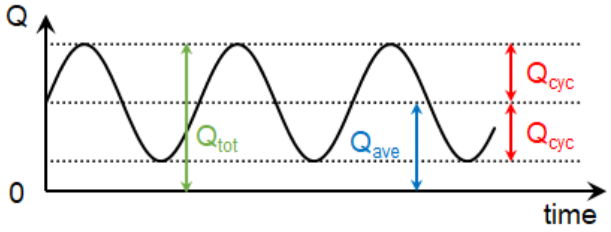

Figure 4-3 Load definitions

Table 4-3 Load parcels for cyclic URI tests.

	Parcel (-):			Parcel (-):			Parcel (-):			Parcel (-):			Parcel (-):			Parcel (-):			Parcel (-):		
	1			2			3			4			5			6			7		
	Ncyc (-)	AVE (kN)	CYC (kN)	Ncyc (-)	AVE (kN)	CYC (kN)	Ncyc (-)	AVE (kN)	CYC (kN)	Ncyc (-)	AVE (kN)	CYC (kN)	Ncyc (-)	AVE (kN)	CYC (kN)	Ncyc (-)	AVE (kN)	CYC (kN)	Ncyc (-)	AVE (kN)	CYC (kN)
URI-P2b *	300	1.4	0.9																		
URI-P2c *	499	2.1	1.5	302	2.5	1.9	156	2.8	2.2	150	3.3	2.7	143	3.5	3.0						
URI-P4	1753	1.9	1.8	2246	2.1	1.7	4058	2.6	2.5	518	3.0	2.5	560	4.2	2.9	560	4.5	3.7	456	5.2	4.2
URI-P5 *	2790	12.8	10.5																		
URI-P6	531	4.2	3.9	7119	13.1	11.8															
Cyclic then monotonic, unless label denoted with an asterisk, for which Monotonic-cyclic-monotonic.																					
Ncyc - number of cycles per packet																					

The UWA-05 (Lehane et al., 2007) method was used to estimate monotonic pile capacities based on SCPT results from the site. Results from this analysis estimated 7-day ultimate tensile capacities ranging from 47-64 kN (varying by SCPT), indicating inherent site variability. It should be noted that the UWA-05 method was calibrated on full-scale piles in the 7-day range after installation, therefore the capacities estimated were expected to differ to some degree with actual capacities at the URI site depending on the time of testing.

Seven days after installation, Pile P1 was tested by applying a series of 4.2-kN load steps, which the UWA-05 method was used to establish. Surprisingly, while setting the initial load for the system, the control system overshot the load control briefly and failed the pile. During this time, the data acquisition system recorded a maximum pile load of 5.84 kN as shown in Figure 4-4.

The tensile capacity of Pile P1, being 12% of the estimated UWA-05 capacity, warranted repeating a monotonic test on Pile P2 using smaller load increments. The results, shown in Figure 4-4, yielded a tensile capacity of 5.83 kN, which further confirmed that the lower than expected monotonic pile capacities were repeatable at the site.

Pile P4 was cyclically loaded before being failed under tension 8 days after installation under cyclic tension loads ranging from about 0 kN (minimum) to 3.4 - 9.5 kN (maximum) as shown in Figure 4-4 and Figure 4-5. Loads were increased during the testing, based on

review of the cycle-by-cycle performance which indicated minimal creep/ movement at lower load levels. The maximum tension load corresponded to about 58% to 163% of the 7-day static monotonic tensile capacity for Pile P2. For the cyclic portion, different sets of cyclic maximum capacities were tested for a total of more than 10,000 eight-second cycles with low frequency (0.125 Hz). The maximum cyclic loads placed on the pile produced no appreciable displacements. Notable displacement 'drift' was observed during testing that was attributed to buoyancy effects during tidal changes, and water table readings from a monitoring well installed on site allowed the displacements to be corrected for these buoyancy effects. Since failure was not reached after ten thousand cycles, a post-cyclic monotonic test was performed on Pile P4, as shown in Figure 4-4, from which the failure load at 1.14 mm (1% pile diameter) of additional displacement was 17.2 kN.

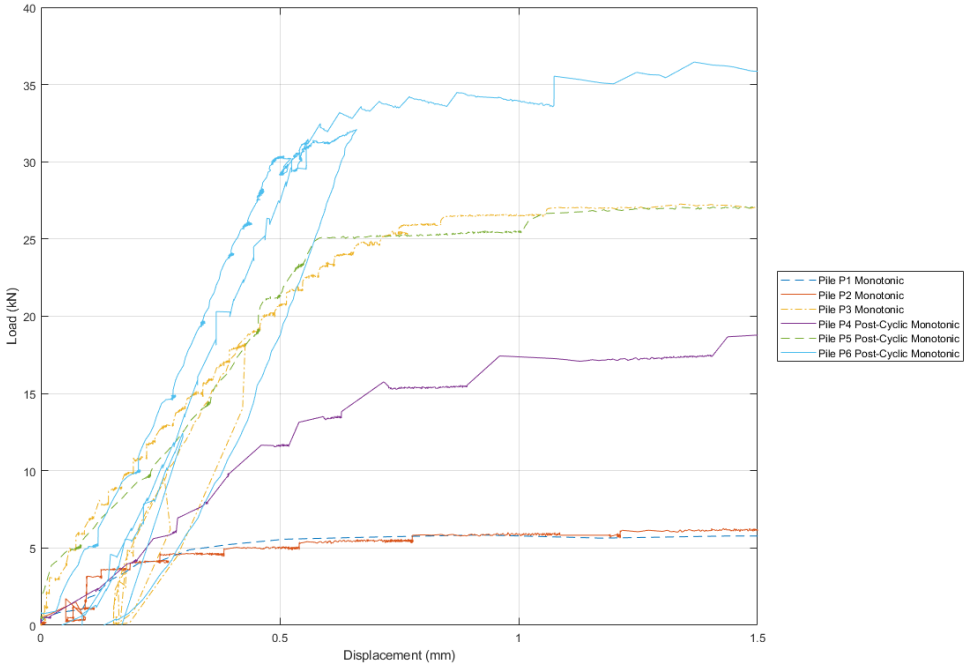

Figure 4-4 URI Load-displacement results for monotonic (P1 and P2) and post LF cyclic (P4,P5,P6)

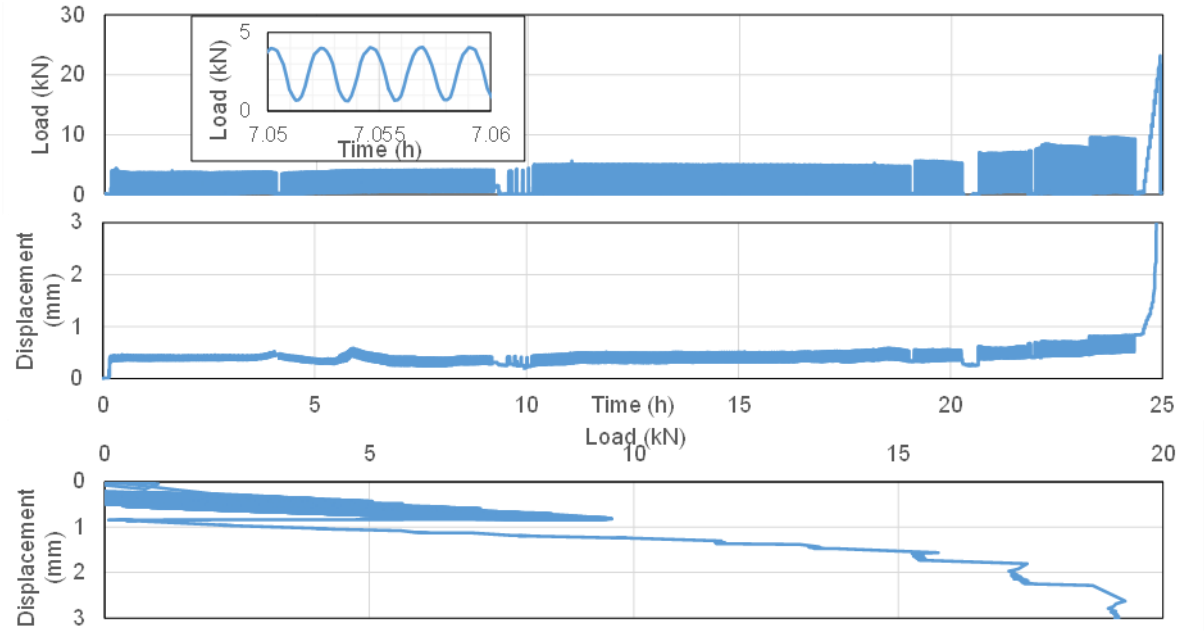

Figure 4-5 Load and displacement variation for pile P4, cyclic (0.125 Hz) & post-cyclic monotonic

Pile P5 and P6 were tested 77 days and 87 days after installation using LF cycles as shown in Figure 4-6 and Figure 4-7 respectively.

P5 was cyclically tested under maximum cyclic load levels ranging from about 0 kN (minimum) to about 22 kN (maximum) (with some over-shoot to 30 kN) as shown in Figure 4-6. This corresponded to about 380% to 517% of the 7-day static monotonic tensile capacity for Pile P2. For the cyclic portion, different sets of cyclic maximum capacities were tested for up to 2,790 eight-second cycles with low frequency (0.125 Hz). The maximum cyclic loads placed on the pile produced no appreciable displacements. Since failure was not reached after cyclic testing for ten thousand cycles, a post-cyclic monotonic test was performed on Pile P5, from which the failure load at 1.14 mm (1% pile diameter) of additional displacement was 17.2 kN. The maximum recorded cyclic load ratio was 1.07.

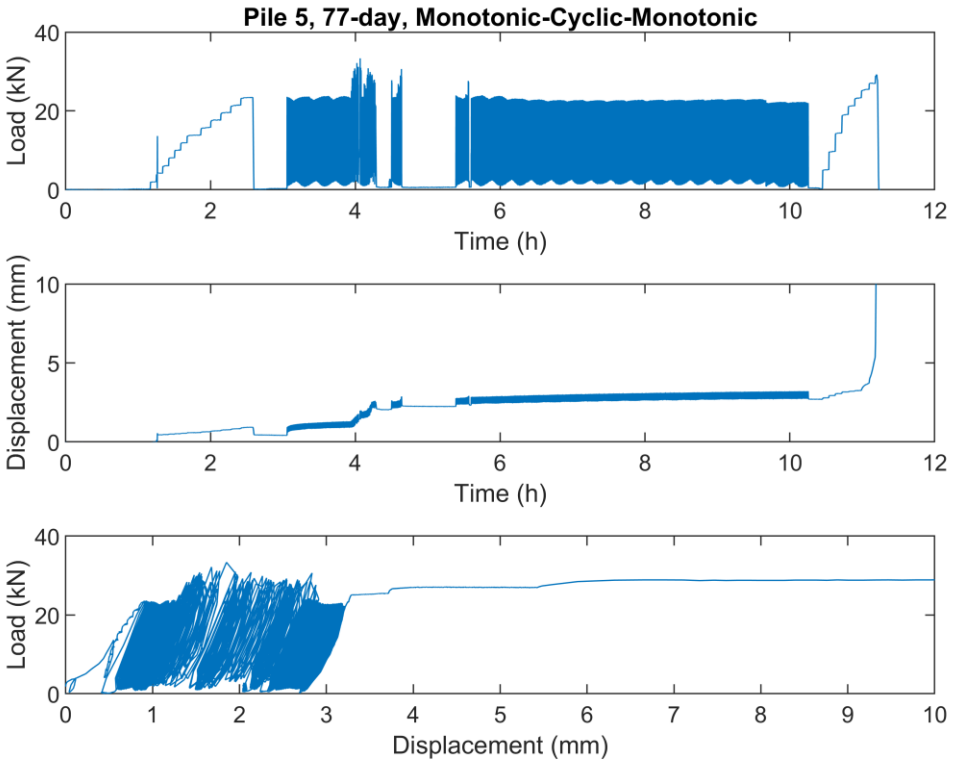

Figure 4-6 Pile 5. 77-day cyclic test, preceded by monotonic testing for cyclic load level determination and followed by monotonic capacity testing

Similarly, P6 was cyclically loaded between 0 to about 25 kN for over 10,000 eight-second cycles with low frequency (0.125 Hz) as shown in Figure 4-7. The maximum recorded cyclic load ratio was 0.82.

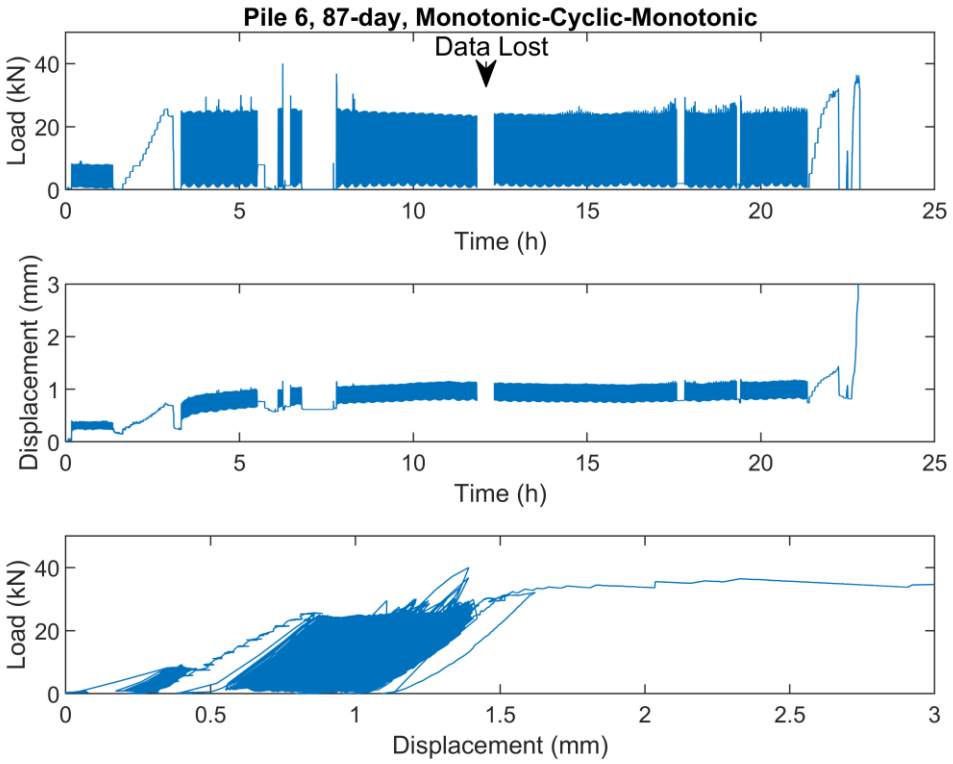

Figure 4-7 Pile 6. 87-day cyclic , preceded by monotonic for cyclic load level determination and followed by monotonic capacity testing

More details of these tests are available in Appendix A of this report.

4.3 Results at UT test site

Table 4-4 provides a summary of the pile tests at UT. The cells highlighted in green are for the low frequency 0.125 Hz (tension cycles) while those in blue are for the high frequency 40 Hz (compression cycles).

Table 4-4 Summary of pile tests at UT

Pile number	Date installed	Type of tests
1	1/15/2020	Practice 1 day monotonic to failure (7 ft short pile)
2	1/15/2020	8 days cyclic HF, then monotonic to failure
3	1/15/2020	8 days monotonic to failure
4	1/15/2020	9 days cyclic HF then monotonic to failure
5	1/15/2020	9 days monotonic to failure
6	1/15/2020	166 days cyclic HF then monotonic to failure
7	1/15/2020	163 days monotonic to failure
8	1/21/2020	0.1 day monotonic
8 re-test	1/21/2020	156 days cyclic LF then monotonic to failure
9	1/15/2020	168 days cyclic HF then monotonic to failure
10	1/21/2020	7 days monotonic
10 re-test	1/21/2020	149 days monotonic to failure
11	1/21/2020	161 days cyclic HF then monotonic to failure
12	1/21/2020	150 days monotonic to failure
13	1/21/2020	153 days monotonic to failure
14	1/21/2020	7 days monotonic then cyclic LF then monotonic to failure
15	1/15/2020	7 ft Short pile
16	1/21/2020	162 days cyclic LF then monotonic to failure

Pile capacity estimations were performed using the UWA-05 (Lehane et al., 2007) method based on parameters estimated from CPT results. The predicted ultimate tensile capacity based on UT-CPT-7 and UT-CPT-8 were 28 kN and 37.5 kN, respectively. Like the URI site, the CPT predictions indicated site variability, and the measured static pile tensile capacities were lower than anticipated.

Table 4-5 Summary of UT monotonic tests

Pile	Aging time	Ultimate monotonic tensile capacity	Net displacement at ultimate capacity	Monotonic capacity at 1% net pile diameter displacement
	(days)	(kN)	(mm)	(kN)
UT-8	0.1	12.2	1.7	11.5
UT-3	8	18.7	1.6	18.0
UT-5	9	11.9	1.2	11.5
UT-10	149	35.7	2.9	28.9
UT-12	150	24.7	1.5	22.2
UT-13	153	37.9	1.8	34.2

Table 4-6 Summary of UT low-frequency (0.125 Hz) cyclic tests

Pile	Aging time	Ultimate post-cyclic monotonic tensile capacity	Net displacement at ultimate capacity[(1)]	Monotonic capacity at 1% net pile diameter displacement[(1)]	Number of cycles	Cyclic load ratio[(2)]	Cyclic displacement
	(days)	(kN)	(mm)	(kN)			(mm)
UT-14	7	19.1	2.0	18.9	9,300	0.77	0.43
UT-8[(3)]	155	31.3	1.1	31.0	2,750	0.70	0.67 [(4)]
UT-16	166	28.6	0.3	28.4	10,000	0.86	0.38 [(4)]
Notes:	[(1)] Net displacement is calculated as 1% of pile OD (1.14 mm) during monotonic loading						
	[(2)] Cyclic load ratio = $(Q_{ave}+Q_{cyc})/Q_t$, where Q_{ave} = average load during cyclic loading, Q_{cyc} = amplitude of cyclic load (for more than one cycle), and Q_t = ultimate post-cyclic monotonic capacity						
	[(3)] Pile was retested 155 days after original failure. Pump failed after about 2,700 cycles						
	[(4)] Does not include displacement caused by uncontrolled jumps in load at start of test						

Table 4-7 Summary of UT high-frequency (40 Hz) cyclic tests

Pile	Aging time	Ultimate post-cyclic monotonic tensile capacity	Net displacement at ultimate capacity[(1)]	Monotonic capacity at 1% net pile diameter displacement[(1)]	Number of cycles	Cyclic load ratio[(2)(3)]	Cyclic displacement
	(days)	(kN)	(mm)	(kN)			(mm)
UT-2	8	12.5	1.1	12.4	150,000	0.23	1.0
UT-4	9	16.0	1.6	15.3	150,000	0.42	1.6
UT-11	161	24.4	2.6	22.3	150,000	0.44	0.1
UT-6	166	26.9	1.6	24.5	150,000	0.84	0.2
UT-9	168	35.6	2.2	33.5	150,000	0.67	0.1
Notes:	[(1)] Net displacement is calculated as 1% of pile OD (1.14 mm) during monotonic loading						
	[(2)] High-frequency cyclic loading was applied in compression						
	[(3)] Cyclic load ratio = $(Q_{ave}+Q_{cyc})/Q_t$, where Q_{ave} = average compressive load during cyclic loading, Q_{cyc} = amplitude of cyclic compressive load (for more than one cycle), and Q_t = ultimate post-cyclic tensile monotonic capacity						

While the magnitude of capacity estimates were higher than the tested capacities, the difference in capacities from the short term tests (~45%) was generally consistent with variability in capacity based on estimates using CPT methods (~30%). Load v displacement results for the short term tests at UT site are shown in Figure 4-8. Piles UT-2 and 4 were

tested with HF (40 Hz) cyclic loading while pile UT-14 was tested with LF (0.125 Hz) cyclic loading.

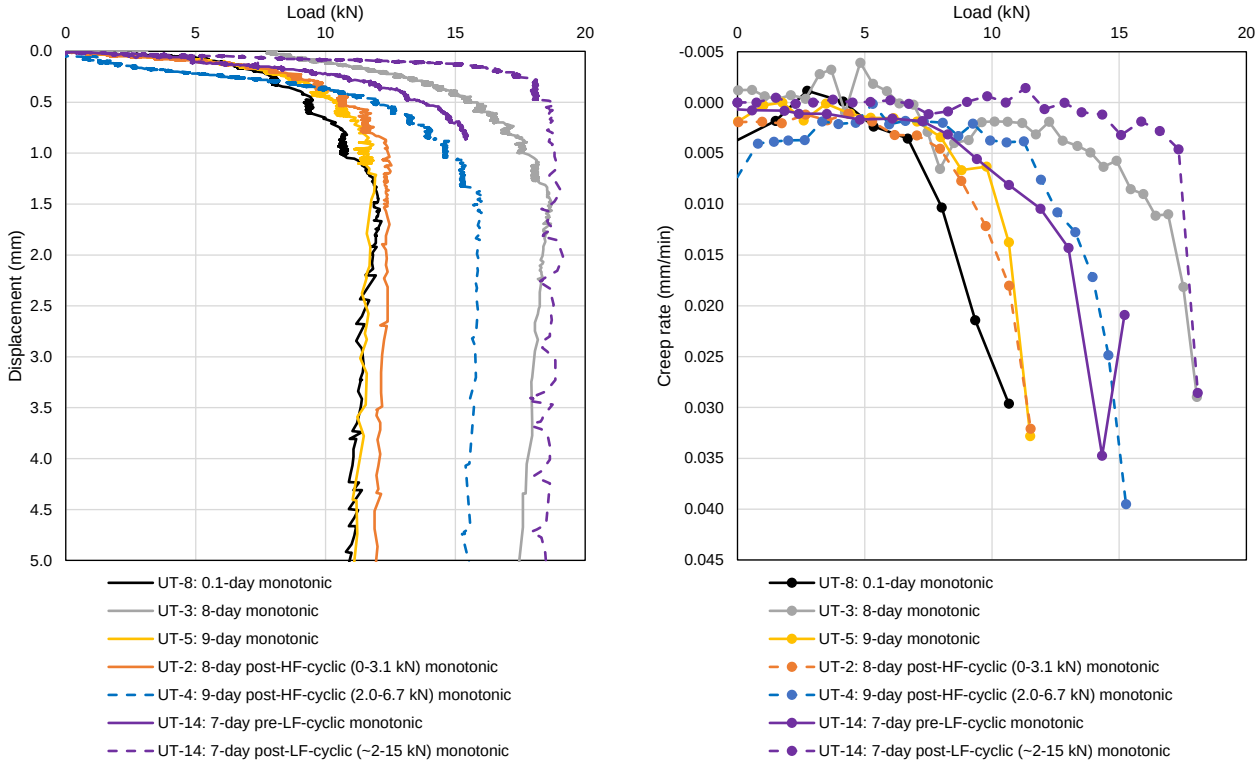

Figure 4-8 Load v displacement for short-term monotonic pile tests

Figure 4-9 shows all the long-term load versus displacement tests for the UT piles. This includes HF (40 Hz) and LF (0.125 Hz) cyclic tests. Note that pile UT-8 was re-tested for long-term conditions.

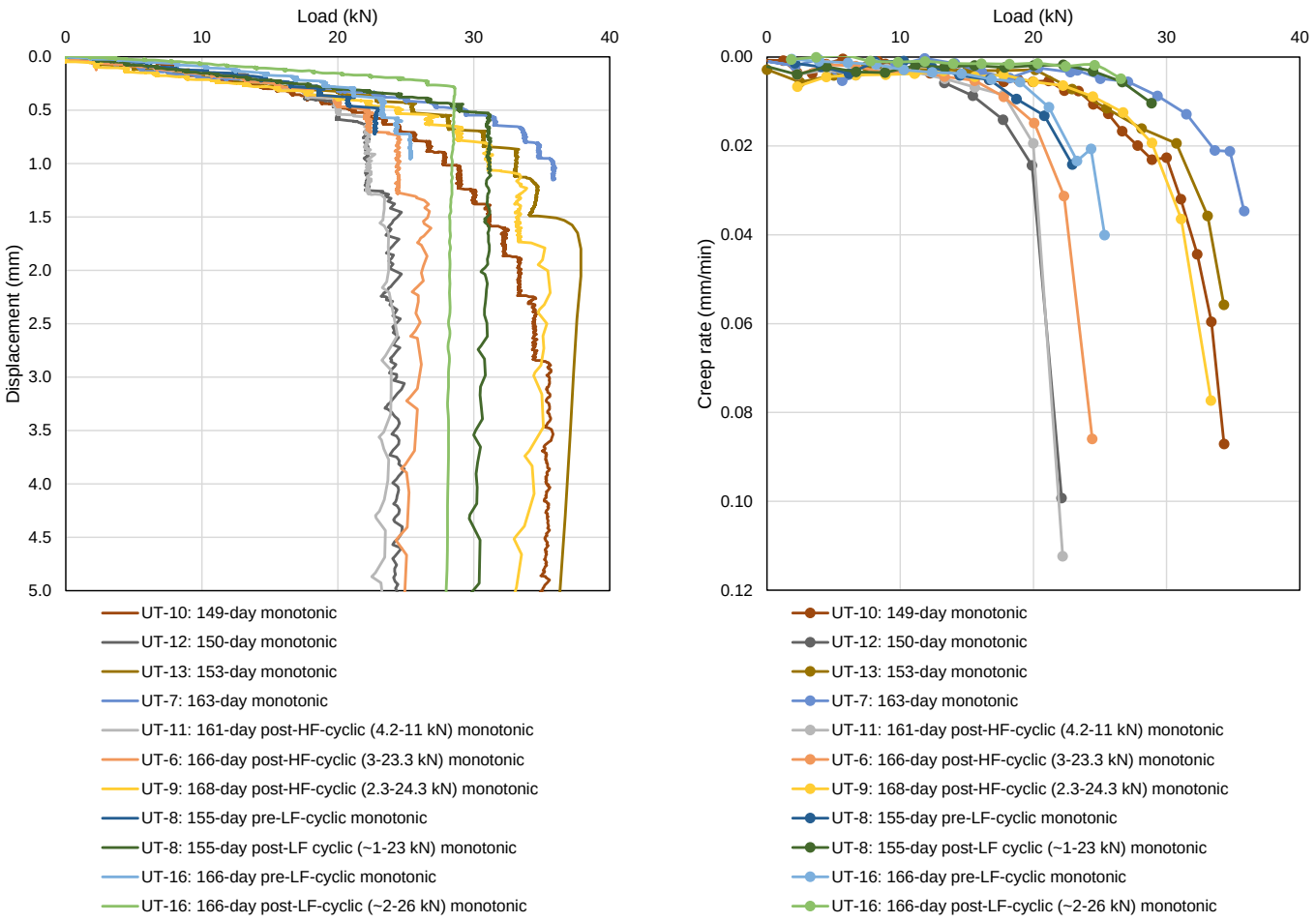

Figure 4-9 Load v displacement for long-term monotonic pile tests

To determine the maximum load to apply in the low-frequency cyclic tests, piles were loaded monotonically in tension with the aim of reaching a pullout rate just over 0.02 mm/min. The piles were then cyclically loaded in tension with a low frequency (0.125 Hz) for approximately 10,000 cycles. As an example, UT-14 was loaded with a minimum and maximum load of approximately 2 and 15 kN, approximately 13-100% of the previous maximum load. A sample of the load and displacement data 6.5 hours into low-frequency cyclic loading is shown in Figure 4-10.

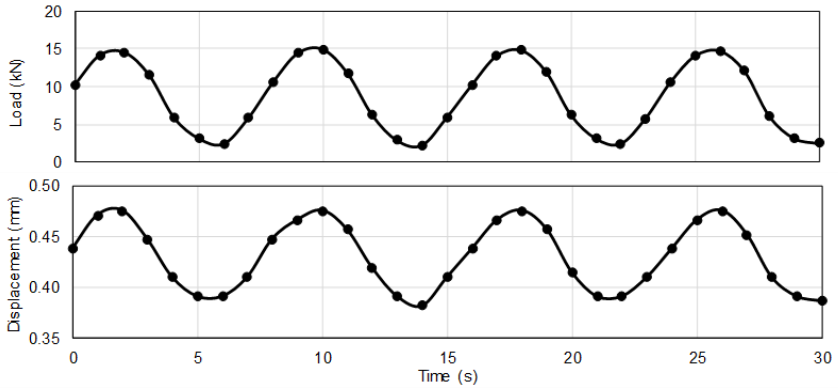

Figure 4-10 Load and displacement variation for UT14 cyclic (0.125 Hz) tension at 6.5 hours

For piles with HF cyclic loading, the piles were cyclically loaded in compression at a high frequency (40 Hz) using the urban shaker *Thumper*. As an example, UT-2 was loaded between 0 and 3.1 kN, approximately 0-26% of the tensile capacity of UT-5. UT-4 was loaded between 2.0 and 6.7 kN, approximately 17-56% of the tensile capacity of UT-5. Samples of the recorded load approximately 30 minutes into the high-frequency cyclic loading for UT-2 and UT-4 are shown in Figure 4-11.

a-UT2

b-UT4

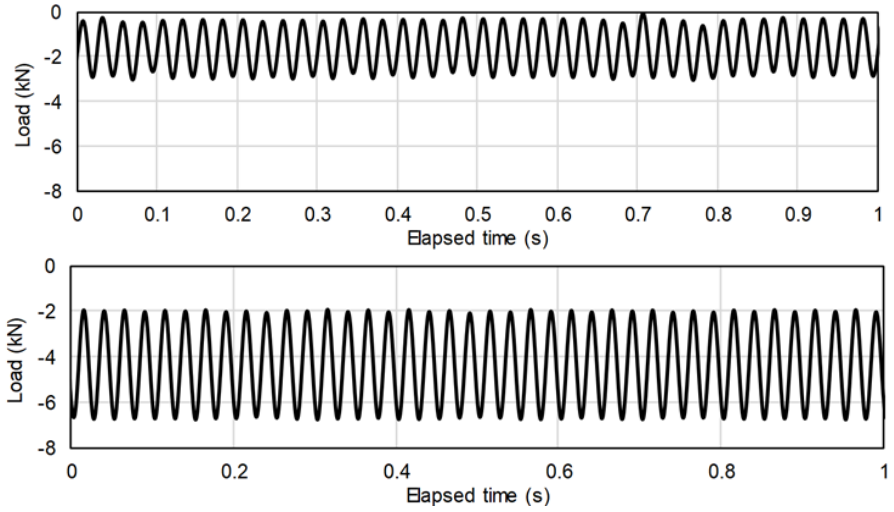

Figure 4-11 Load variation for UT2 and UT4 cyclic (40 Hz) compression at approximately 30 minutes

After cyclically loading, monotonic tensile load tests were performed.

Figure 4-12 shows the full load v displacement graph for pile UT-16 which was tested with LF cyclic loading. The aim of the figure is to highlight the change in stiffness with cyclic loading.

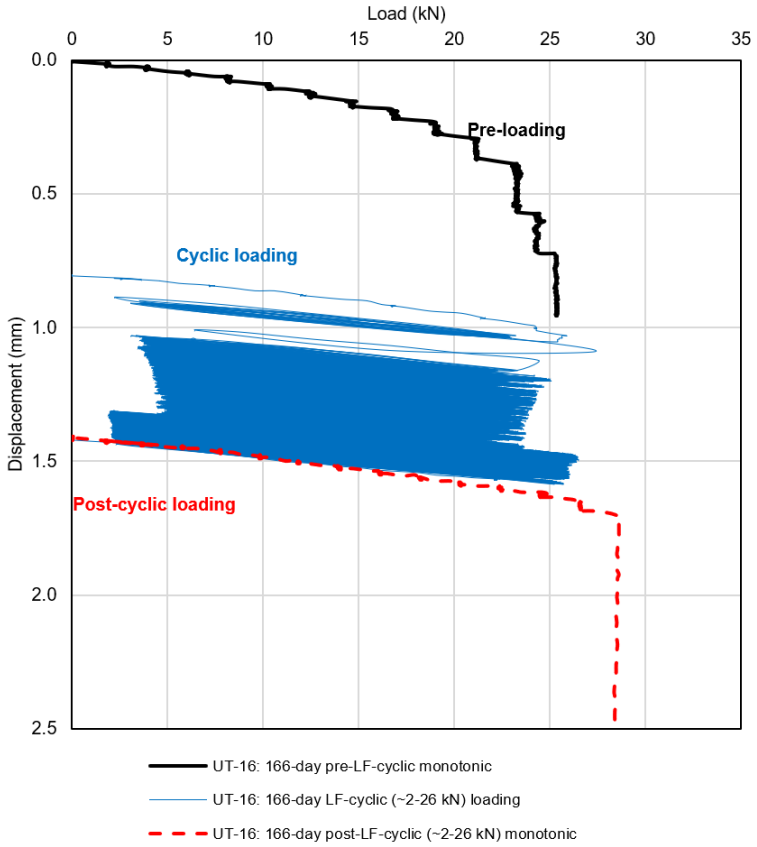

Figure 4-12 Load v displacement for pile UT-16 with LF cyclic loading

The complete monotonic, high-frequency, and low-frequency test results for the UT site are shown in given in Appendix B.

5 Discussion

5.1 Overview

The key aims of this work are to investigate the effects of time (aging) and cycles on pile capacity. Section 5.1.1 summarises the time effects data, and Section 5.1.2 the cyclic stability data. The interaction between these effects is discussed within those sections.

5.1.1 Ageing

Figure 5-1 and Figure 5-2 summarise the changes in pile capacity with time, and marks cyclic tests for URI and UT respectively. Pile capacity increased with time; and is seemingly not detrimentally affected by cycles (1-way, tension or compression) applied prior to monotonic loading.

- The gain in capacity with time at the URI site was large (about 4.0-5.0), and exceeds that typically reported in the literature (which is about 1.5 to 2.5, Gavin et al. 2015).
    - This might be because the initial capacity at the URI site was particularly low, when assessed relative to standard CPTU design methods; as illustrated on Figure 5-3.
    - Low capacity might be due to low pile roughness (unrusted), and friction fatigue during driving (See Section 5.1.3), exaggerated due to the high stiffness of the site soils combined with the small pile diameter. High soil stiffness and small pile diameter yielded a very high value of normal stiffness in this case, meaning that small shear band contractions resulted in very large reductions in the normal stress on the pile: and high friction fatigue, and due to the low roughness, low dilation on loading. In turn the low initial capacity is more likely to re-gain.
    - Additionally, low short-term capacities at the test sites may be due to higher than typical blow counts during installation (and hence more friction fatigue during installation, see also Sections 5.1.3 to 5.3.3)
- One particular test (URI-P4) showed very high tensile capacity:
    - This pile was tested monotonically 8 days after installation.
    - ~10,000 LF cycles were applied to this pile, varying in magnitude (see next section), the maximum load was about 41% of the ultimate capacity (measured in the subsequent monotonic load test).
    - The capacity increase compared to the other piles (about 3 times greater), is higher than can be related to site variability (about 1.5 times, max/ min CPTU capacity).
    - This leads to the hypothesis that cyclic loading of URI Pile 4 may have initiated an enhanced creep type ‘aging’ (Bowman & Soga, 2005, Deeks, 2008). It is noted no other piles showed this degree of accelerated aging.

    - Note the tidal range at the URI site is low (+/-0.5 m, say) hence any rusted zone (where the interface roughness can increase) is small in length, and is located near the top of the pile, which has minimal influence on overall axial capacity.
- The UT data indicated a capacity gain (about 2.0, over 100 days) in line with typical data
    - The hammer at UT provided an order of magnitude greater energy, hence blow counts were lower at this site; and this is a reason that the UT pile capacities are potentially both closer to those predicted by the UWA method (Figure 5-3), and the strength gain is lower (Figure 5-2)
    - One-way LF cycles were applied in tension (~10,000) and compression (~150,000) prior to the monotonic tension pull-outs, and no detrimental effect on aged-capacity was noted, in the context of overall site variability.
- As stated neither pile showed particular degradation due to the applied cycles.
    - URI CNS data (Figure 3-2) shows stress decrease for large and small displacement cycles (i.e. also pre-failure cycles). It could be competing CNS compaction at small cycles, with hoop stress equalisation / stiffening in background (after White & Deeks 2007).

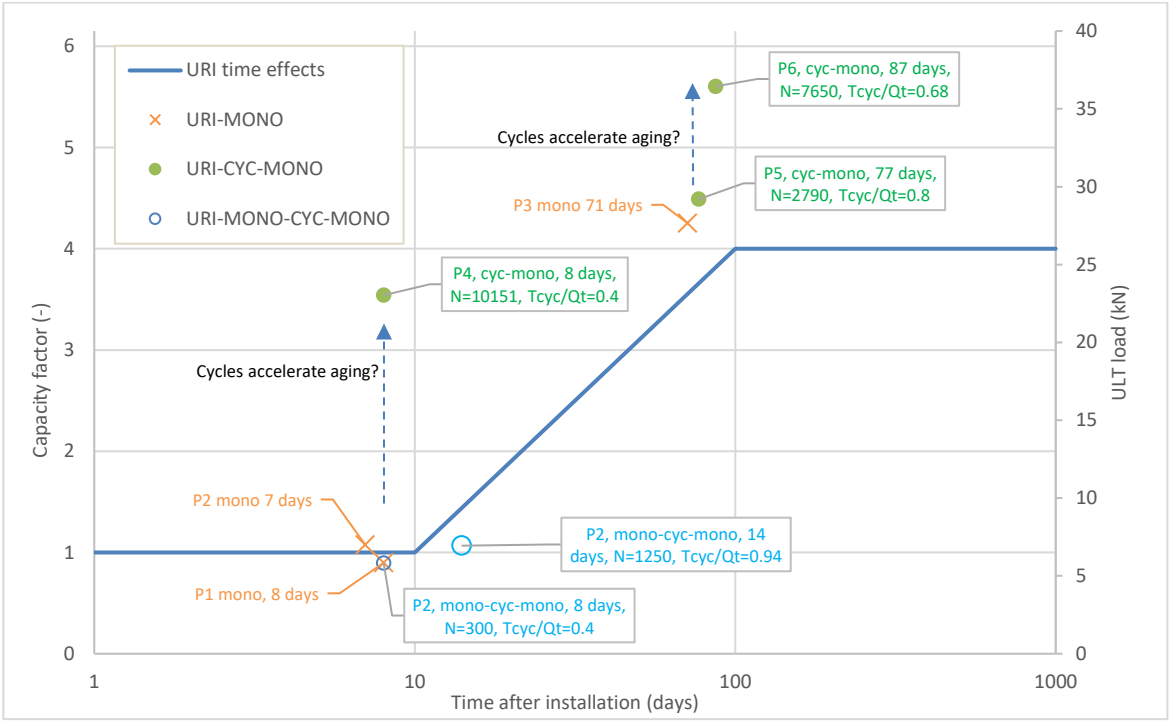

Figure 5-1 Pile capacity variation with time for URI. Ultimate tension capacity presented.

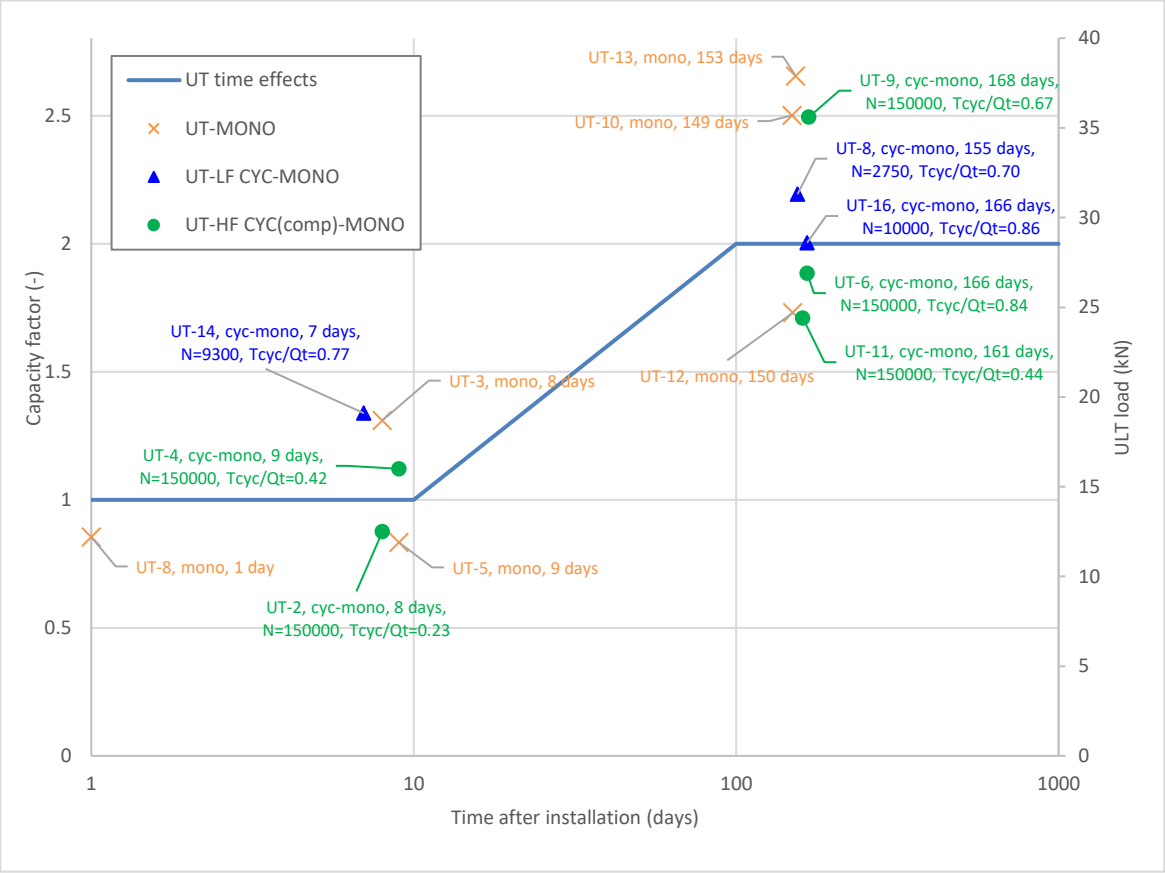

Figure 5-2 Pile capacity variation with time for UT. Ultimate tension capacity presented.

It should be noted that the UWA-05 average shaft shear strength used in Figure 5-3 is the predicted pile capacity based on CPT data divided by the pile outer wall surface area. In Figure 5-3, tests labeled "cyc" refer to low frequency cyclic test while tests labeled as "cyc HF" refer to high frequency cyclic tests.

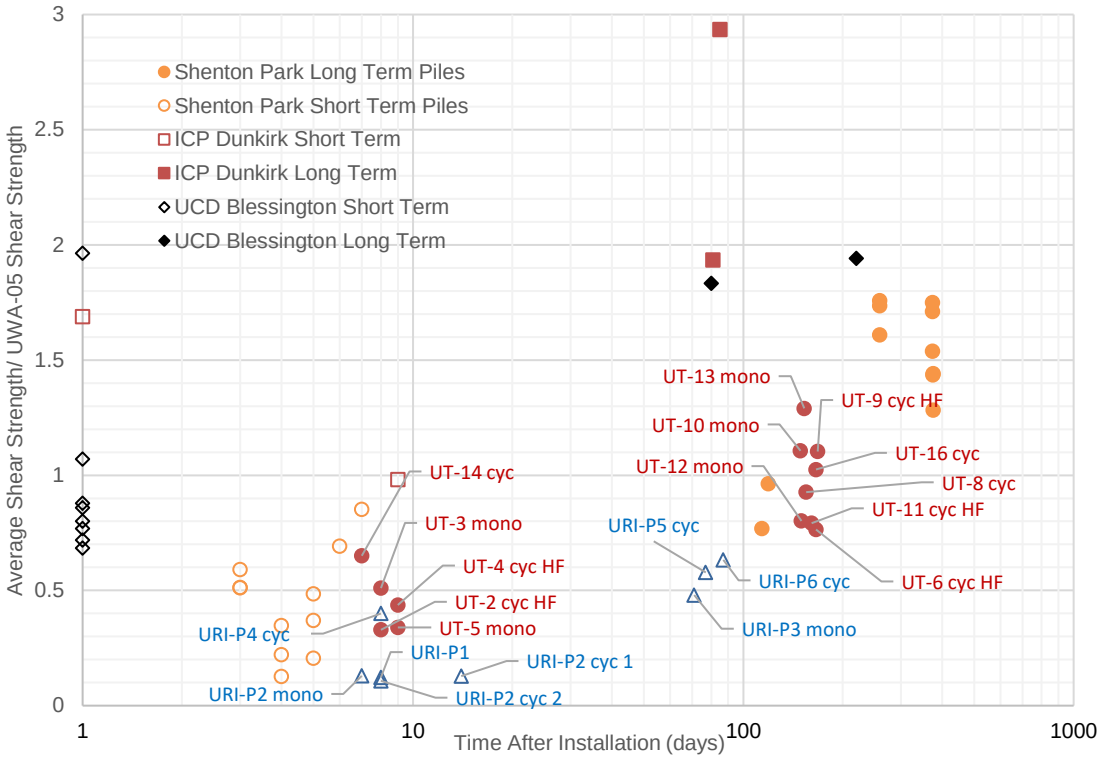

Figure 5-3 Normalized ultimate tension pile capacity variation with time. UWA-05 used as normalization.

5.1.2 Cyclic stability

Following on research into static capacity, and particularly to address concerns related to the design of offshore wind turbines, large programs related to cyclic resistance were undertaken from about 2008 to 2012. The main program was the SOLCYP program centered in France (e.g., Peuch 2012, Andersen et al. 2012, Peuch & Garnier 2017). Experiments related to cyclic loading of piles driven in sands confirmed the concepts of previously proposed cyclic stability diagrams (e.g., Poulos 1988b) that include the following conditions:

(i) Unstable: A point during cyclic loading is reached where continued plastic deformation occurs at or below the applied loading condition.

(ii) Metastable: A state where plastic displacements continue to accumulate during each cycle. Failure is often defined during a metastable condition based on a serviceability requirement.

(iii) Stable: Deformations may initially accumulate during cycling, however, a point is reached after a certain number of cycles where displacements become stable. 'Stable' can be a somewhat arbitrary definition of cyclic stability based on a maximum number of expected cycles. The maximum number of expected cycles is estimated to be much higher for offshore wind turbines as compared to offshore oil and gas structures, which would lead to lower apparent stable positions within the cyclic stability diagram.

a. In practice a threshold for accumulated displacement rate (e.g. 0.00003 mm/s, Jardine et al. 2012) is often defined (c.f. a value of zero).

Figure 5-4 presents all the data in a cyclic stability framework. Only a single load package failed during cycling (illustrated on figure). All other tests the displacement rates (of accumulated cyclic displacement) were low, typically < 0.00003 mm/s which is similar to the Jardine et al. 2012 definition of stability (stable/metastable boundary).

Site specific stability lines are proposed. These indicate significantly greater stability and meta-stability than proposed by others. The stability lines are likely valid for one to two orders of magnitude greater load cycles (10,000 to 100,000 cycles), for the particular site-pile combination tested.

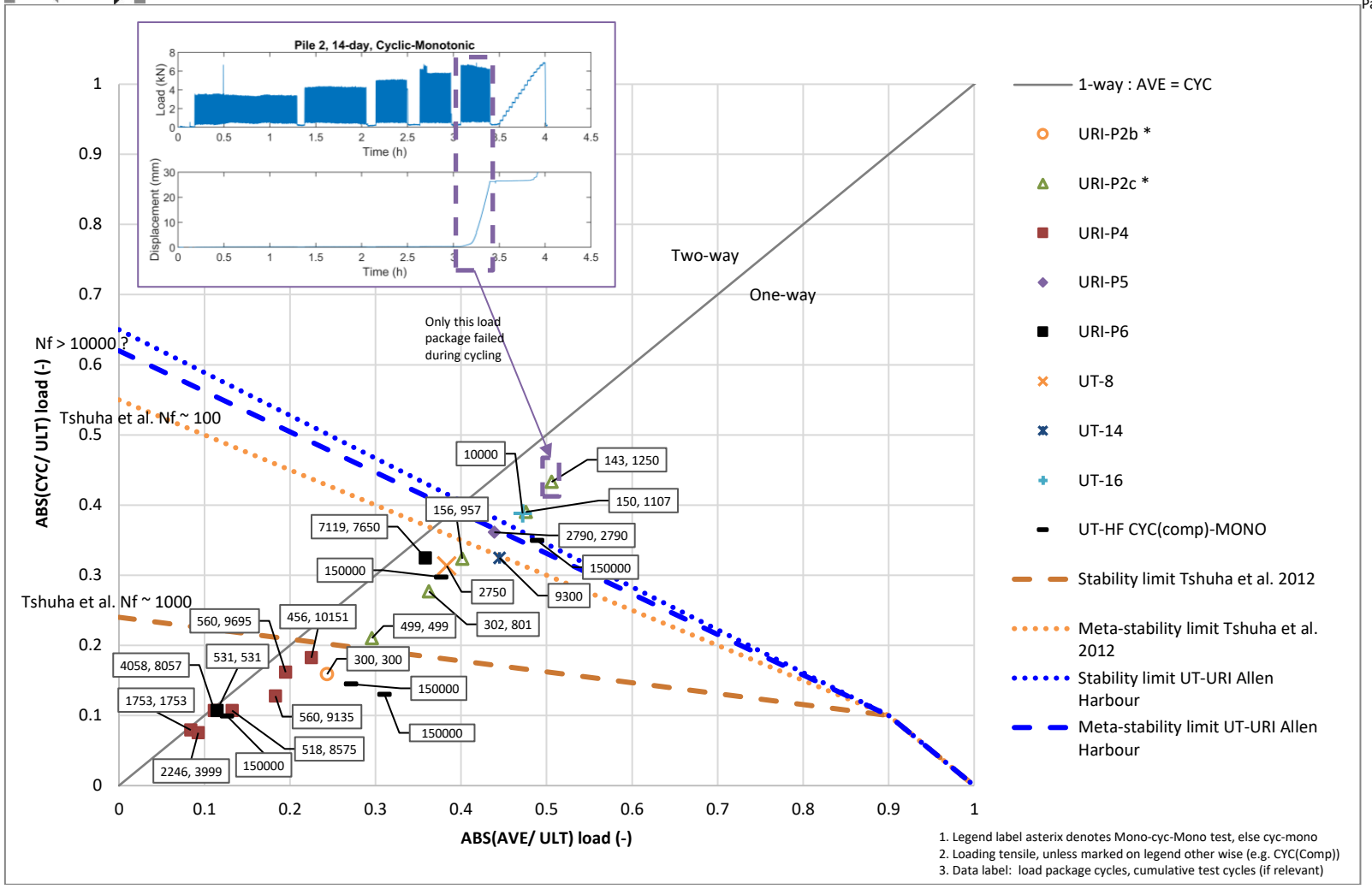

Figure 5-4 Cyclic stability diagram URI (tensile) and UT (tensile and compressive) data.

5.1.3 Cyclic stiffness

Figure 5-5 to Figure 5-7 present the load displacement responses during initial static loading, the cyclic load packages, and subsequent maintained load tests. The secant pile head stiffness is indicated on these figures. The stiffness during low frequency cyclic loading wass about 2 to 4 times greater than that under static maintained load. This is hypothesized to be a soil rate of loading (viscosity) effect.

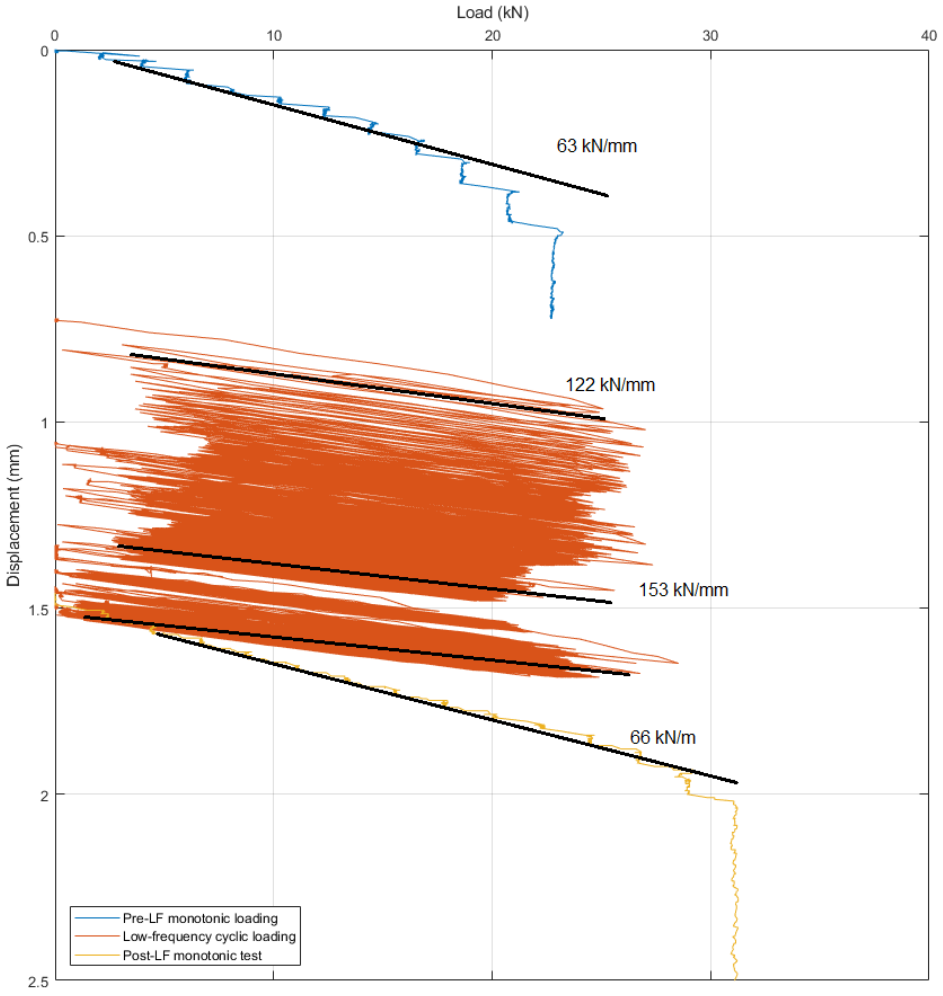

Figure 5-5 UT Pile 8: Load displacement response and selected pile head stiffness values.

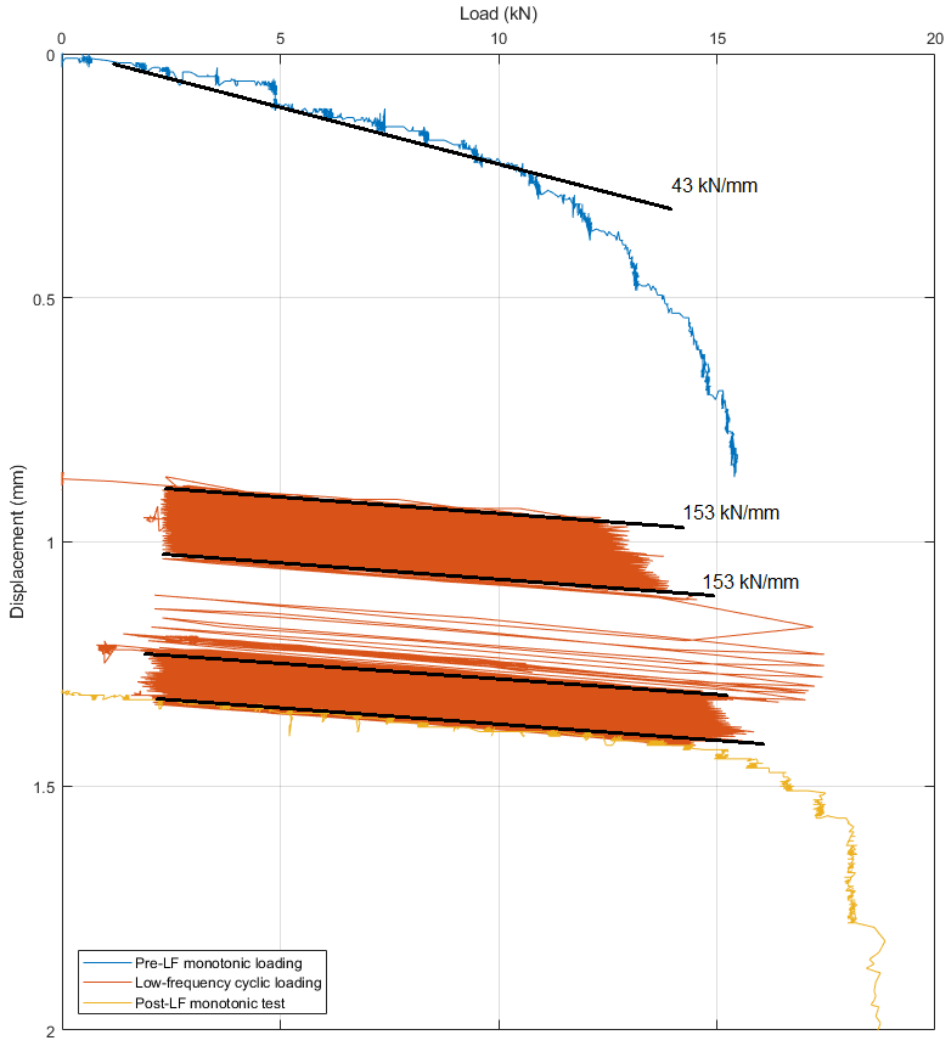

Figure 5-6 UT Pile 14: Load displacement response and selected pile head stiffness values.

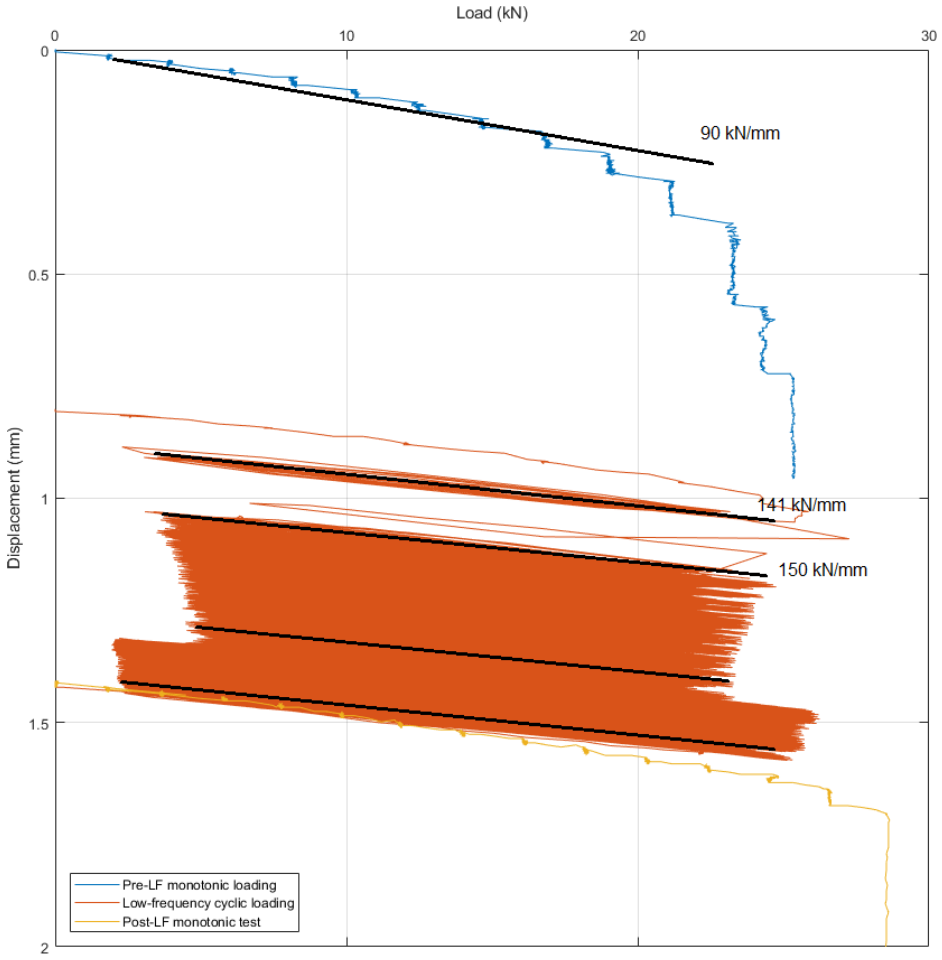

Figure 5-7 UT pile 16: Load displacement response and selected pile head stiffness values.

5.2 Design observations

The stability data collected indicates significant safety for driven piles subsequently subjected to high amplitude cyclic loads, either early (1-10 days) or later (~100 days) in life, for the site, pile and load frequency combinations tested.

As design methods in sand are typically calibrated for 7 to 10 day capacity, this indicates there is significant safety margin for driven piles to cyclic loads. This might differ for other installation types, e.g. jacked piles.

If the structure needs to be designed for hurricane or storm loads that may occur in the first 1 to 10 days after foundation installation, this needs to be considered very carefully. There is greater robustness if turbines are to be loaded several weeks or months after pile installation (which is more typical): the aging effect could double pile capacity, if it can be relied upon (it is typically not relied upon).

The safety to cyclic loads is contingent on (i) reliable design (7 to 10 day) capacity assessment, and (ii) the cyclic load characterization.

Regarding reliable (7 to 10 day capacity):

- URI and UT piles showed low capacity relative to a selected design method that includes friction fatigue (UWA-05), as indicated in Figure 5-3 , i.e. the short and long term test results have capacities relative to the UWA-05 method below unity.
    - This is surprising as the base UWA-05 method is for large diameter piles, and smaller diameter piles would be expected to have higher capacity due to confined dilation effects related to their smaller diameter.
    - Figure 5-3 also shows data from other test sites collated by Anusic et al. 2018, typically this other data is also from small diameter piles; and so in that regard it is noted many of those data points are also below unity, however our site (UT and URI) capacities are still low as compared to those. We reviewed the UT and URI sites as compared to the other test sites and they are broadly similar.
- It may be that the pile interface has affected these results.
    - On the one hand, these piles reflect typical design materials (steel), but due to pipe sizes the provided finish was relatively smooth and un-rusted. Hence the interface friction angle and dilation induced at the interface on loading is low (Mortara et al. 2007).
    - In contrast, field scale piles typically have a rough finish (and hence dilate on loading, after cyclic compaction).

Regarding cyclic load characterization, modern control systems for wind turbines (e.g. for pitch and yaw) have developed extensively over the last decade, and in NGI's experience typically the operational window for a jacket turbine is approximately (though noting project specific analysis is required):

- Operation (power production):
  - around 1-way loading, at say 0.1 to 0.3 Hz (structure-wind-geotechnical dominated)
- Storm (idling):
  - say 1-way loading on compression pile, 1- to 2-way loading on tension pile, at around 0.1 Hz (wave dominated)
- Seismic (potentially operating):
  - say 0.1 to 1 Hz (or greater) depending on the soil column-structure natural frequency (1 and 2 way)

Project constraints dictated this work focused around 1-way loading; inherently there is greater uncertainty for 2-way loading (as it was not tested), and the influence of soil rate effects should be considered further.

The data collected in this study is not sufficient to develop a holistic design approach, rather indicates further work is required (Section 5.4).

5.3 Discussion of pile capacity degradation as compared to previous BOEM study

The results of the present study did not show clear cyclic degradation of capacity under axial loading for cycles applied after pile installation, which is counter to the findings of an earlier centrifuge study presented in MMI (2016).

5.3.1 Background

The differences can be explained by considering the mechanics of the soil shear band that forms immediately adjacent to the pile when it is subjected to axial loading. The shear band generally has a thickness between 2 to 10 times the median grain diameter depending on interface roughness (DeJong and Westgate 2009) and is constrained by the soil outside the shear band under Constant Normal Stiffness Conditions (CNS). Changes in the normal stress on the pile can be represented by the following simple mechanical spring model (Boulon and Foray 1986):

$$\Delta\sigma = -k * y \qquad \text{Equation (5.1)}$$

$$k = \frac{4*G}{B} \qquad \text{Equation (5.2)}$$

where
k=normal stiffness in units of kPa/mm,
y=shear band normal displacement in mm (positive sign for contraction),
G = shear modulus of the soil constraining dilation,
and B=pile diameter.

As shown by Equation 5.1, contraction of the shear band leads to a reduction in normal (radial) stress on the pile and dilation leads to an increase in normal stress. The shear stress on the pile is simply the normal stress times the tangent of the interface friction angle.

This simple model in combination with the critical state framework proposed by DeJong et al. (2006) is used to explain the observations in both the MMI (2016) study as well as the current study. The framework is shown conceptually in Figure 5-8, which shows the critical state space for the interface shear band. The upper range of void ratio is bounded by the maximum void ratio (e_{max}) and the lower range is bounded by the minimum void ratio (e_{min}), whose values are normal stress dependent. The soil in the shear band starts at some initial void ratio and moves up and down a stress path line having a slope of one over the shear band thickness (h_t) times the normal stiffness. Cyclic loading tends to incrementally move the soil toward e_{min} and monotonic loading (with dilation) tends to move the soil toward e_{max}.

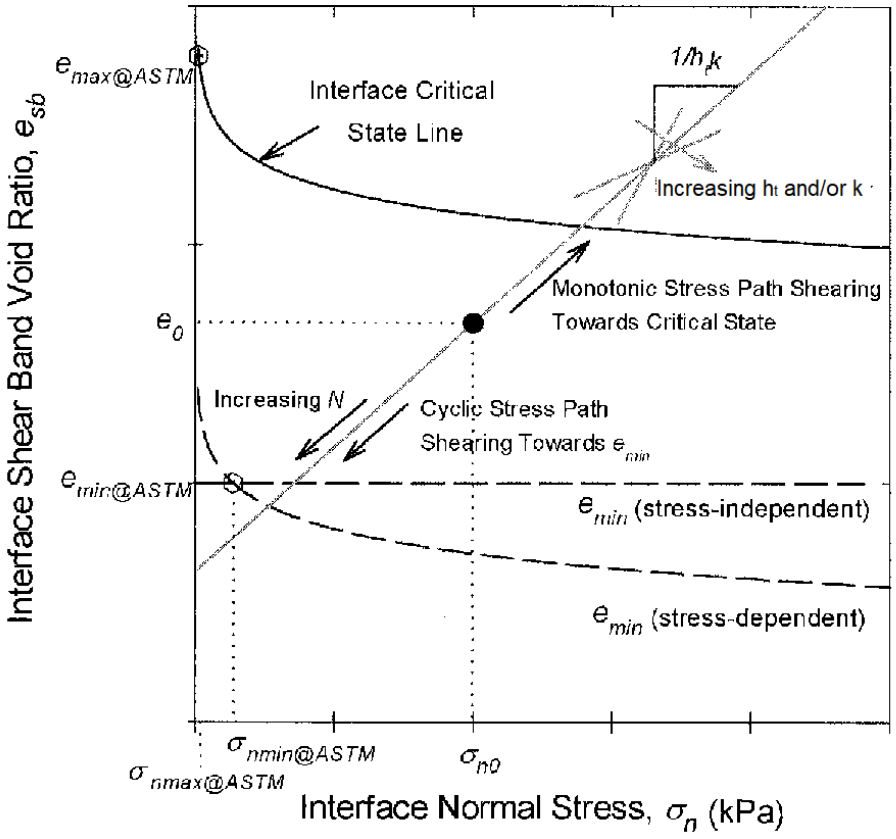

Figure 5-8 Critical state framework used to describe changes to the void ratio within the shear band constrained under constant normal stiffness conditions (DeJong et al. 2006).

5.3.2 Centrifuge Study by MMI (2016)

The centrifuge tests were performed on very small diameter (~8 mm), closed-ended, fully rough piles (i.e. sand glued to pile), installed by in-flight jacking, and tested by alternating monotonic tensile tests with cyclic load packets. The soils were prepared to an initial relative density of between 65% and 70%. After installation, the piles were tested by first performing a tensile load test to a displacement of 2 mm which formed the baseline capacity. Then cyclic load packets were applied alternating with additional monotonic tensile tests. The study compared the tensile test results to assess the degradation in capacity over the duration of loading sequence.

Installation of any pile forces the lateral expansion of a soil cavity just below the toe of the pile. The expanding cavity results in very high normal (radial) stresses that are higher in high displacement piles (i.e. closed-ended or solid piles) as compared to low-displacement

piles. Since the centrifuge piles were installed by jacking and the pile was rough, the good interface coupling induced large shear strains within the band during installation, which likely brought the soil to the critical state void ratio (Figure 5-8). It is likely that this caused some increase in the shear band void ratio relative to the pre-installation void ratio since the soil was initially dense (reported relative densities between 65% and 70%).

At installation the pile was jacked/monotonically installed, so very little compaction of the interface would have occurred during pile installation, hence the interface is susceptible to compaction with any subsequent load cycles.

This effect of this is exaggerated since the model pile had a very small diameter, the normal stiffness was high (Equation 1) and thus even small changes in void ratio resulted in large increases in the normal stress relative to the initial cavity expansion stress.

In detail, since the shear band was likely at critical state at the end of installation, the first tensile test likely did not induce any additional shear band dilation or normal stress changes, and used as the baseline capacity for the subsequent tensile tests within the sequence. The second step, which consisted of a packet of cyclic loading, would have reduced the shear band void ratio depending on the amplitude of cyclic loading and number of cycles. This in turn would have reduced the normal stress on the pile. The second tensile test would have caused some dilation of the shear band again toward the critical state void ratio and increased the normal stress. However, the dilation from monotonic loading was not enough to restore the normal stress to the pre-cyclic condition. As a result, the monotonic capacity was lower in the second tensile test. This process was just repeated over the load sequence, which explains the observed reduction or degradation in tensile capacity after each packet of cyclic loading.

5.3.3 Current Study

As compared to the centrifuge tests, the load testing in the current study were done on larger piles having a smooth (non-rusted) steel surface, that were driven open-ended with an impact hammer, and were not subjected to any prior tensile testing before cyclic loading. As such, the installation regime of the test piles are more representative of full-scale jacket piles that are installed by driving and then put into service (albeit these are likely already rusted). However, relative densities in the current study were more varied than in the centrifuge tests and estimated to be between 50% to 100% over the pile embedment depth (Keefe et al. 2020).

Driving of the open-ended pipe piles still requires initial cavity expansion at the pile toe but less than for a closed-ended pile because of the lower soil displacement (White, 2005). In this case the impact driving caused cyclic loading of the shear band, which incrementally reduced the shear band void ratio toward e_{min} along with the normal stress. After driving,

when the pile is monotonically load tested, there would be very little shear band dilation that would occur because the pile is smoother and particle slippage suppresses dilation (Mortara et al. 2007). As a result, the low normal stresses would result in a relatively low initial tensile capacity. The loss in capacity associated with pile driving is commonly referred to as friction fatigue. Previous work indicates that the strength loss is highest toward the ground surface where the soil experiences the highest numbers of cycles and lowest at the pile toe (White and Lehane 2004; Gavin and O'Kelly 2007). Also, friction fatigue generally increases with an increase in the number of driving blows as shown in Figure 5-9 (White 2005). In the current study, since the diameter of the test piles was still relatively small, the high normal stiffness exacerbated the friction fatigue process.

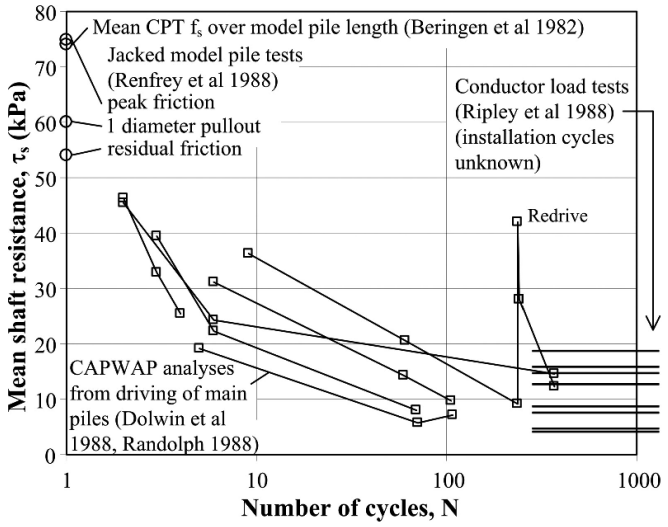

Figure 5-9 Data showing the reduction of shaft resistance with an increase in blow count (White 2005).

Although the driving process reduced the shear capacity of the test piles through friction fatigue, the net result is that the shear band becomes denser and more resistant to further densification from subsequent "service" cyclic loading. This is because the pile driving process likely brought the shear band to e_{min} (Figure 5-8) or even lower where the potential for additional volume change from cyclic loading is very low. Therefore, there was no further shear band contraction and losses in normal stress by the end of cyclic loading. This explains why there was no observed degradation in capacity in the test piles, despite that fact that the applied cyclic load levels were as high as ~90% of the tensile capacity.

5.4 Recommendations

This work has demonstrated the necessity of replicating field scale installation techniques and the viability of model scale piles to develop meaningful design insights.

Further field scale testing, accompanied with detailed soil element testing, is recommended to investigate, and clarify for design if the findings of resilience to post-installation cyclic loads can be relied upon to investigate:

- Pipe roughness
  - Do rougher piles activate cyclic degradation proactively?
- End condition
  - Does the stress regime induced by installation of piles with a different area ratio (e.g., thinner wall, closed ended) change the aging and cyclic response?
- Diameter
  - Are large diameter piles less susceptible due to lower confining stiffness?
- Cycles for installation (e.g. jacked c.f. driven)
  - Are piles installed with low cycles more susceptible to future degradation?
- Maintained load over time
  - Can strength gains with time be relied upon if a pile had been subject to maintained working load throughout its life?
- Cyclic load characterisation
  - Extending the existing work to probe further load combinations (e.g. 2-way), and different loading frequencies (e.g. additionally around 1 Hz).

6 Acknowledgements

In addition to the BOEM & NSF funding (Section 1.1), the Authors extend thanks to Fred Pease and Paul Sauco of URI, Justin Caccamise of Northeast Engineering, the employees of The Hose Connection, Inc; Benchen Zhang, Chihun Sung, and Jiali Han of UT, Robert Kent and Andrew Valentine of NHERI@UTexas, and Ensoft, Inc. Thanks are also extended to Kai Feng from UT for his help some of the field work. Finally, thanks to Marcus Rasulo, currently with DNV, for his earlier management of this project for NGI.

7 References

Andersen, K.H., Puech, A., and Jardine, R.J. (2012).
Cyclic resistant geotechnical design and parameter selection for offshore engineering and other applications. Proceedings of TC209 Workshop – Design for cyclic loading: Piles and other foundations, 18th ICSMGE, Paris: 9-44.

Anusic, I., Lehane, B.M., Eiksund, G.R., and Liingaard, M.A. 2018.
Evaluation of installation effects on set-up of field displacement piles in sand. Canadian Geotechnical Journal, 56(4). 461-472.

Boulon, M. & Foray, P. 1986.
Physical and numerical simulation of lateral shaft friction along offshore piles in sand. Proceedings, 3rd International Conference on Numerical Methods in Offshore Piling. Nantes, France. 1:127-147.

Bowman, E.T., and Soga, K. 2005.
Mechanisms of setup of displacement piles in sand: laboratory creep tests. Canadian Geotechnical Journal, 42(5). 1391-1407.

Deeks. A.D. 2008.
An investigation into the strength and stiffness of jacked piles in sand. PhD dissertation. Engineering Department, Cambridge University, Cambridge, United Kingdom.

DeJong, J.T., White, D.J., and Randolph, M.F. (2006).
Microscale Observation and Modeling of Soil-Structure Interaction Behavior Using Particle Image Velocimetry. *Soils and Foundations*, 46(1), 15-28.

DeJong, J.T. and Westgate, Z.J. (2009).
Role of Initial State, Material Properties, and Confinement Condition on Local and Global Soil-Structure Interface Behavior. *Journal of Geotechnical and Geoenvironmental Engineering*, 135(11), 1646-1660.

Gavin, K.G. and O'Kelly, B.C. (2007).
Effect of Friction Fatigue on Pile Capacity in Dense Sand. *Journal of Geotechnical and Geoenvironmental Engineering*, 133(1), 63-71.

Gavin, K.; Jardine, R., Karlsrud, K. And Lehane, B. (2015). *"The effects of pile ageing on the shaft capacity of offshore piles in sand". ISFOG: International Symposium Frontiers in Offshore Geotechnics. Oslo, Norway, 2015.*

Jamiolkowski, M., Diego, L. P., Manassero, M (2003)
Evaluation of Relative Density and Shear Strength of Sands from CPT and DMT
Geotechnical Special Publication, SN - 978-0-7844-0659-5, DO - 10.1061/40659(2003)7
January, 2003

Jardine, R.J. Puech, A.E., and Andersen, K.H. 2012.
Cyclic Loading of Offshore Piles: Potential Effects and Practical Design. Offshore Site Investigation and Geotechnics: Integrated Technologies - Present and Future, 12-14 September, London, UK. 1-39.

Jardine, R.J., Thomsen, N.V., Mygind, M., Lingaard, M.A., and Thilsted, C.L. 2015.
Axial Capacity Design Practice for North European Wind-turbine Projects. ISFOG 2015. 581.

Lehane, B.M., Schneider, J.A., and Xu, X. 2007.
Development of the UWA-05 Design Method for Open and Closed Ended Driven Piles in Siliceous Sand. Geo-Denver 2007. 1-10.

MMI (2016).
Final Report- Model Testing to Evaluate Degradation of Axial Capacity from Cyclic Loading. BSEE Contract No. E14PC00007. March 22, 2016.

Mortara, G., Mangiola, A., and Ghionna, V. N. (2007).
Cyclic Shear Stress Degradation and Post-Cyclic Behaviour from Sand-Steel Interface Direct Shear Tests. Can. Geotech. J., 44(7), 739–752.

NGI (2018)
Model testing of cycle axial loading on piles for jacket foundations
BSEE Technological Assessment Program Project Execution and Management Plan (PEP & PMP), NGI Doc. No. 17-1082-01-R, Rev 0, 2018-10-31

NGI (2019a)
Field Work Plan -Additional Model Testing of Cyclic Axial Loading on Piles for Jacket Foundations
NGI Technical Note 18-1076-02, Rev 0, 2019-03-20

NGI (2019b)
In-situ characterization -Additional Model Testing of Cyclic Axial Loading on Piles for Jacket Foundations
NGI Technical Note 18-1076-03, Rev 0, 2019-06-24

N&N Drilling. 2019.
Steel Casing. N&N Drilling Supply Manufacturer. Jessup, PA, USA.

Puech, A. (2012).
Advances in axial cyclic pile design: Contributions of the SOLCYP project. Proceedings of TC209 Workshop – Design for cyclic loading: Piles and other foundations, 18th ICSMGE, Paris: 9-44.

Puech, A., and Garnier, J. ed. (2017)
Design of piles under cyclic loading: SOLCYP Recommendations, John Wiley & Sons.

Poulos, H.G. (1988a).
The mechanics of calcareous sediments. Australian Geomechanics, ANZ Geomechanics Conference, 8-41.

Poulos, H.G. (1988b)
Cyclic stability diagram for axially loaded piles, Journal of Geotechnical Engineering, 114(8): 877-895.

Stokoe, K., Cox, B., Clayton, P., and Menq, F. 2017.
NHERI@UTexas Experimental Facility: Large-scale mobile shakers for natural-hazards field studies. Proceedings, 16th World Conference on Earthquake, Santiago, Chile, January 9-13.

White, D.J. and Lehane, B.M. (2004).
Friction Fatigue on Displacement Piles in Sand. *Geotechnique*, 54(10).

White, D.J. 2005.
A general framework for shaft resistance on displacement piles in sand, Proceedings, International Symposium on Frontiers in Offshore Geotechnics, ISFOG, Perth: 697-703.

White, D.J. & Deeks A.D. 2007.
Recent research into the behaviour of jacked foundation piles. Proceedings, International Workshop on Recent Advances of Deep Foundations (IWDPF07), Yokosuka, Japan. 1-23.

8 Appendix A: URI pile test results

Detailed graphs of monotonic and cyclic tests on piles carried out at URI

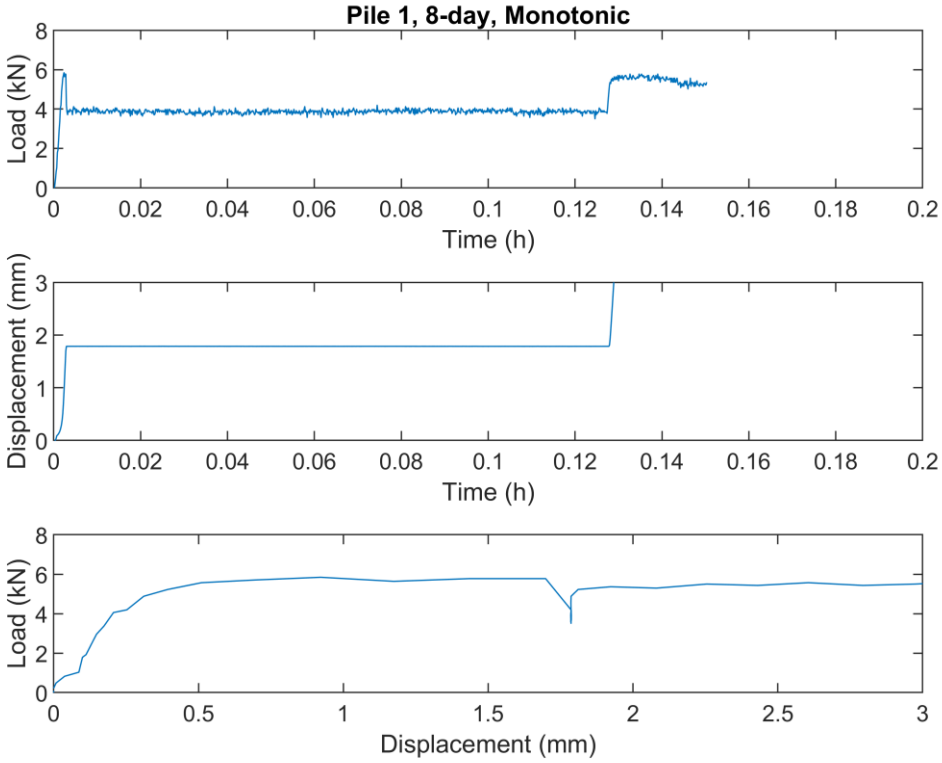

Figure 8-1 Pile 1. Eight day monotonic load test

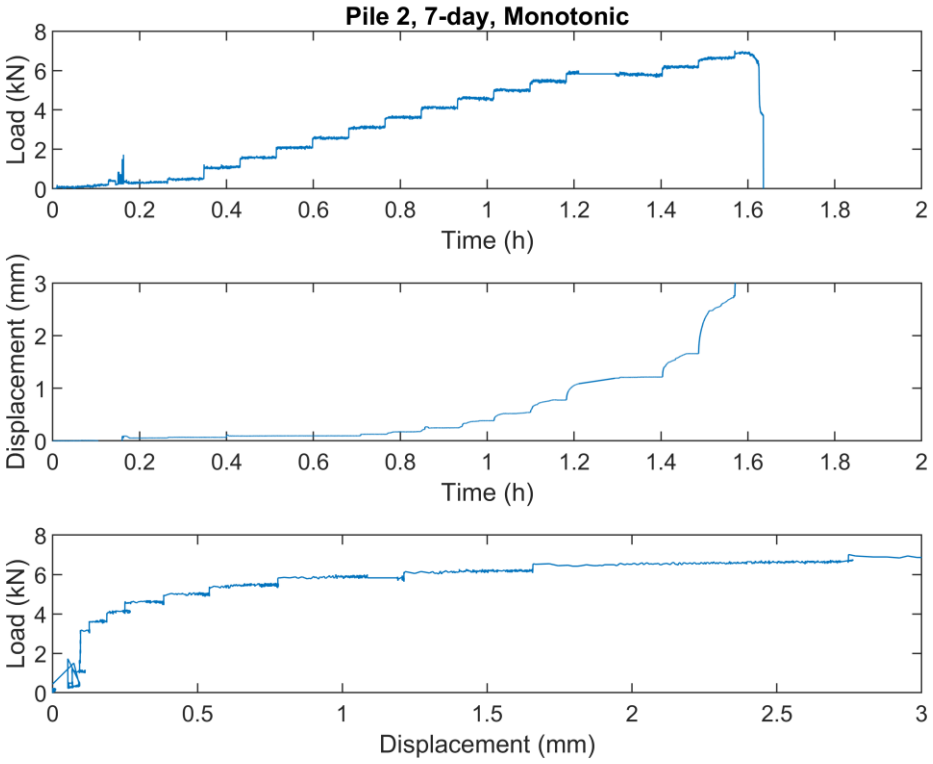

Figure 8-2 Pile 2 Seven day monotonic load test

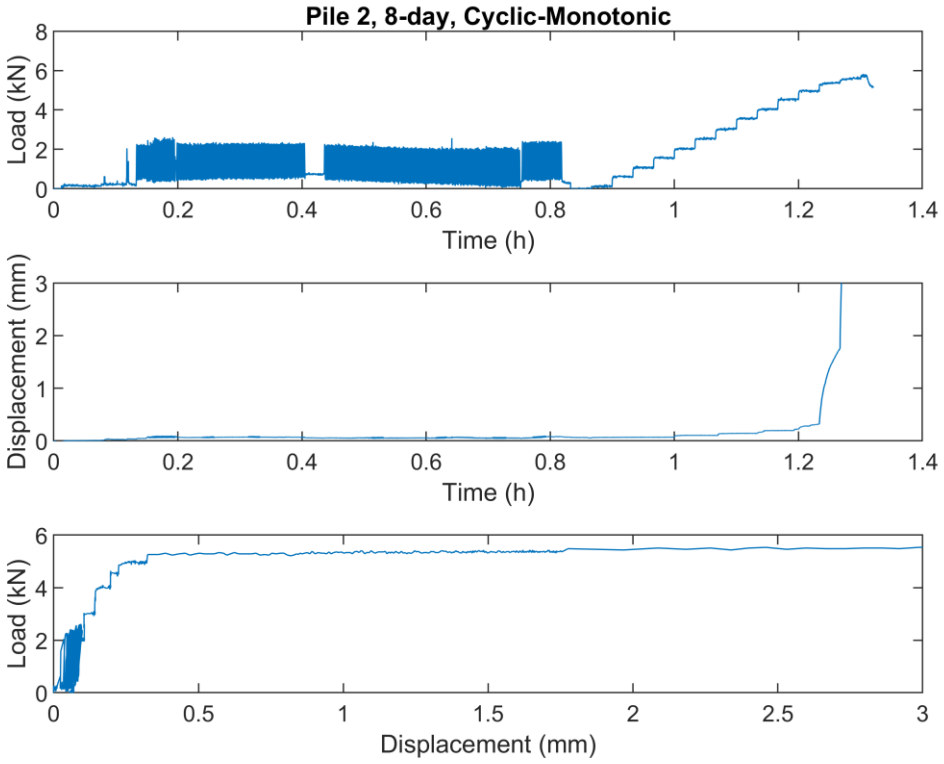

Figure 8-3 Pile 2 Eight day cyclic test, followed by monotonic test

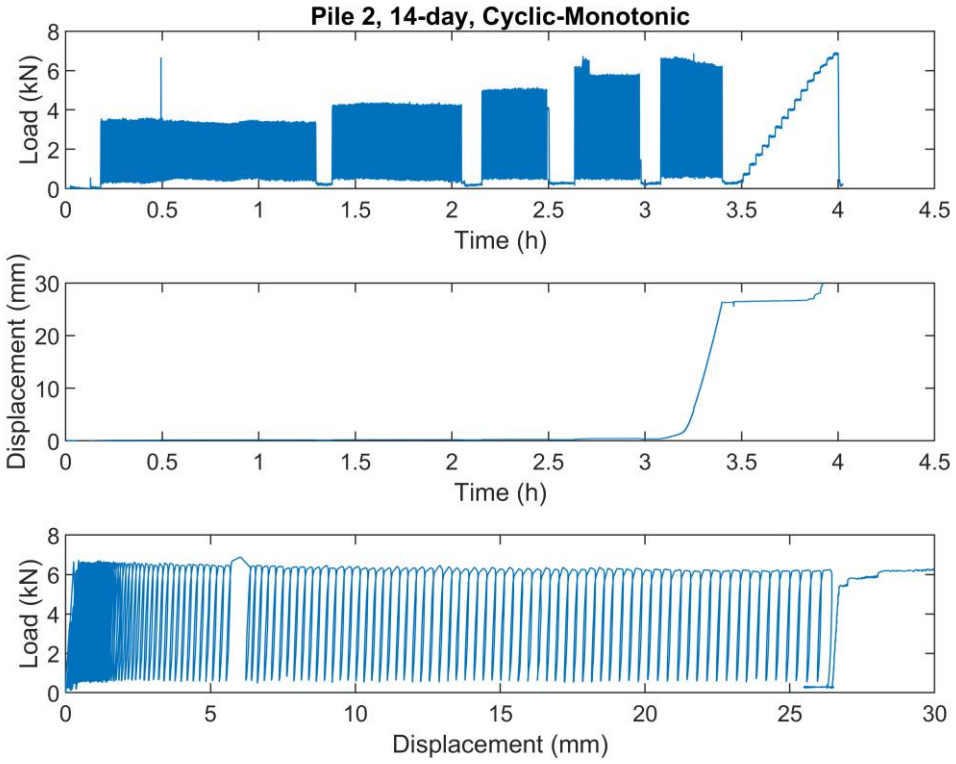

Figure 8-4 Pile 2 14-day cyclic test, followed by monotonic test

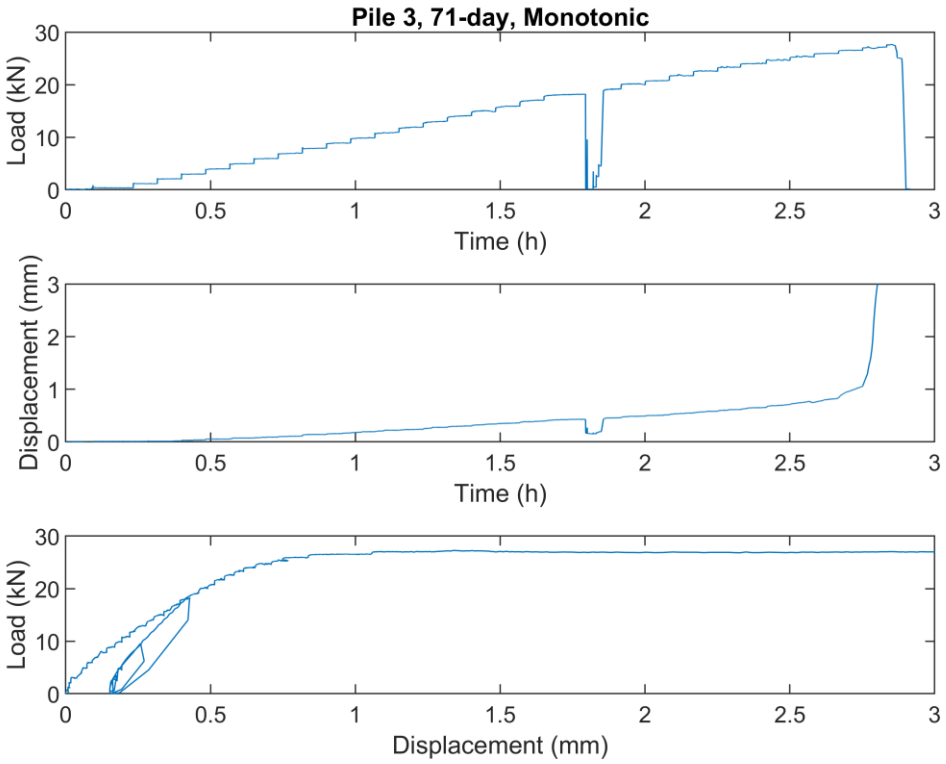

Figure 8-5 Pile 3. Seventy one day monotonic load test

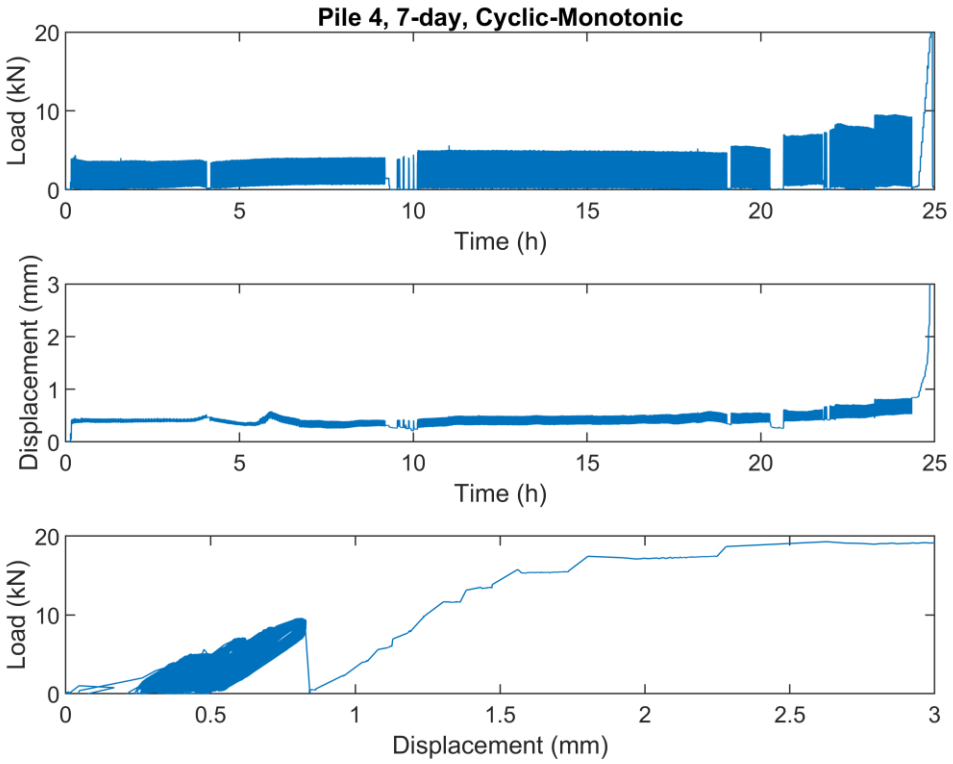

Figure 8-6 Pile 4 . Seven day cyclic test, then followed by a monotonic load test

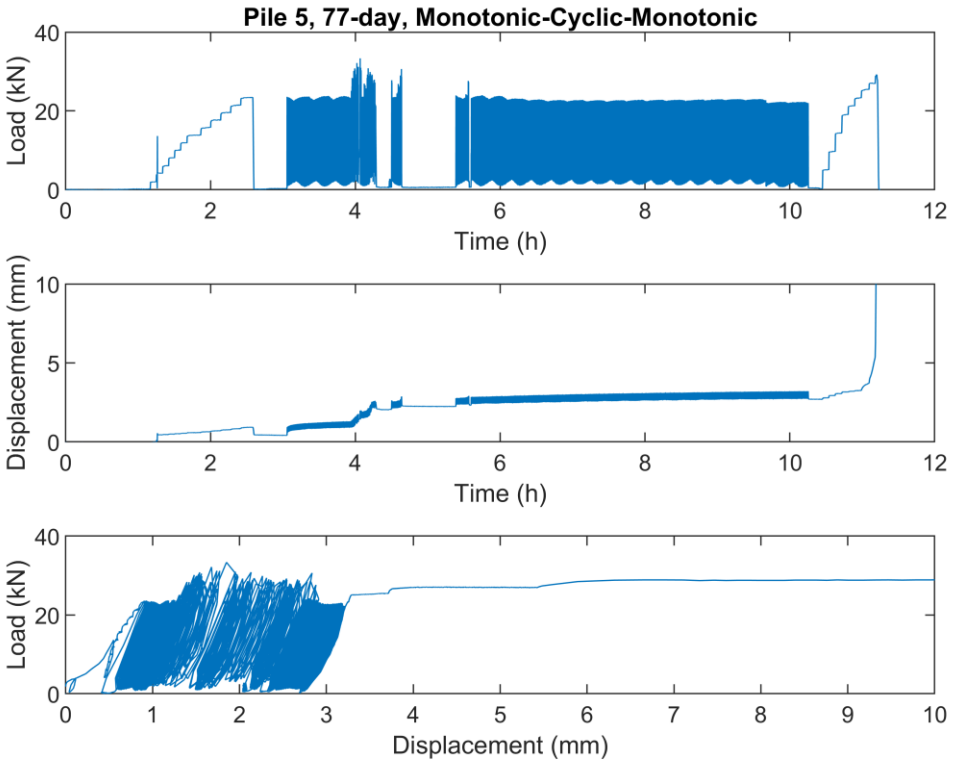

Figure 8-7 Pile 5. 77-day cyclic , preceded by monotonic for cyclic load level determination and followed by monotonic capacity testing

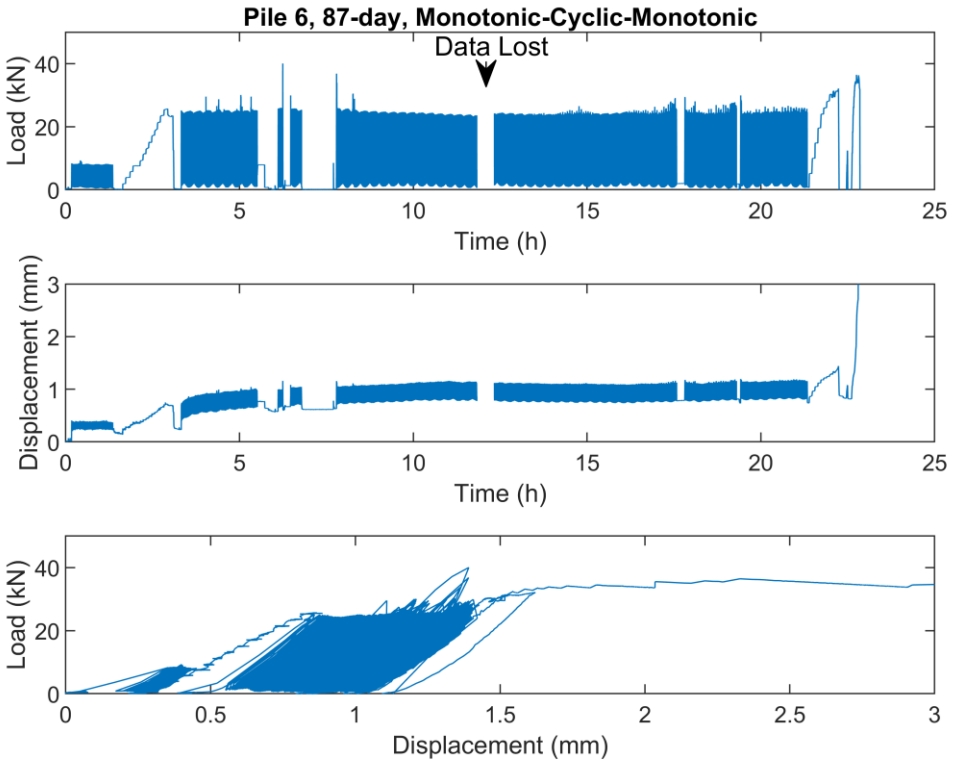

Figure 8-8 Pile 6. 87-day cyclic , preceded by monotonic for cyclic load level determination and followed by monotonic capacity testing

9 Appendix B: UT pile test results

9.1 Monotonic tests:

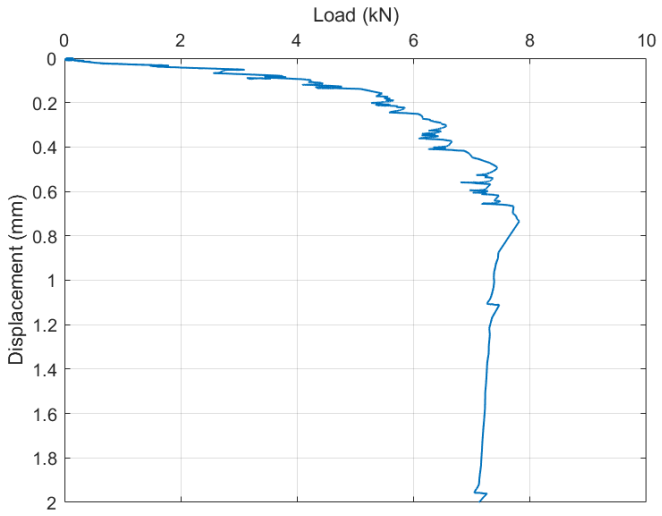

Figure 9-1 Pile 1. 0.1-day monotonic test (shorter practice pile)

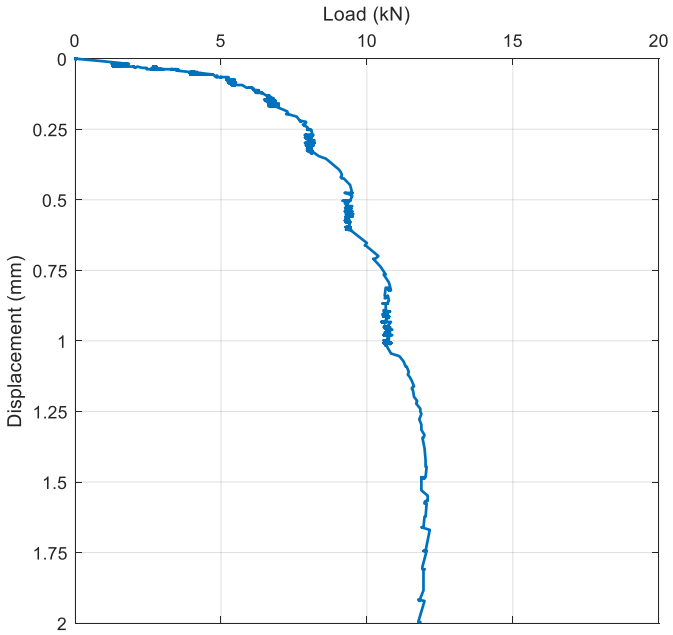

Figure 9-2 Pile 8. 0.1-day monotonic test

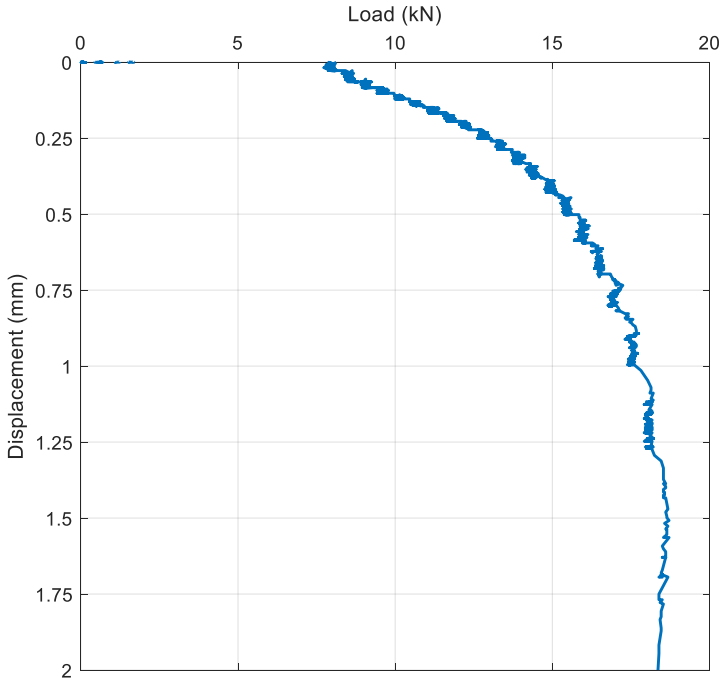

Figure 9-3 Pile 3. 8-day monotonic test

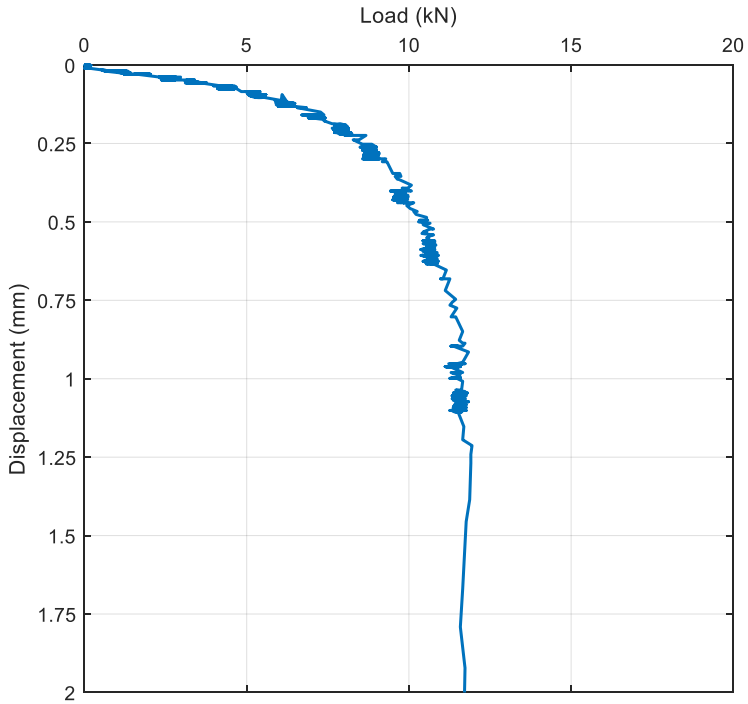

Figure 9-4 Pile 5. 9-day monotonic test

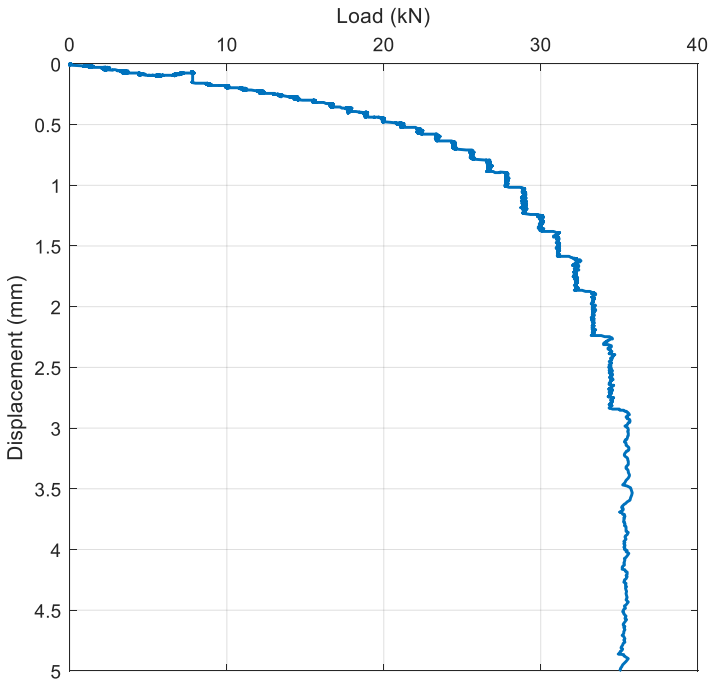

Figure 9-5 Pile 10. 149-day monotonic test

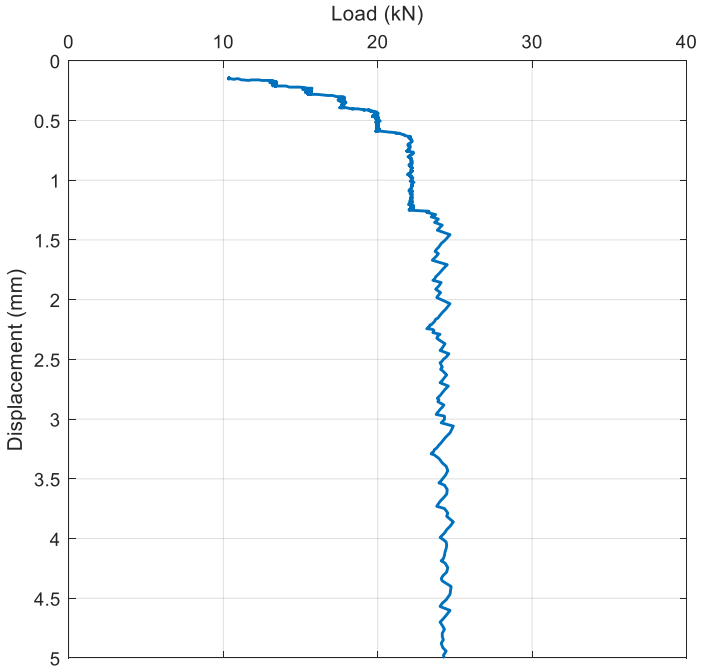

Figure 9-6 Pile 12. 150-day monotonic test (LVDT record is erroneous during early load steps)

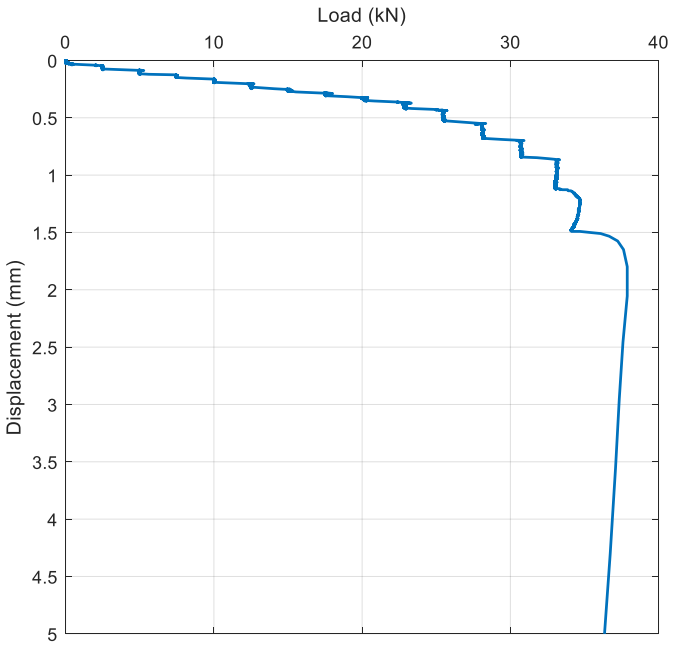

Figure 9-7 Pile 13. 153-day monotonic test

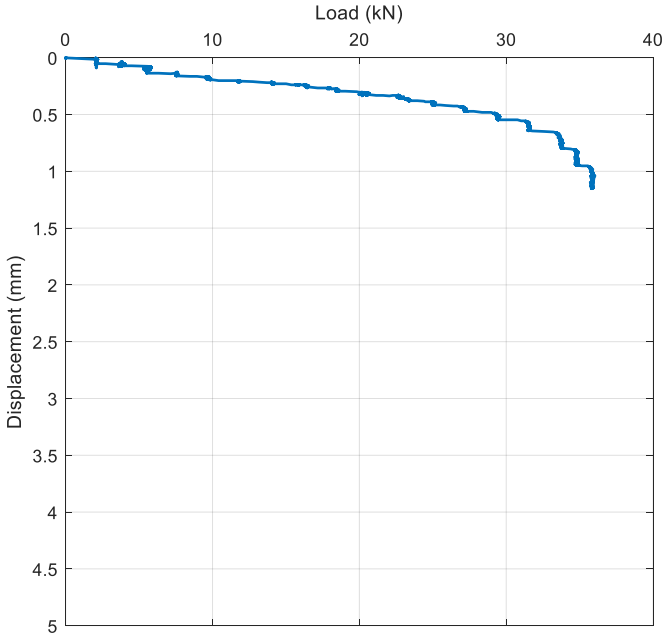

Figure 9-8 Pile 7. 163-day monotonic. Pile intended for a LF cyclic, but failed during first cycle due to equipment malfunction.

9.2 Low-frequency cyclic loading and pre/post-cyclic monotonic

9.2.1 Pile 14 - 7-days after installation

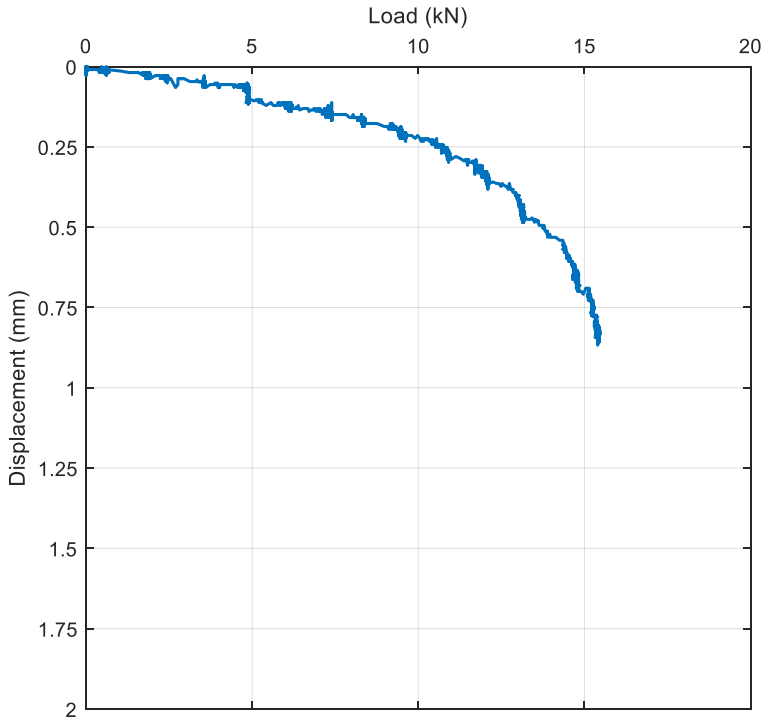

Figure 9-9 Pile 14. 7-day monotonic loading before low-frequency cyclic loading

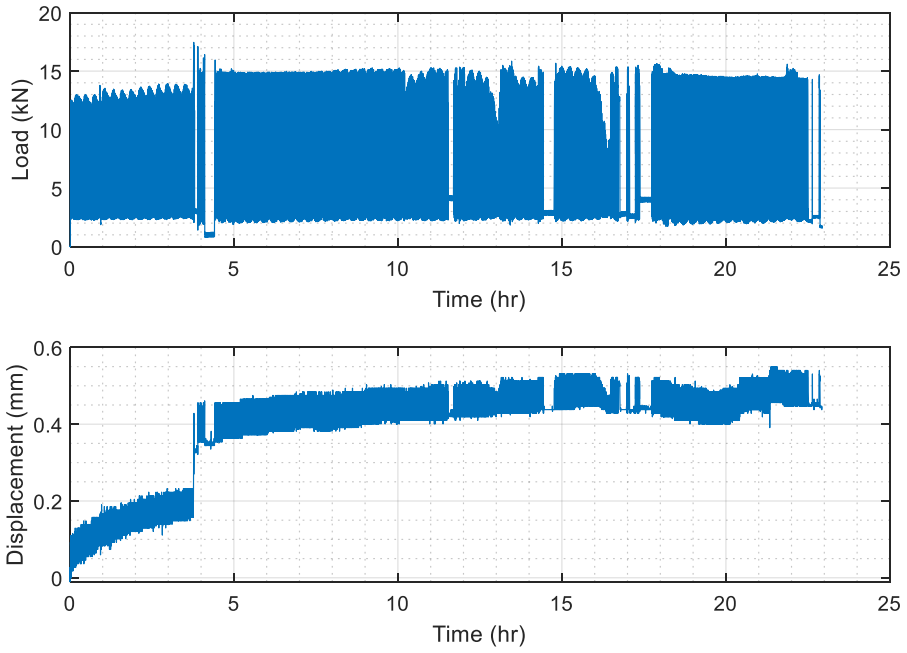

Figure 9-10 Pile 14. 7-day cyclic loading time history

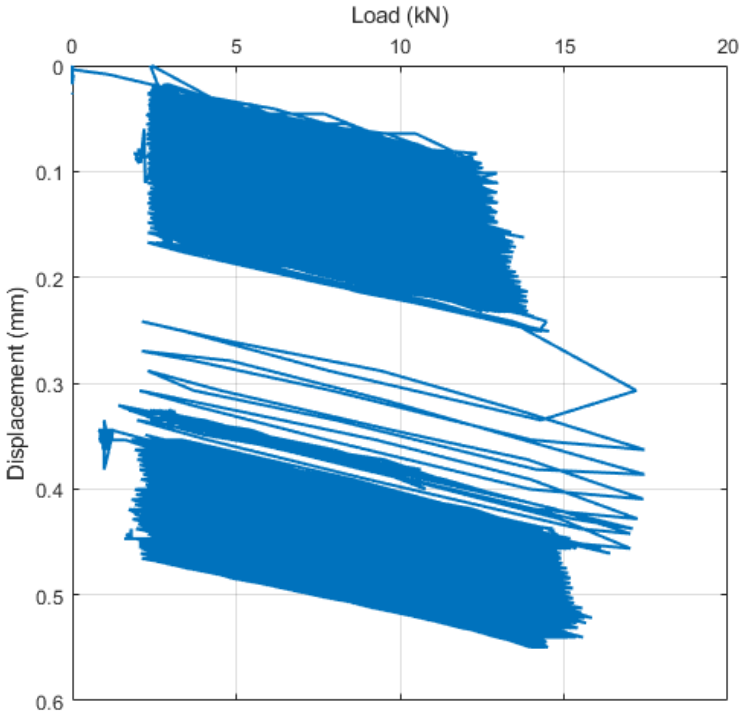

Figure 9-11 Pile 14. 7-day cyclic load-displacement curve

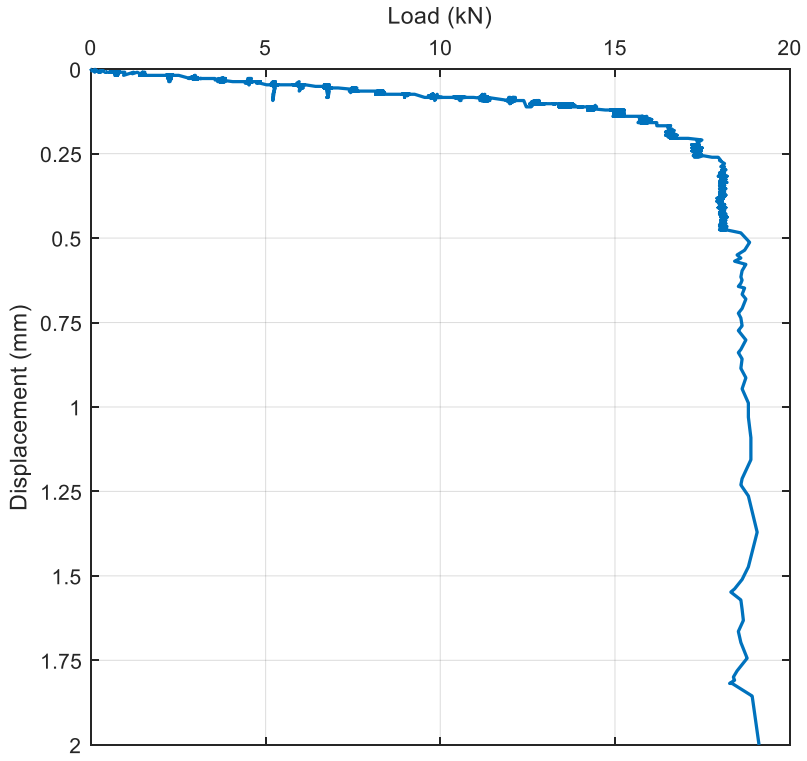

Figure 9-12 Pile 14. 7-day monotonic test after low-frequency cyclic loading

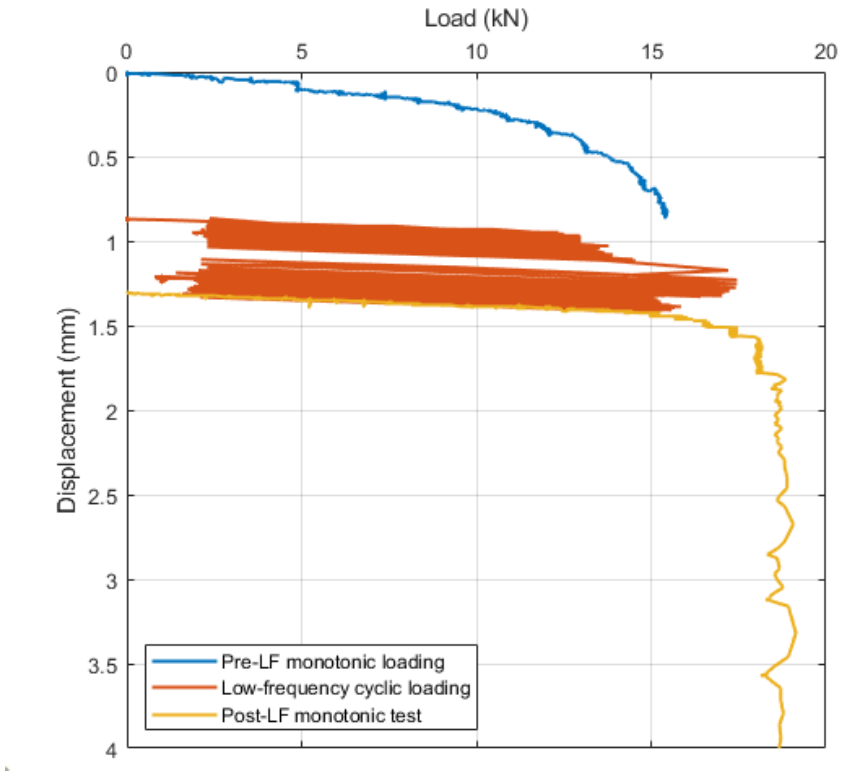

Figure 9-13 Pile 14. 7-day monotonic loading, low-frequency cyclic loading, and monotonic test

9.2.2 Pile 8 - 155-days after installation

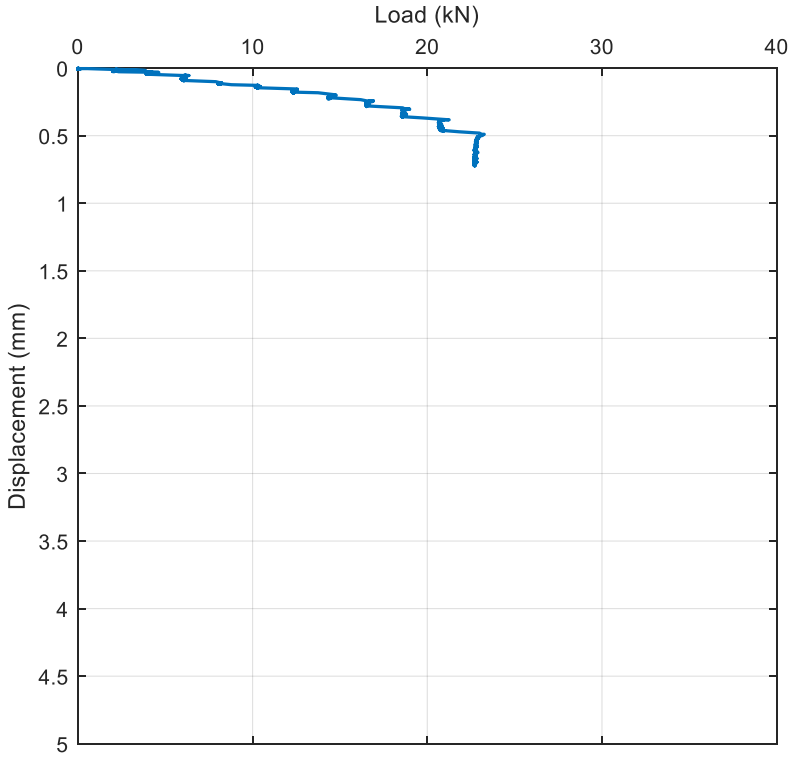

Figure 9-14 Pile 8. 155-day monotonic loading before low-frequency cyclic loading

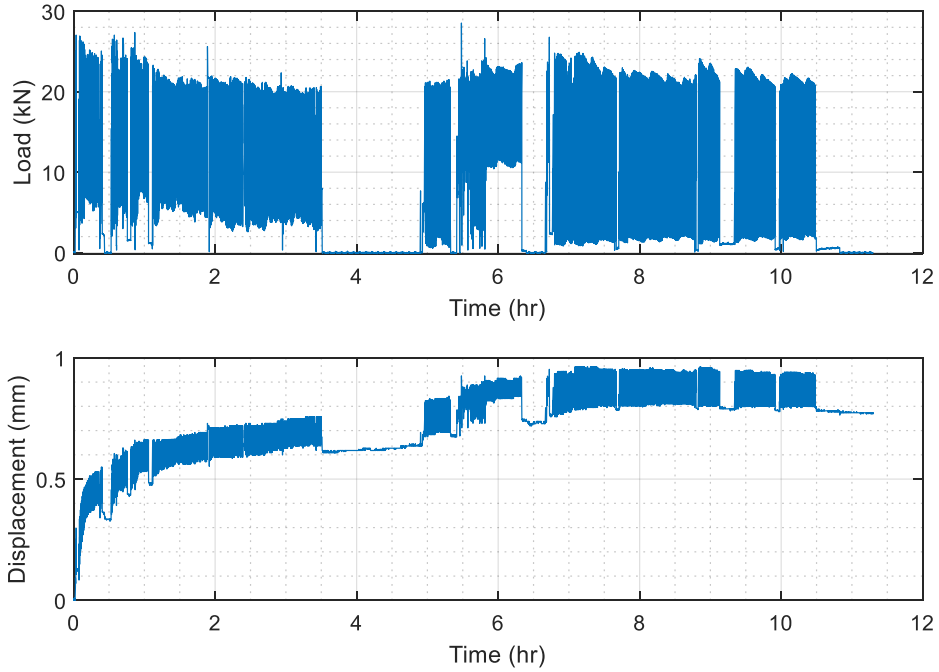

Figure 9-15 Pile 8. 155-day cyclic loading time history. Hydraulic pump failed after 2,700 cycles

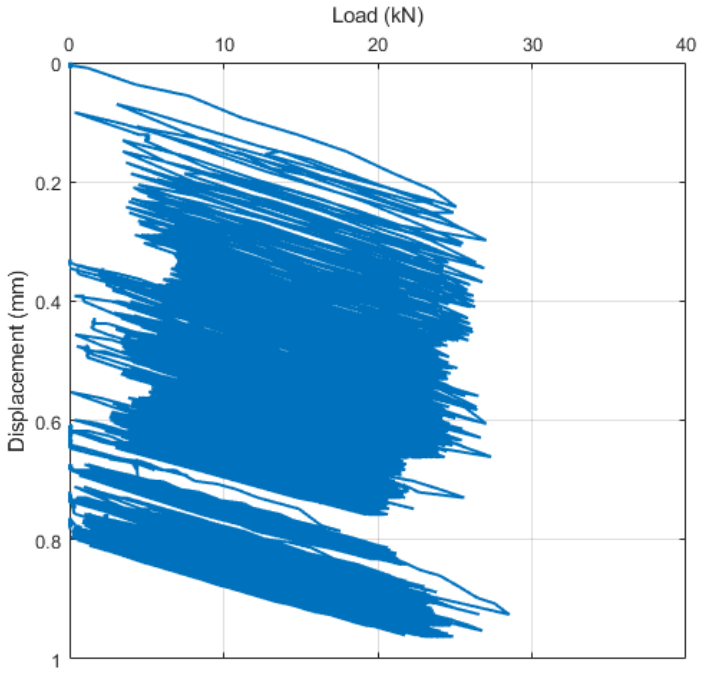

Figure 9-16 Pile 8. 155-day cyclic load-displacement curve. Hydraulic pump failed after 2,700 cycles

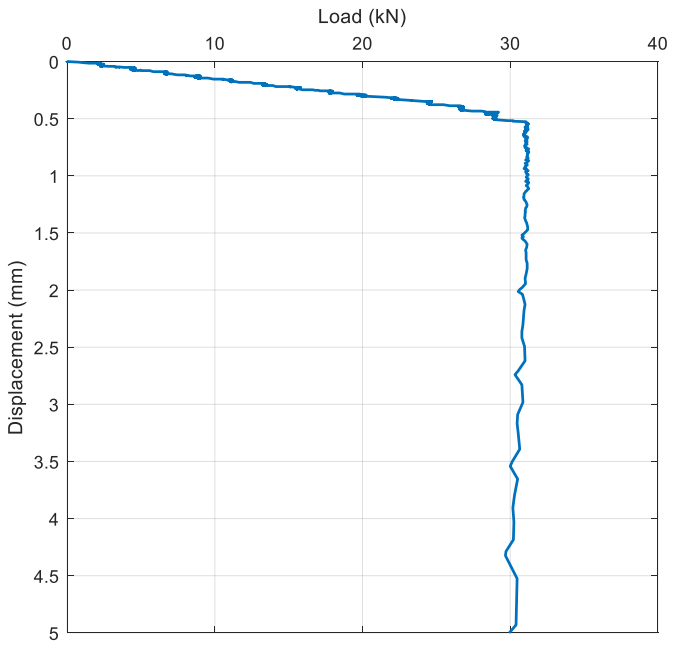

Figure 9-17 Pile 8. 155-day monotonic test after low-frequency cyclic loading

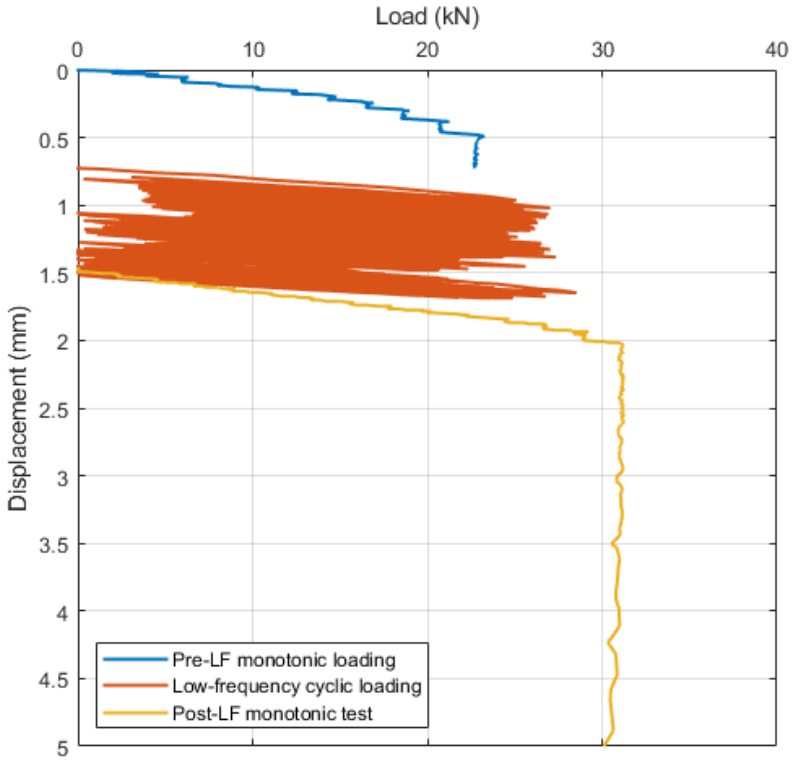

Figure 9-18 Pile 8. 155-day monotonic loading, low-frequency cyclic loading, and monotonic test

9.2.3 Pile 16 - 166-days after installation

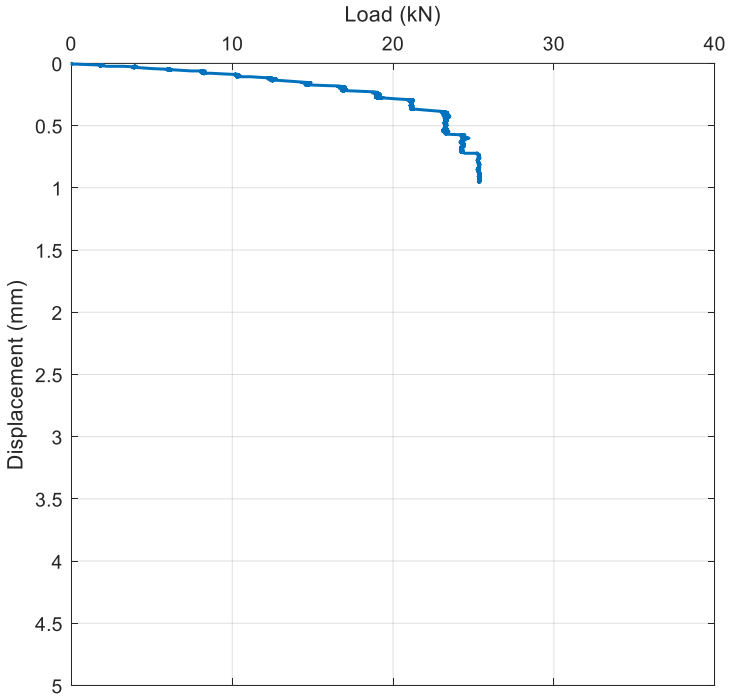

Figure 9-19 Pile 16. 166-day monotonic loading before low-frequency cyclic loading

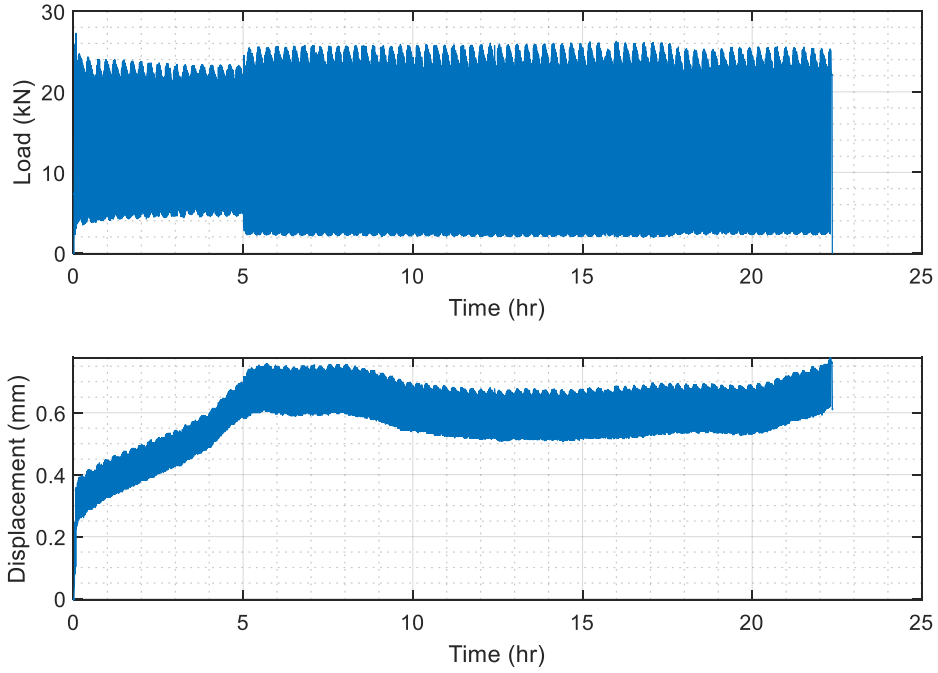

Figure 9-20 Pile 16. 166-day cyclic loading time history

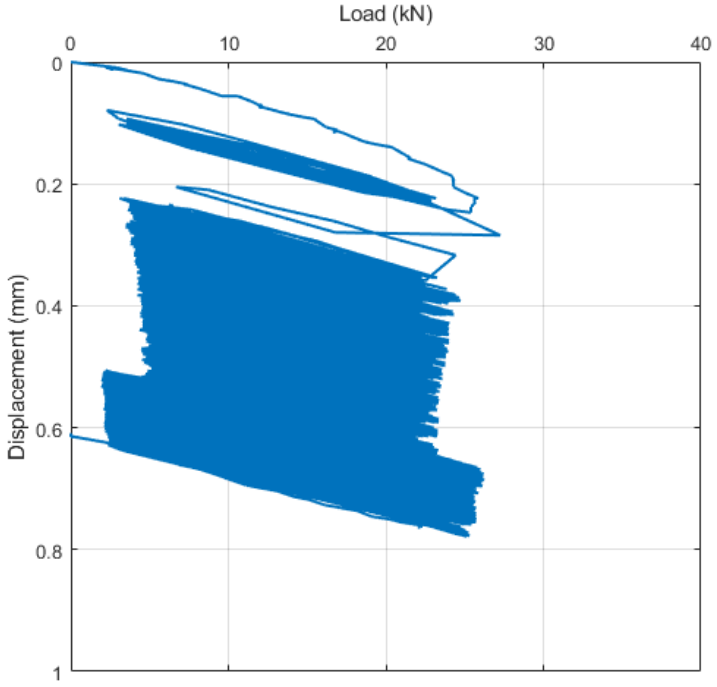

Figure 9-21 Pile 16. 166-day cyclic load-displacement curve

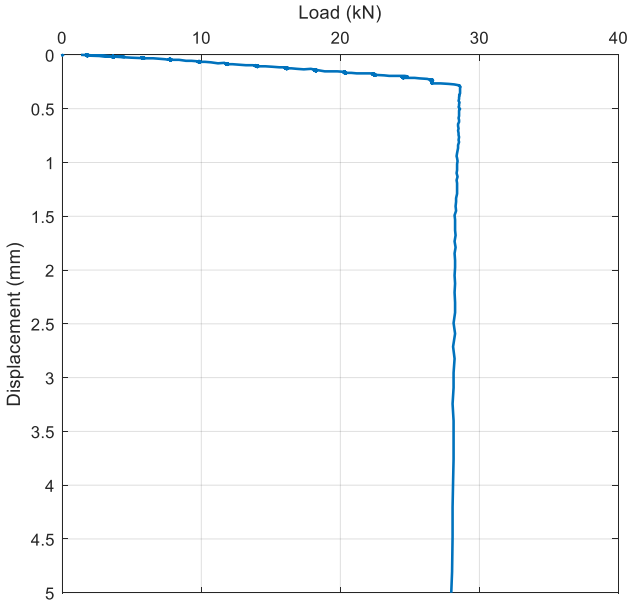

Figure 9-22 Pile 16. 166-day monotonic test after low-frequency cyclic loading

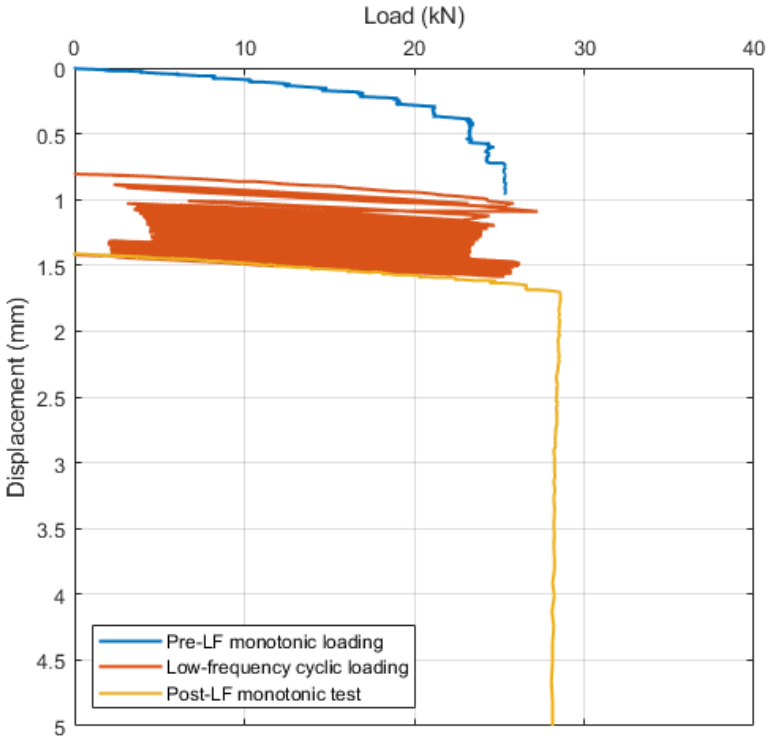

Figure 9-23 Pile 16. 166-day monotonic, LF cyclic, and monotonic test

9.3 High-frequency cyclic loading and post-cyclic monotonic

9.3.1 Pile 2 - 8-days after installation

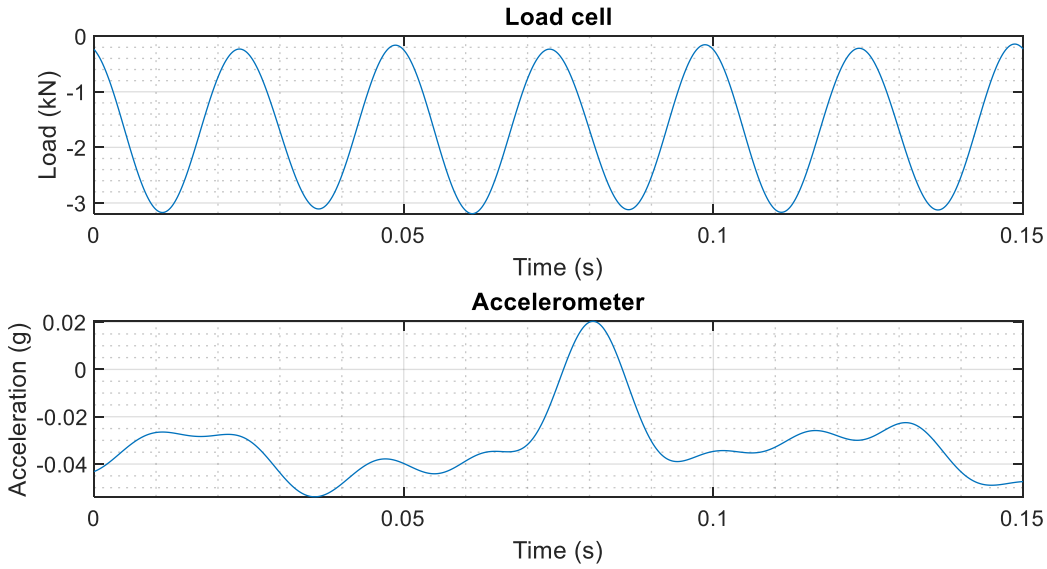

Figure 9-24 Pile 2. 8-day HF cyclic - Snapshot about 1 minute into shaking

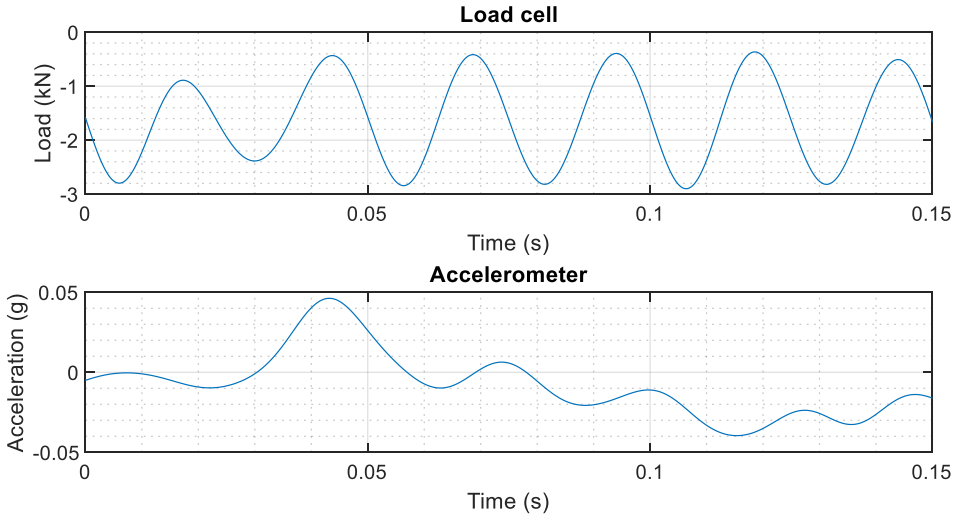

Figure 9-25 Pile 2. 8-day HF cyclic - Snapshot about 2.5 minutes into shaking

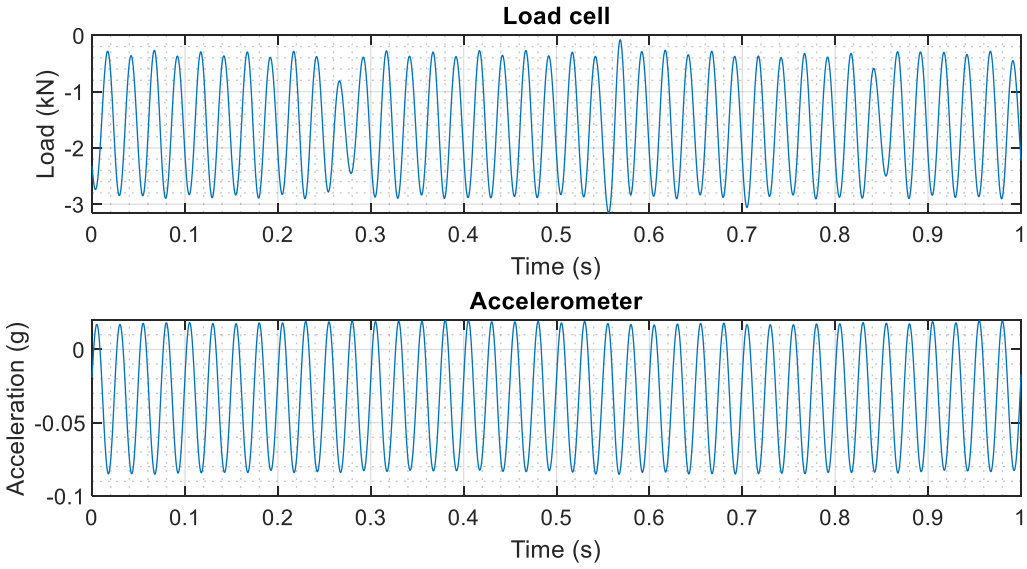

Figure 9-26 Pile 2. 8-day HF cyclic loading - Snapshot about 7.5 minutes into shaking

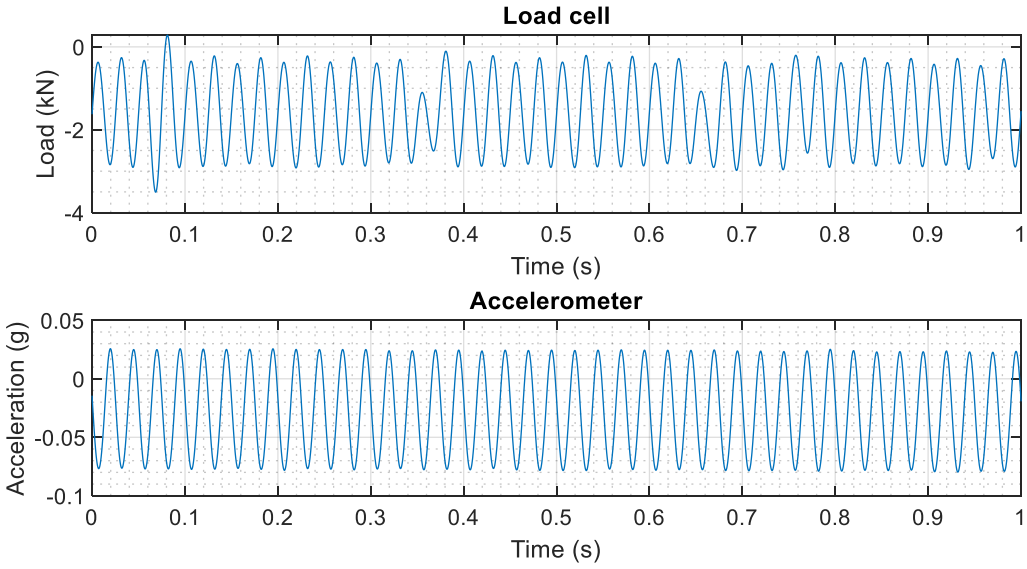

Figure 9-27 Pile 2. 8-day HF cyclic - Snapshot about 12.5 minutes into shaking

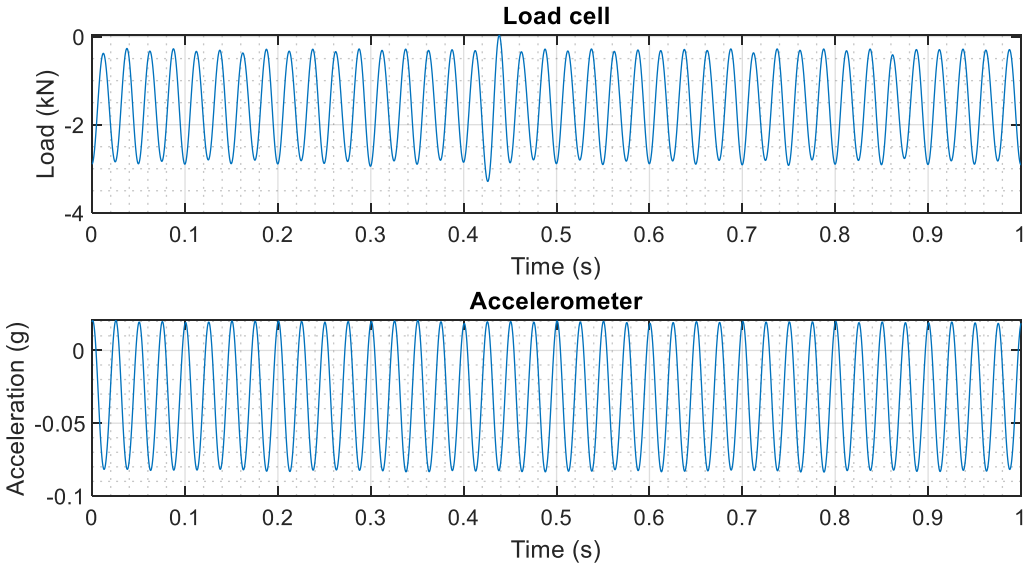

Figure 9-28 Pile 2. 8-day HF cyclic - Snapshot about 17.5 minutes into shaking

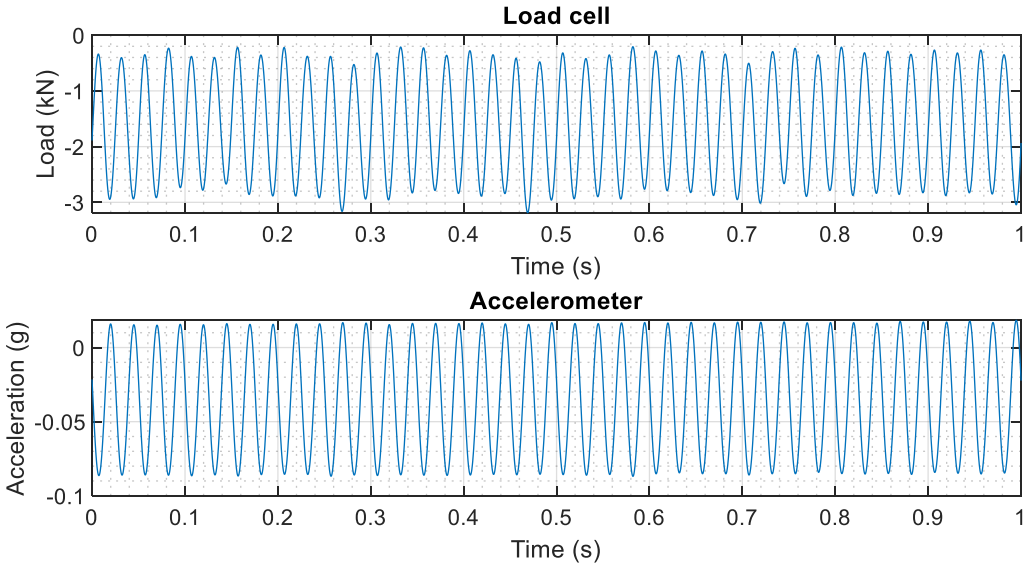

Figure 9-29 Pile 2. 8-day HF cyclic - Snapshot about 22.5 minutes into shaking

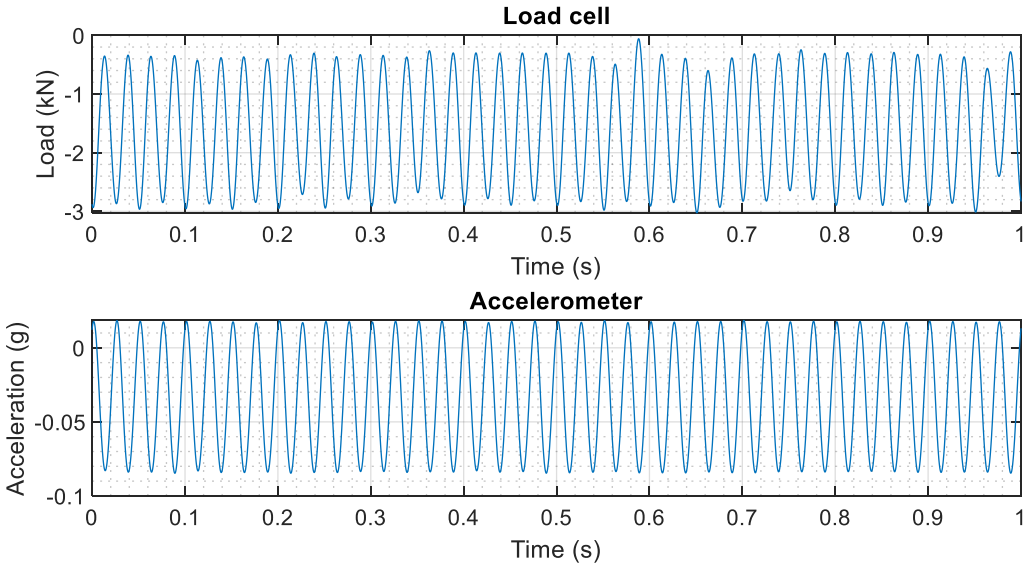

Figure 9-30 Pile 2. 8-day HF cyclic - Snapshot about 27.5 minutes into shaking

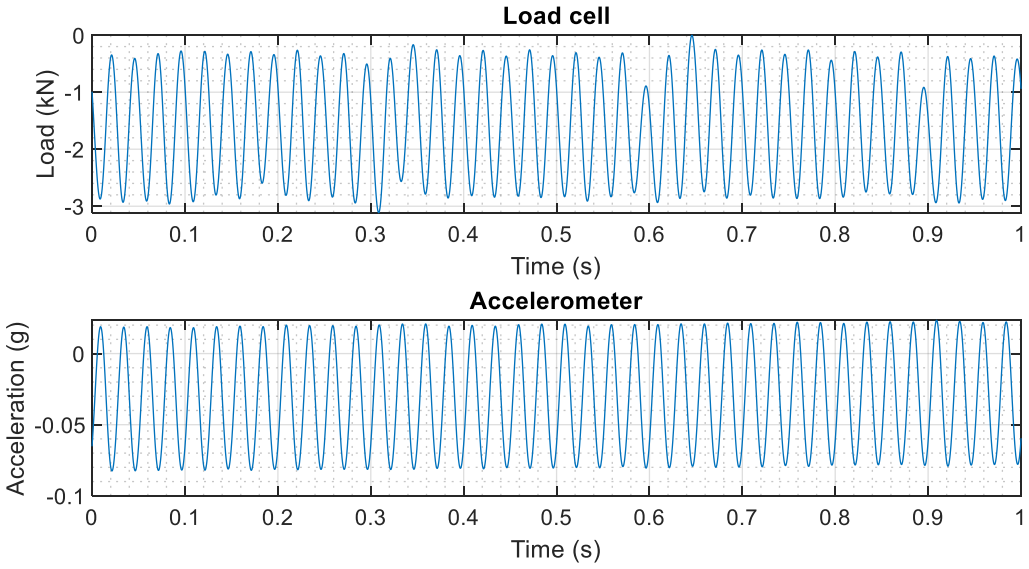

Figure 9-31 Pile 2. 8-day HF cyclic - Snapshot about 32.5 minutes into shaking

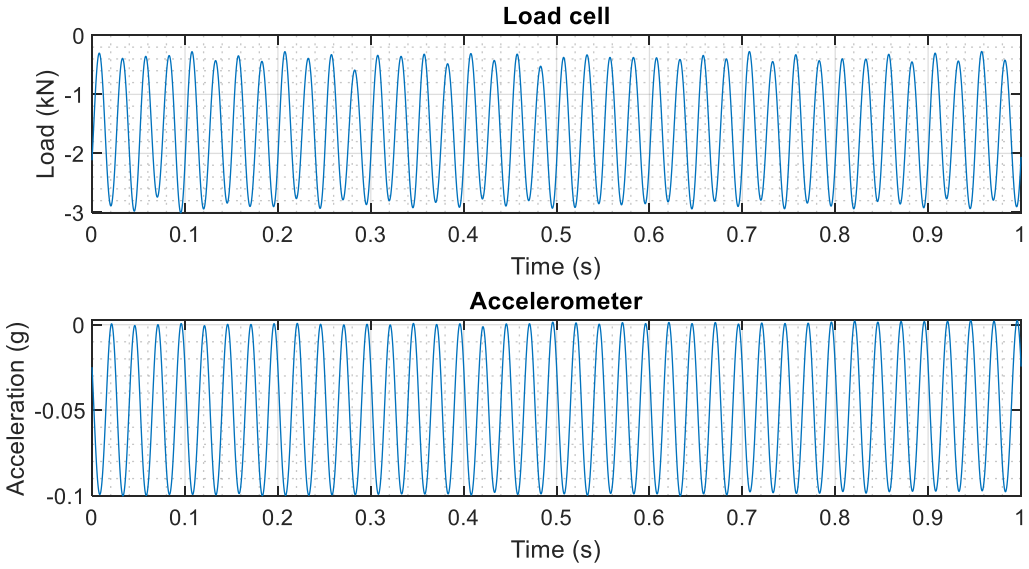

Figure 9-32 Pile 2. 8-day HF cyclic - Snapshot about 37.5 minutes into shaking

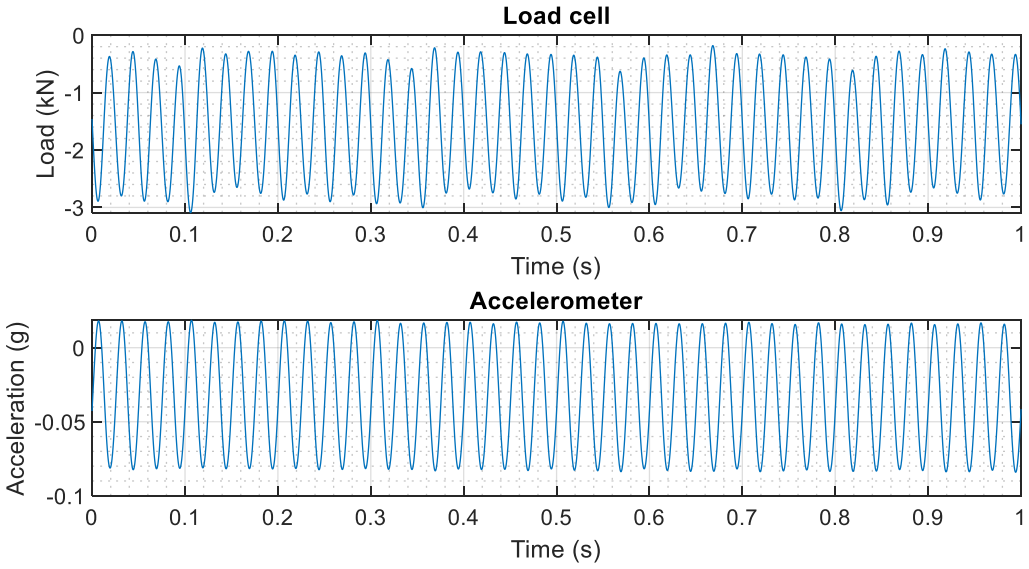

Figure 9-33 Pile 2. 8-day HF cyclic - Snapshot about 42.5 minutes into shaking

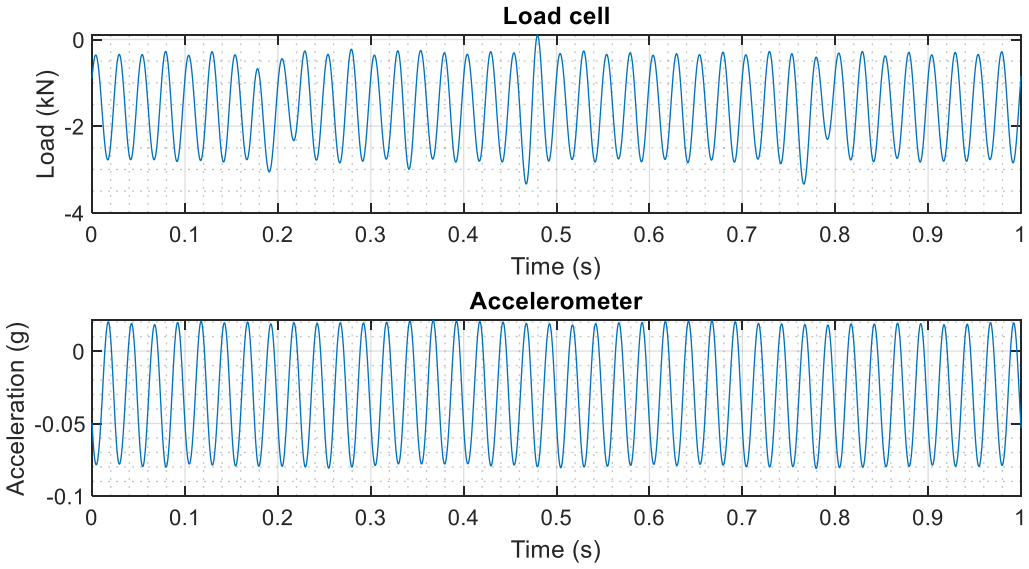

Figure 9-34 Pile 2. 8-day HF cyclic - Snapshot about 47.5 minutes into shaking

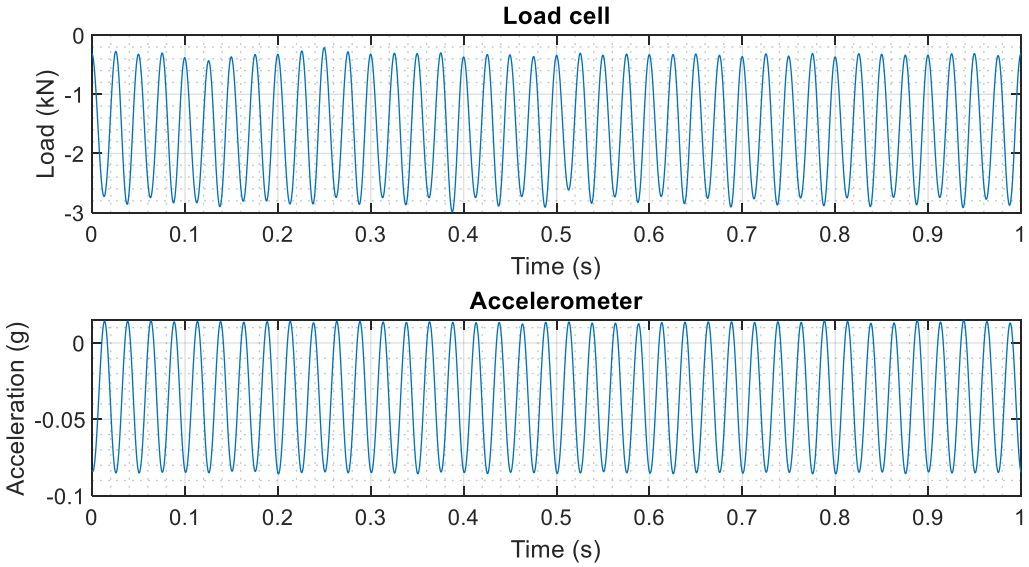

Figure 9-35 Pile 2. 8-day HF cyclic - Snapshot about 52.5 minutes into shaking

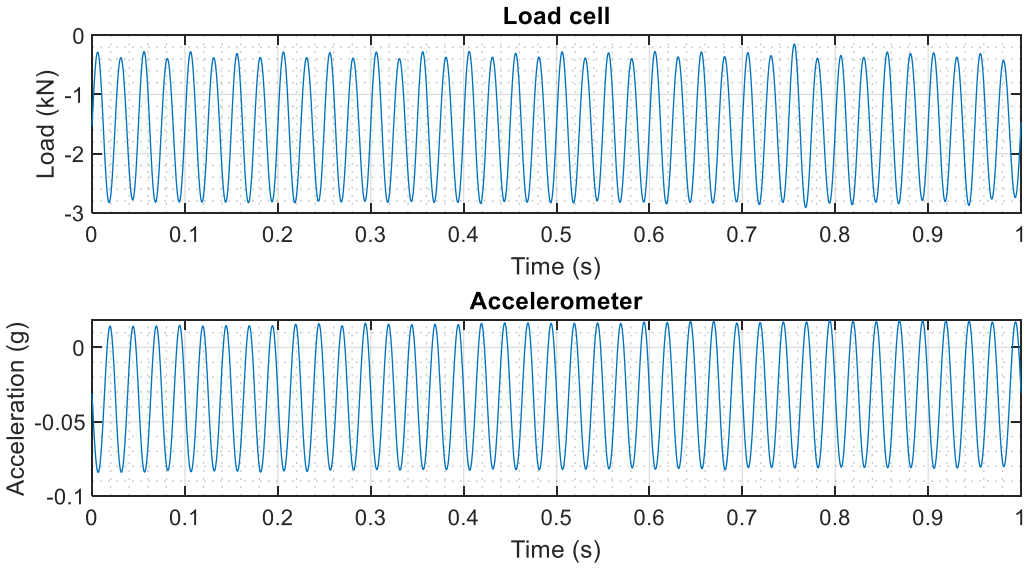

Figure 9-36 Pile 2. 8-day HF cyclic - Snapshot about 57.5 minutes into shaking

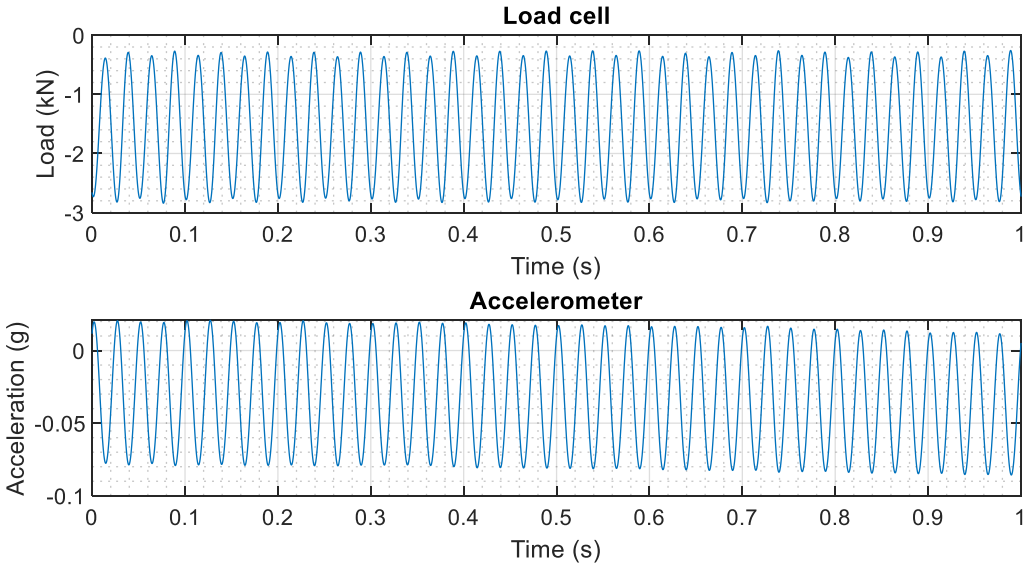

Figure 9-37 Pile 2. 8-day HF cyclic - Snapshot about 62.5 minutes into shaking

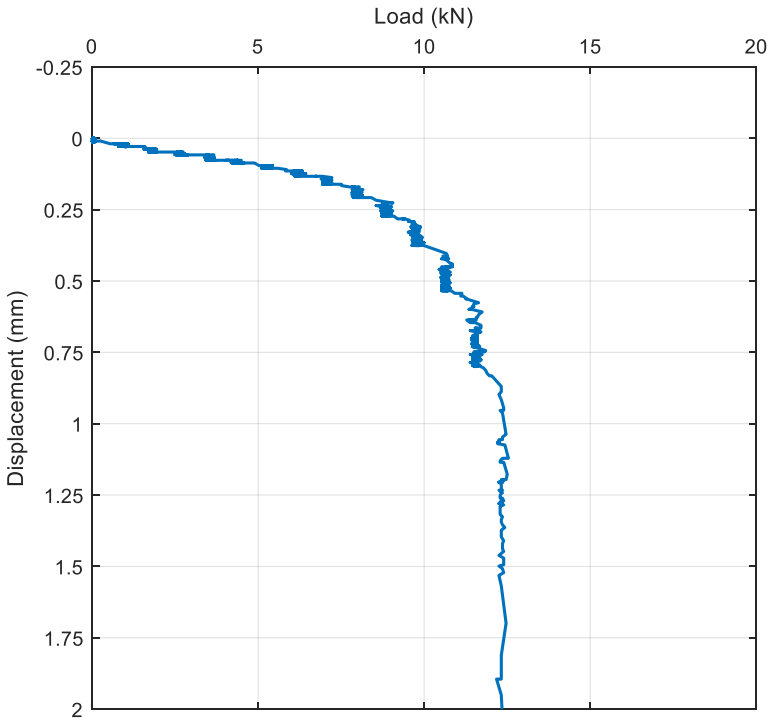

Figure 9-38 Pile 2. 8-day monotonic after HF cyclic

9.3.2 Pile 4 - 9-days after installation

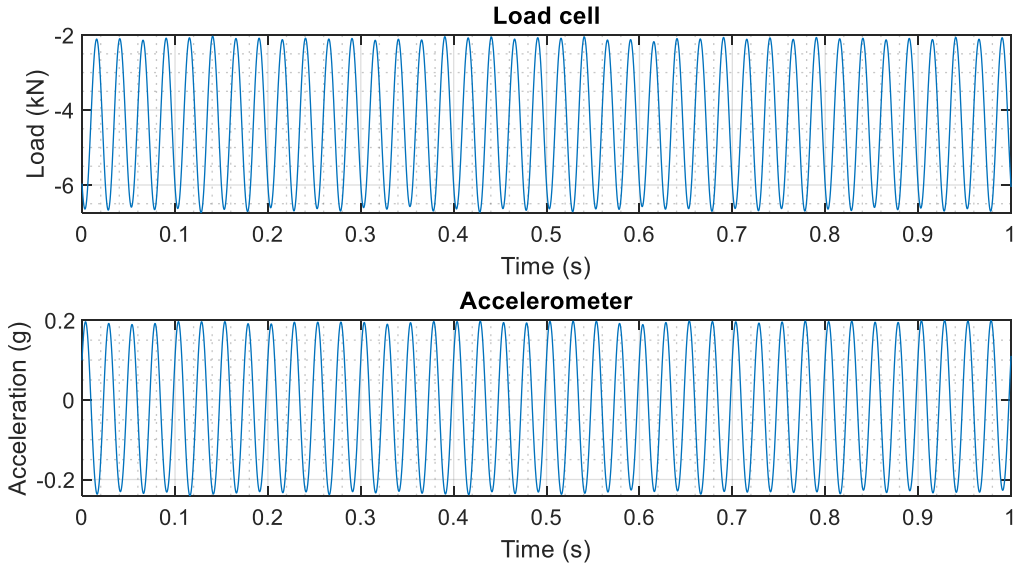

Figure 9-39 Pile 4. 9-day HF cyclic - Snapshot about 1 minute into shaking

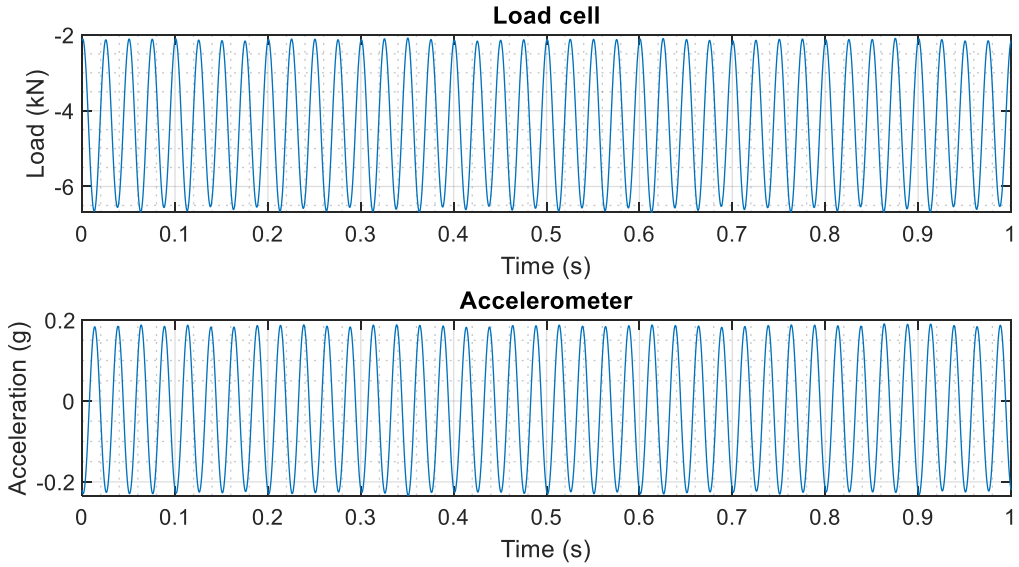

Figure 9-40 Pile 4. 9-day HF cyclic - Snapshot about 2.5 minutes into shaking

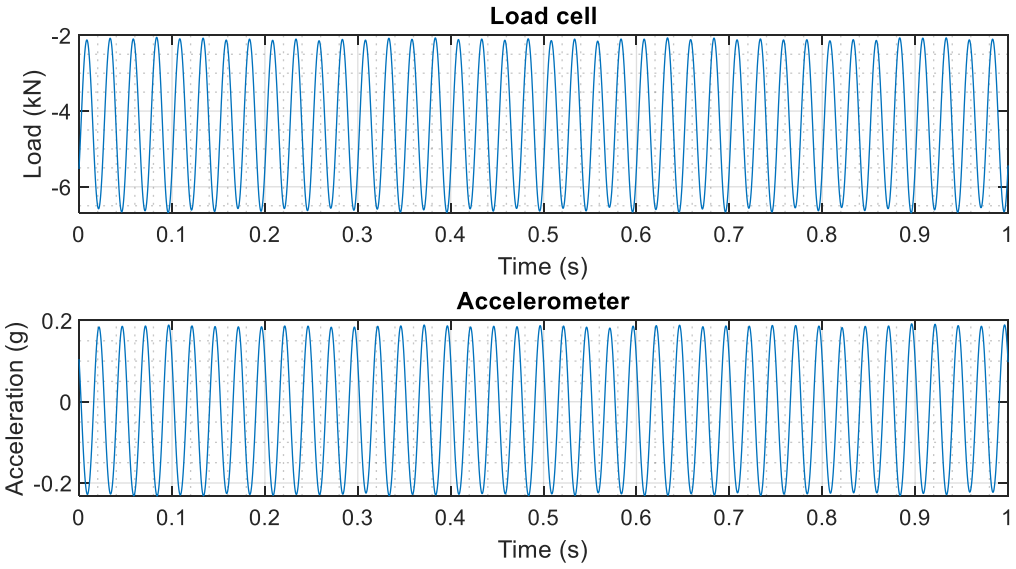

Figure 9-41 Pile 4. 9-day HF cyclic - Snapshot about 7.5 minutes into shaking

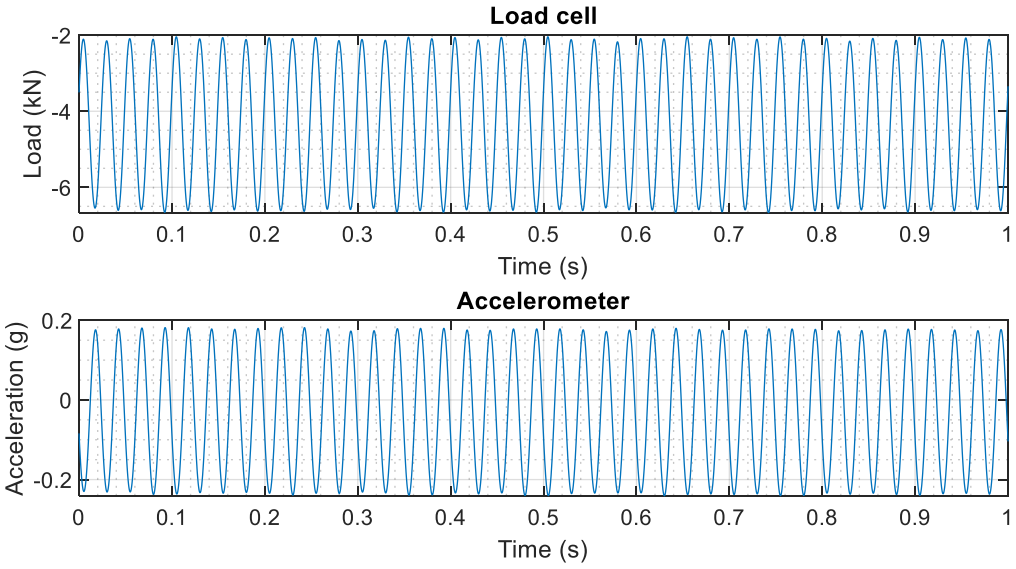

Figure 9-42 Pile 4. 9-day HF cyclic - Snapshot about 12.5 minutes into shaking

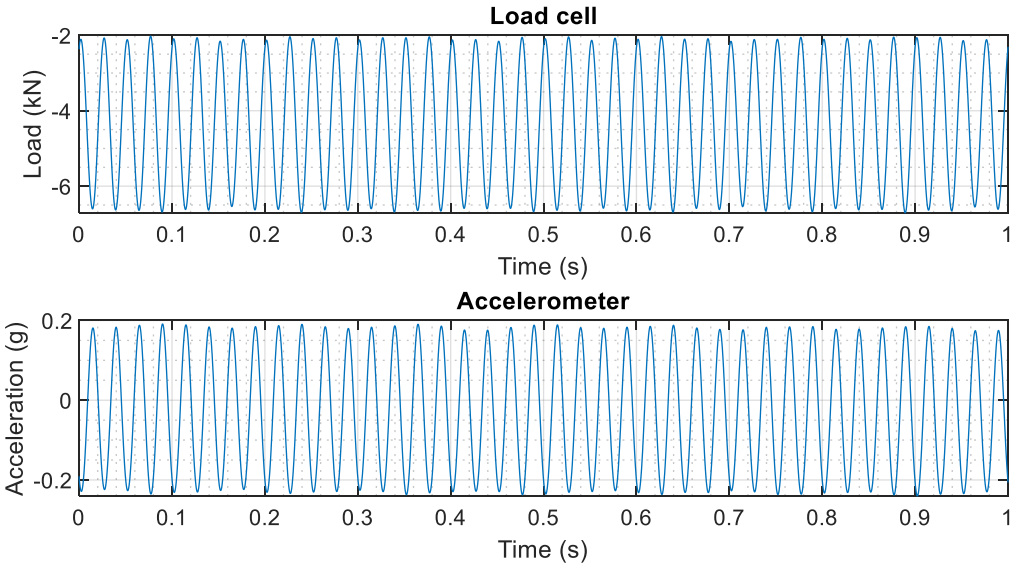

Figure 9-43 Pile 4. 9-day HF cyclic - Snapshot about 17.5 minutes into shaking

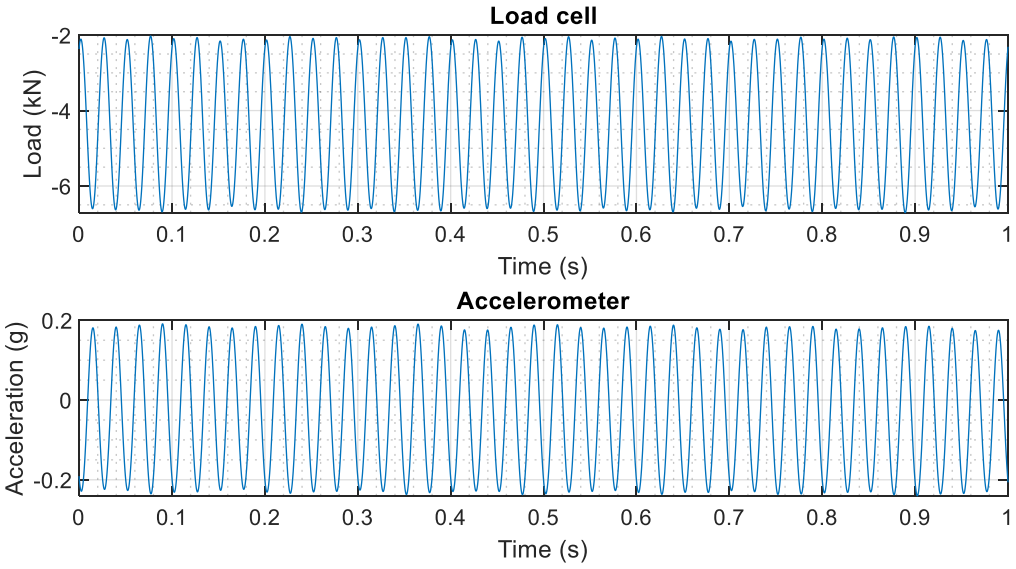

Figure 9-44 Pile 4. 9-day HF cyclic - Snapshot about 22.5 minutes into shaking

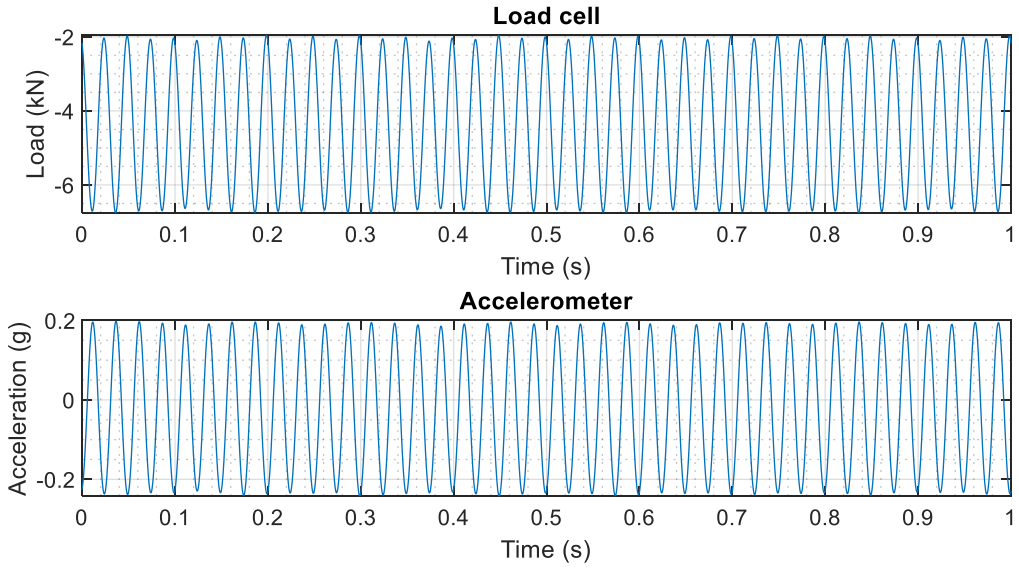

Figure 9-45 Pile 4. 9-day HF cyclic - Snapshot about 27.5 minutes into shaking

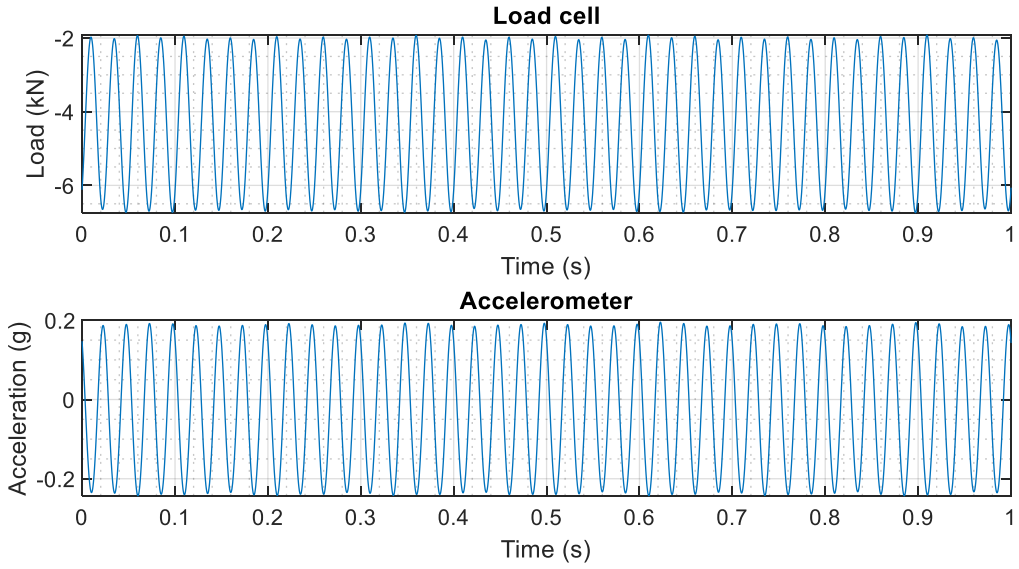

Figure 9-46 Pile 4. 9-day HF cyclic - Snapshot about 32.5 minutes into shaking

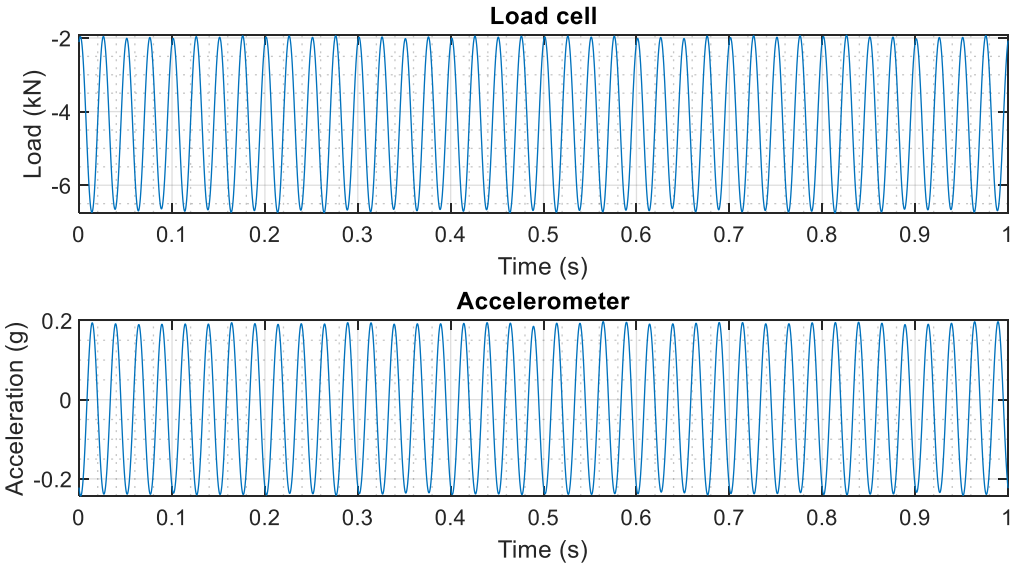

Figure 9-47 Pile 4. 9-day HF cyclic - Snapshot about 37.5 minutes into shaking

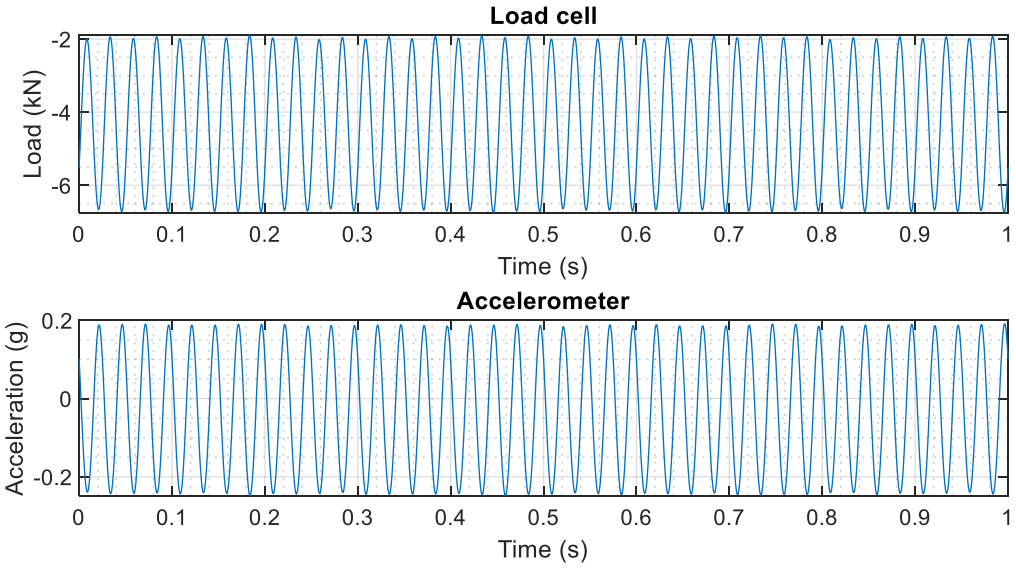

Figure 9-48 Pile 4. 9-day HF cyclic - Snapshot about 42.5 minutes into shaking

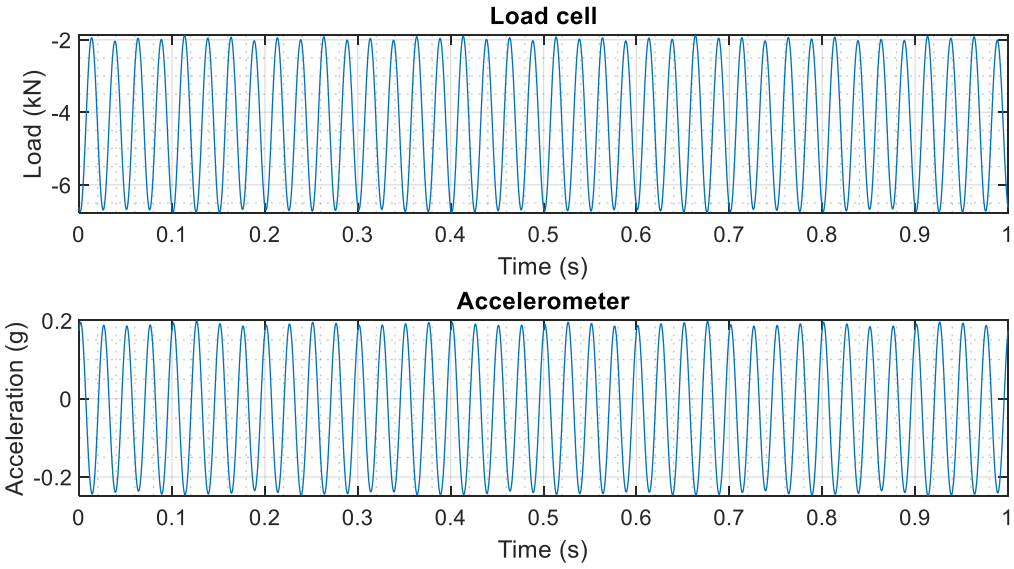

Figure 9-49 Pile 4. 9-day HF cyclic - Snapshot about 47.5 minutes into shaking

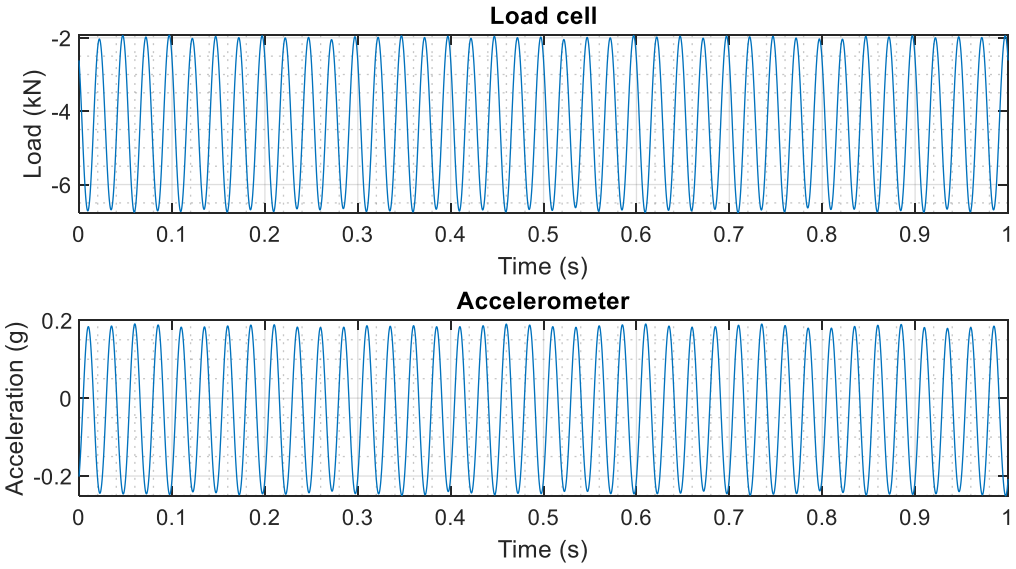

Figure 9-50 Pile 4. 9-day HF cyclic - Snapshot about 52.5 minutes into shaking

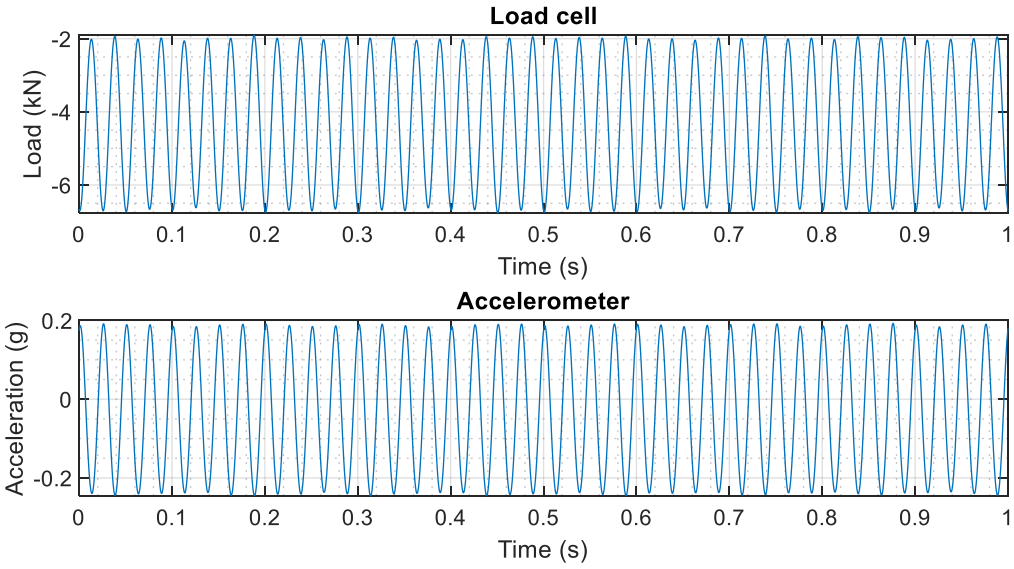

Figure 9-51 Pile 4. 9-day HF cyclic - Snapshot about 57.5 minutes into shaking

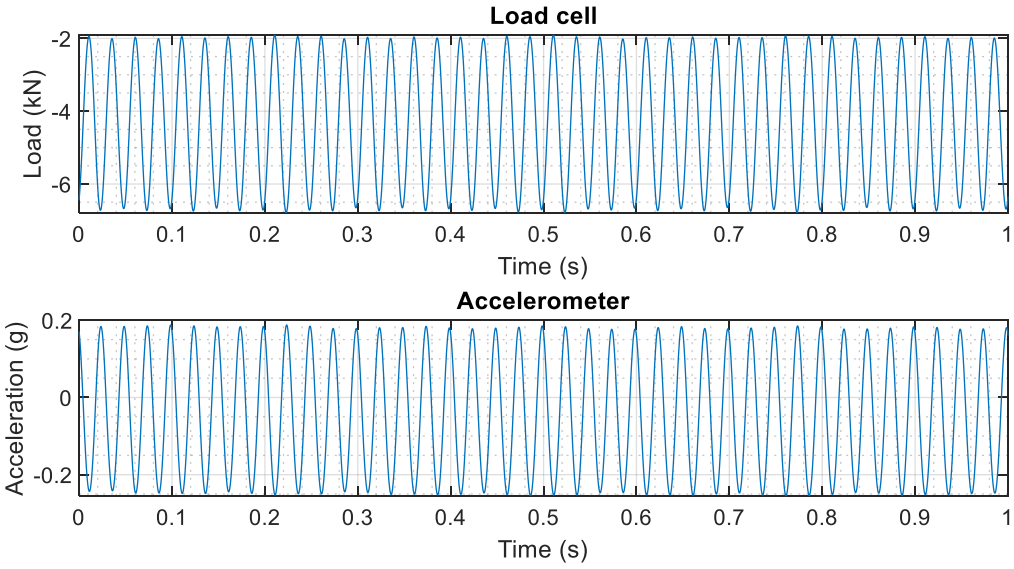

Figure 9-52 Pile 4. 9-day HF cyclic - Snapshot about 62.5 minutes into shaking

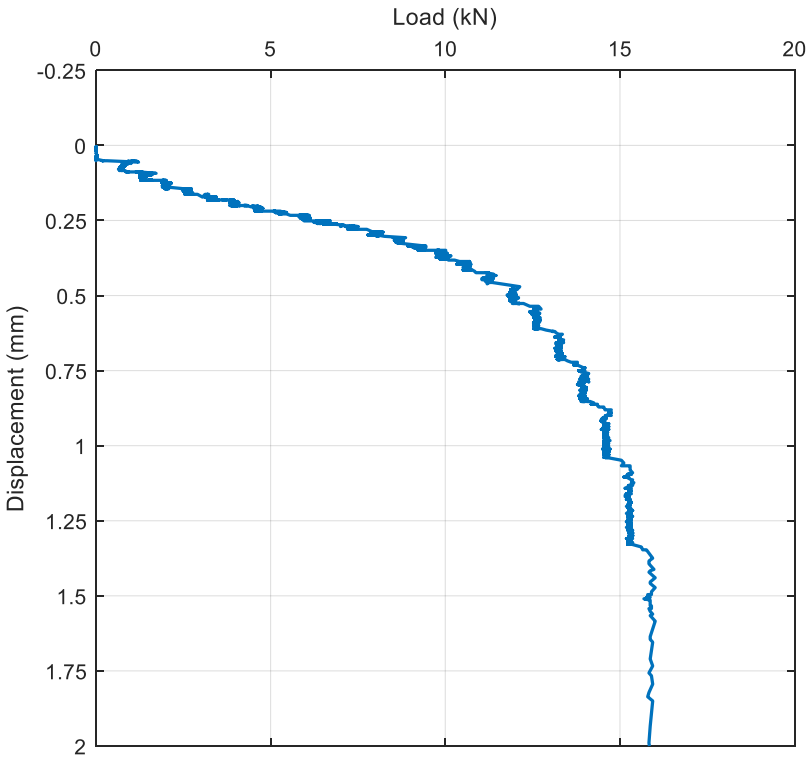

Figure 9-53 Pile 4. 9-day monotonic after HF cyclic

9.3.3 Pile 11 - 161-days after installation

Note: Accelerometer did not record during this test.

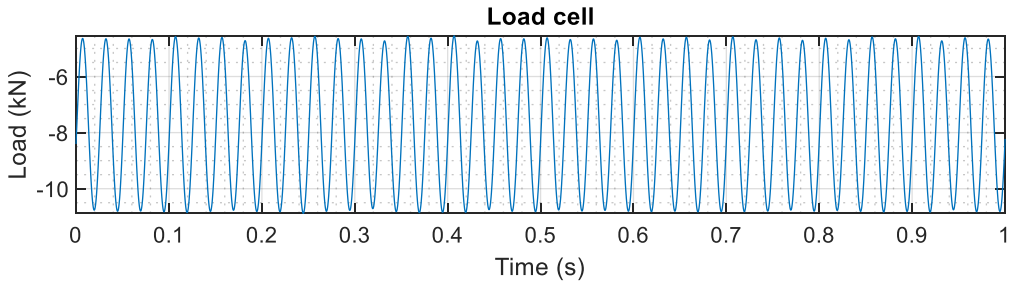

Figure 9-54 Pile 11. 161-day HF cyclic - Snapshot about 2.5 minutes into shaking

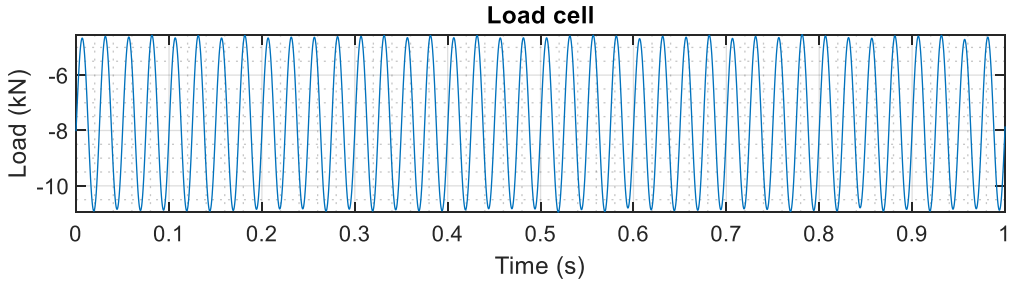

Figure 9-55 Pile 11. 161-day HF cyclic - Snapshot about 7.5 minutes into shaking

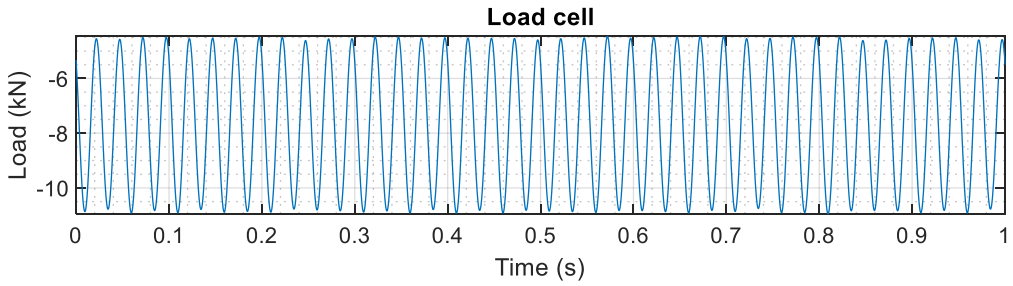

Figure 9-56 Pile 11. 161-day HF cyclic - Snapshot about 12.5 minutes into shaking

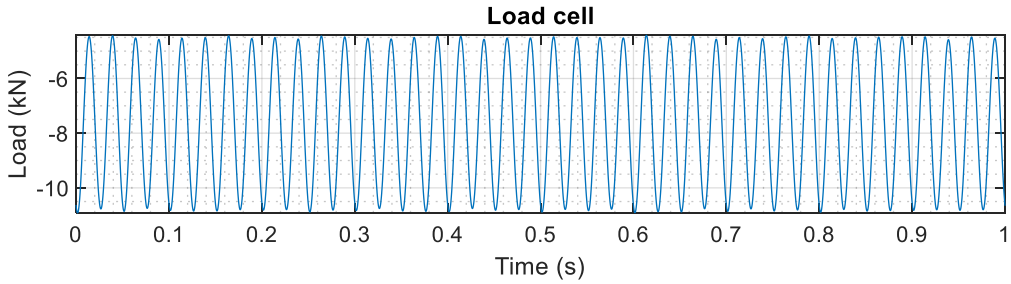

Figure 9-57 Pile 11. 161-day HF cyclic - Snapshot about 17.5 minutes into shaking

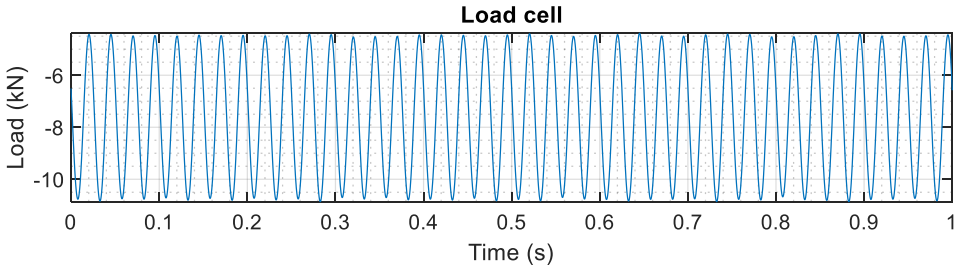

Figure 9-58 Pile 11. 161-day HF cyclic - Snapshot about 22.5 minutes into shaking

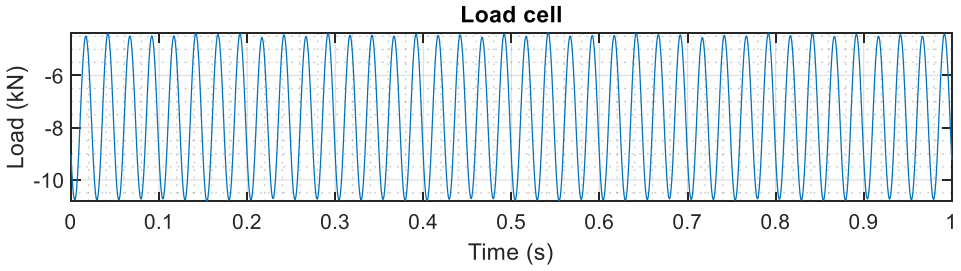

Figure 9-59 Pile 11. 161-day HF cyclic - Snapshot about 27.5 minutes into shaking

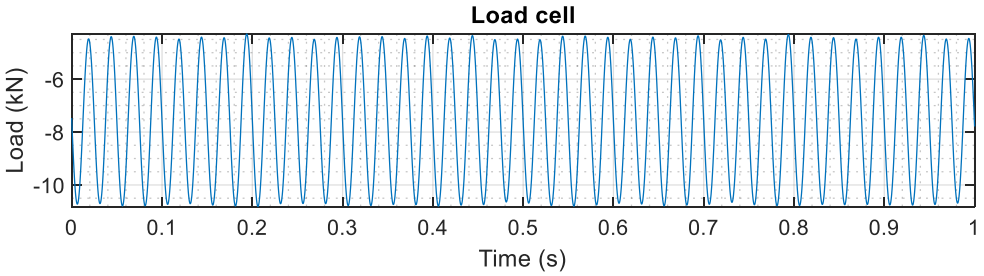

Figure 9-60 Pile 11. 161-day HF cyclic - Snapshot about 32.5 minutes into shaking

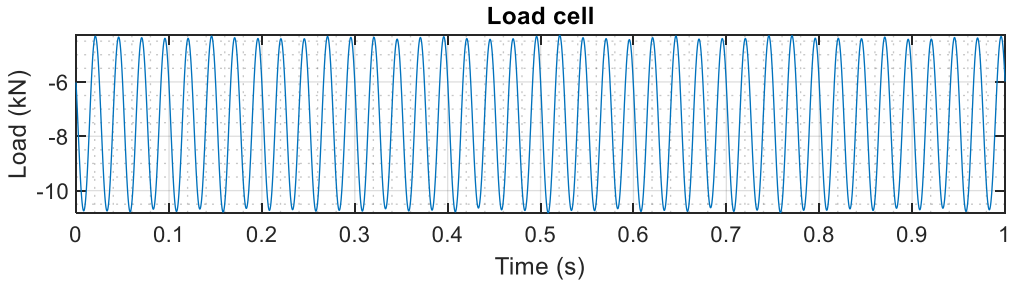

Figure 9-61 Pile 11. 161-day HF cyclic - Snapshot about 37.5 minutes into shaking

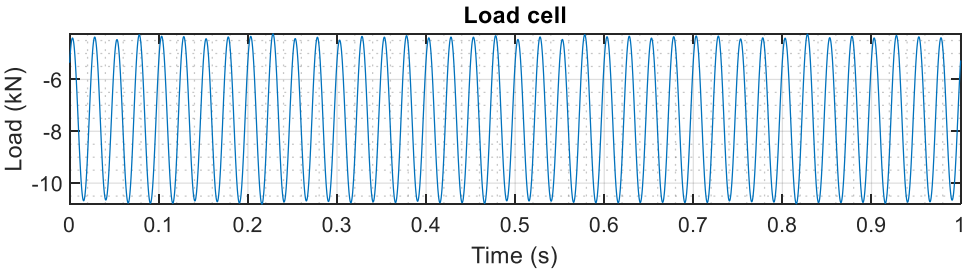

Figure 9-62 Pile 11. 161-day HF cyclic - Snapshot about 42.5 minutes into shaking

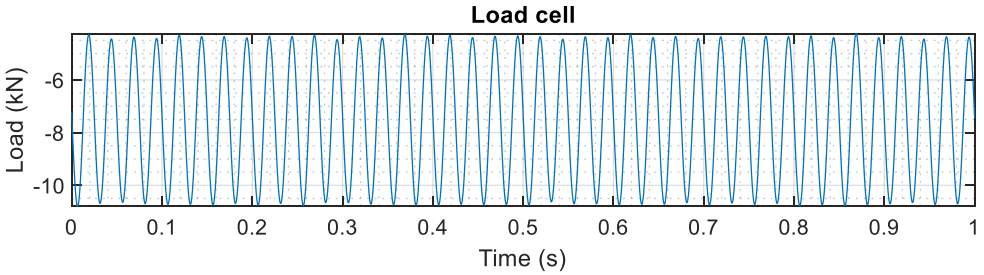

Figure 9-63 Pile 11. 161-day HF cyclic - Snapshot about 47.5 minutes into shaking

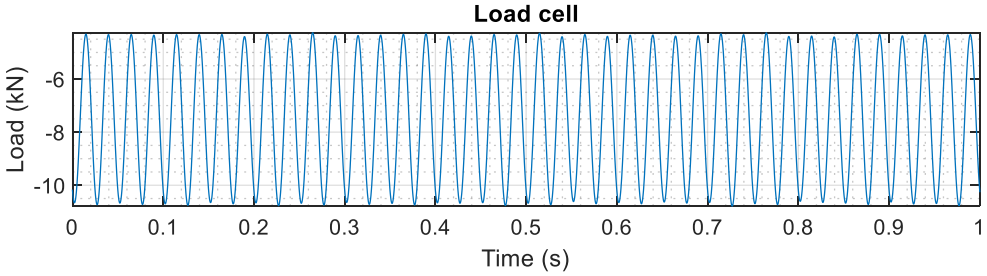

Figure 9-64 Pile 11. 161-day HF cyclic - Snapshot about 52.5 minutes into shaking

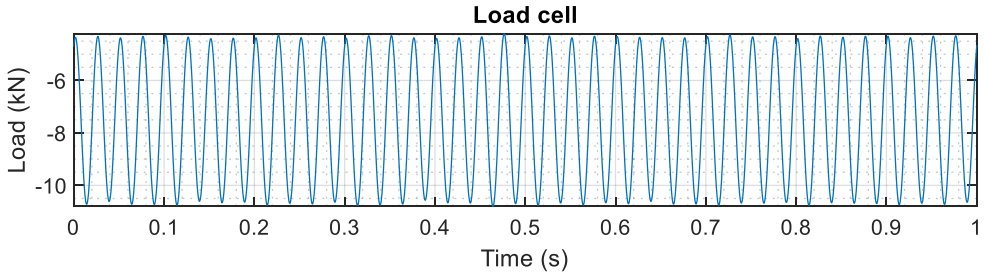

Figure 9-65 Pile 11. 161-day HF cyclic - Snapshot about 57.5 minutes into shaking

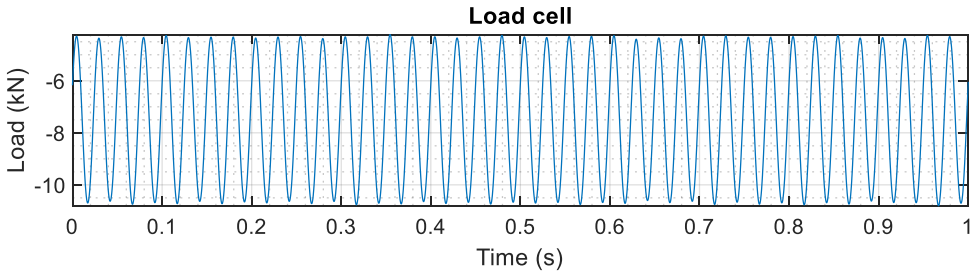

Figure 9-66 Pile 11. 161-day HF cyclic - Snapshot about 62.5 minutes into shaking

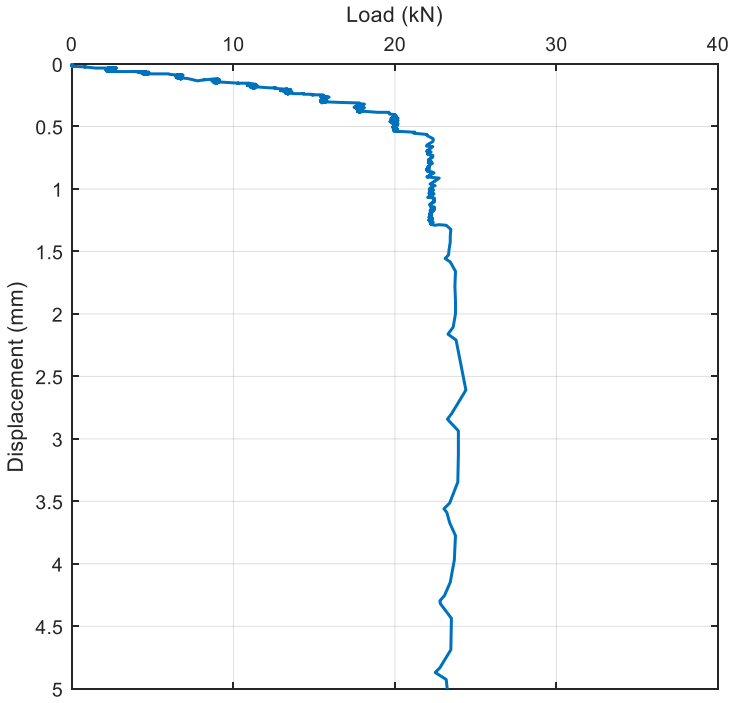

Figure 9-67 Pile 11. 161-day monotonic after HF cyclic

9.3.4 Pile 6 - 166-days after installation

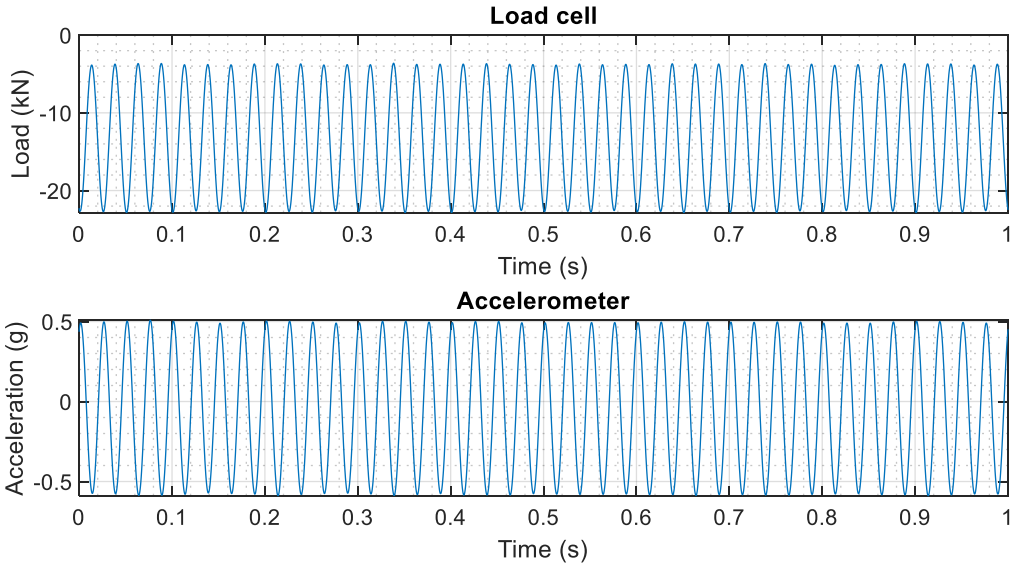

Figure 9-68 Pile 6. 166-day HF cyclic - Snapshot about 2.5 minutes into shaking

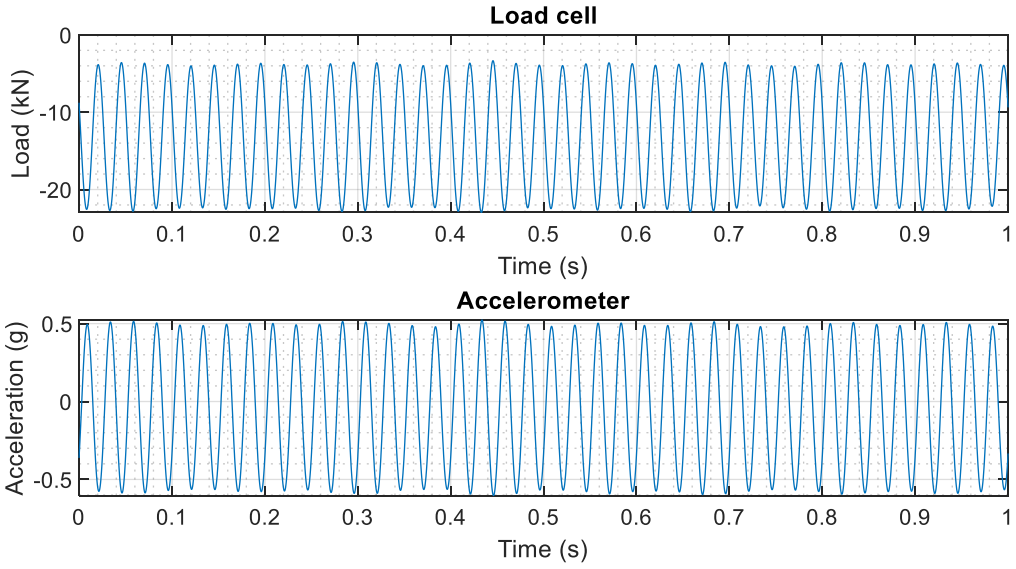

Figure 9-69 Pile 6. 166-day HF cyclic - Snapshot about 7.5 minutes into shaking

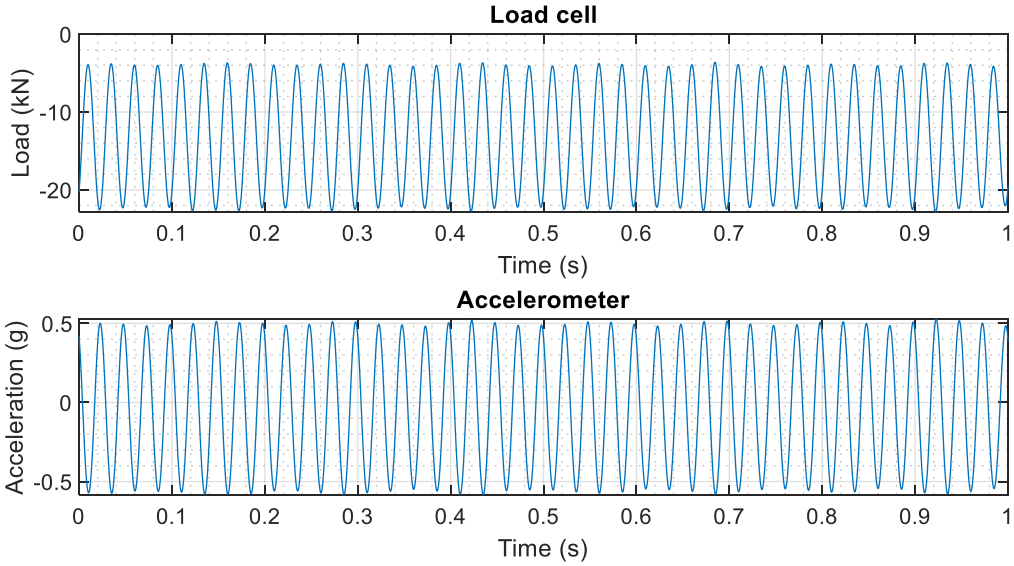

Figure 9-70 Pile 6. 166-day HF cyclic - Snapshot about 12.5 minutes into shaking

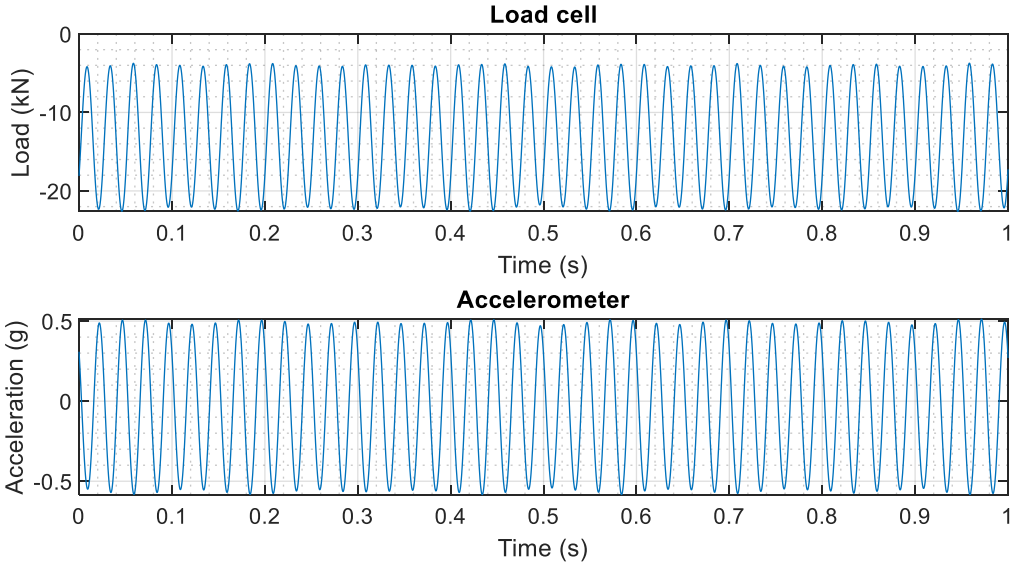

Figure 9-71 Pile 6. 166-day HF cyclic - Snapshot about 17.5 minutes into shaking

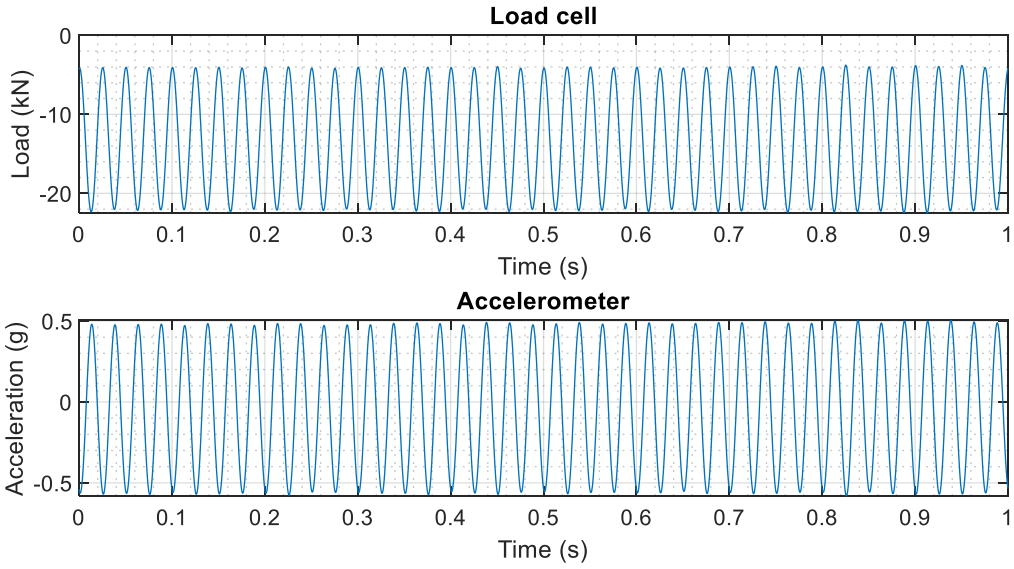

Figure 9-72 Pile 6. 166-day HF cyclic - Snapshot about 22.5 minutes into shaking

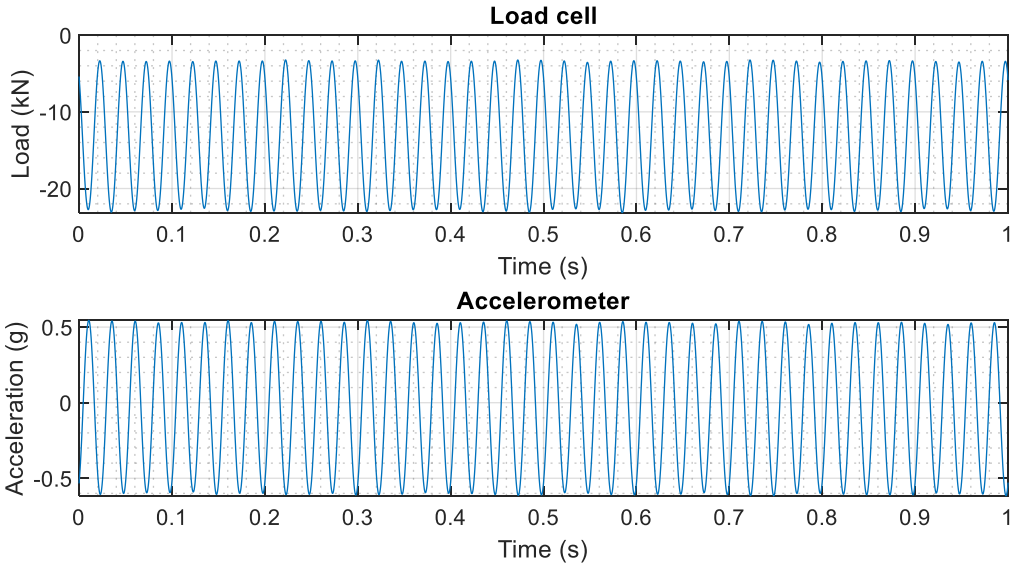

Figure 9-73 Pile 6. 166-day HF cyclic - Snapshot about 27.5 minutes into shaking

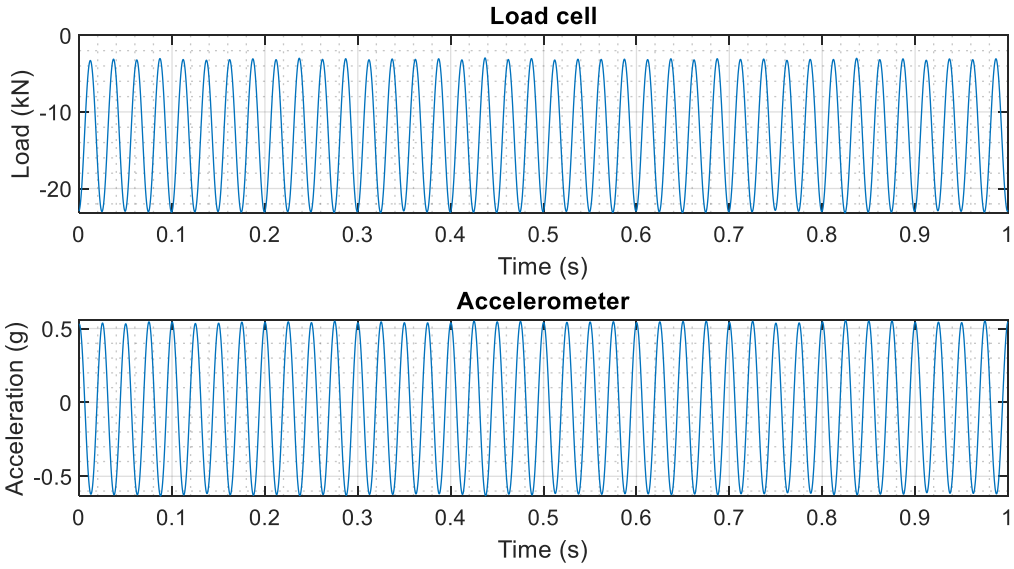

Figure 9-74 Pile 6. 166-day HF cyclic - Snapshot about 32.5 minutes into shaking

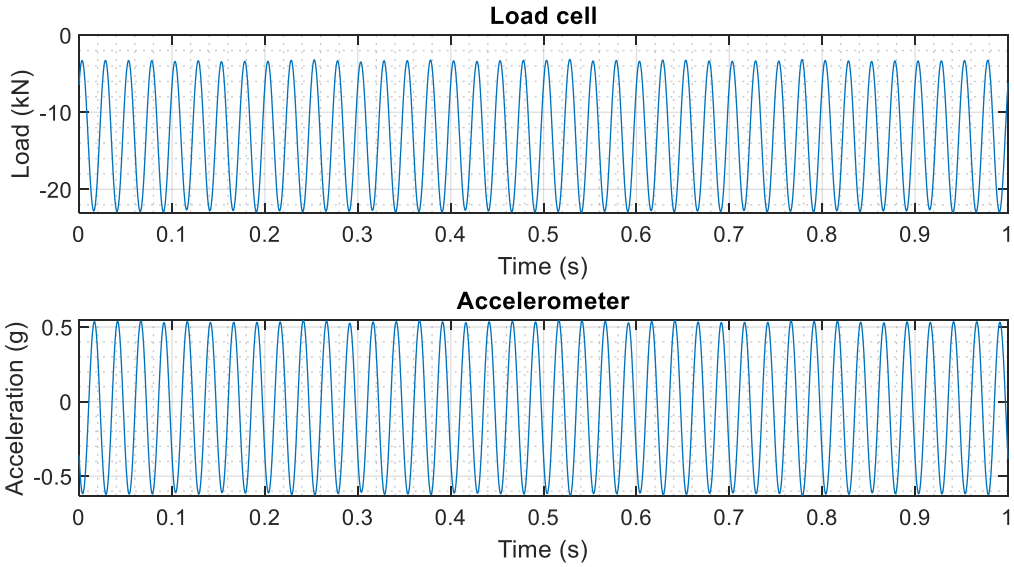

Figure 9-75 Pile 6. 166-day HF cyclic - Snapshot about 37.5 minutes into shaking

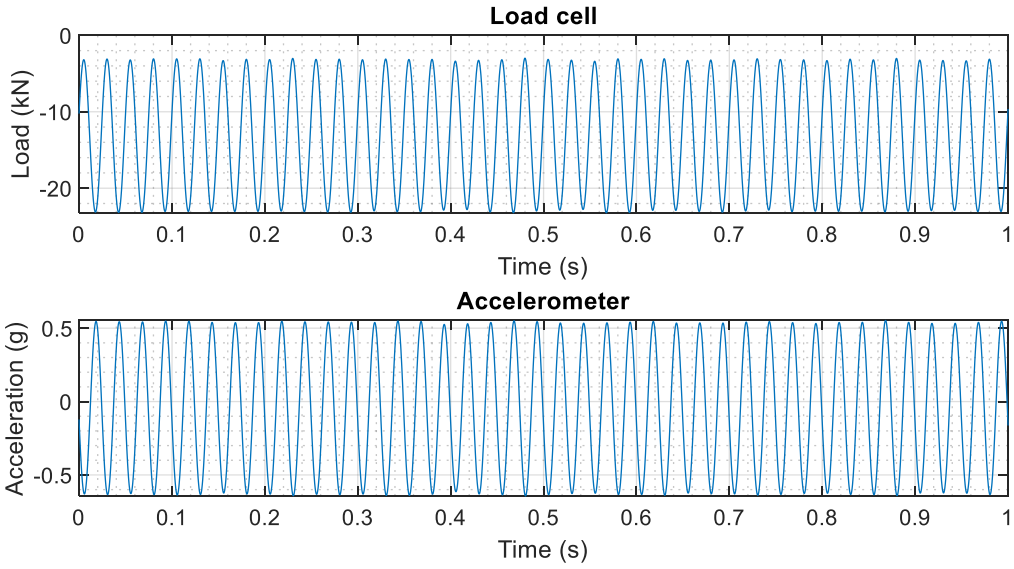

Figure 9-76 Pile 6. 166-day HF cyclic - Snapshot about 42.5 minutes into shaking

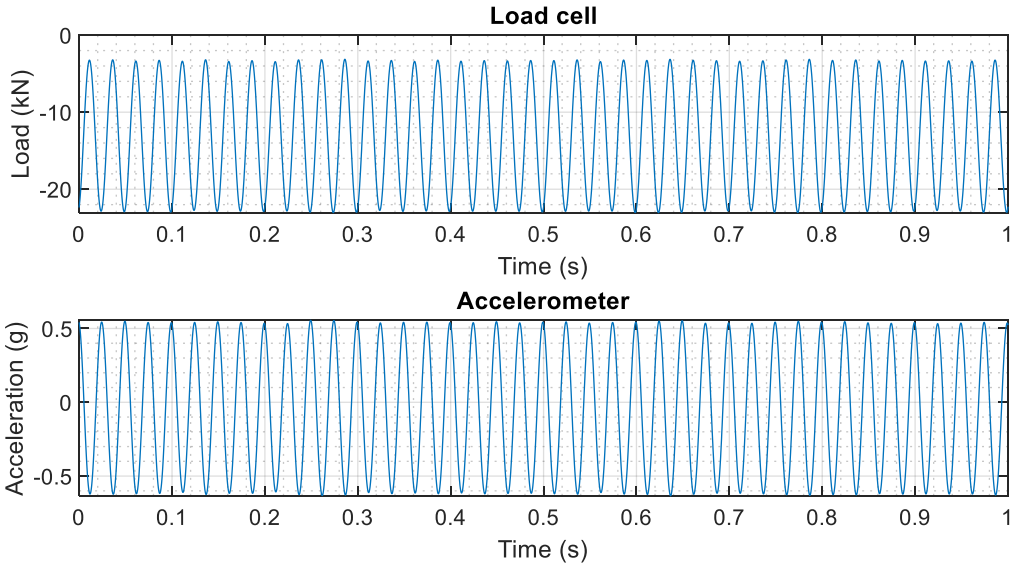

Figure 9-77 Pile 6. 166-day HF cyclic - Snapshot about 47.5 minutes into shaking

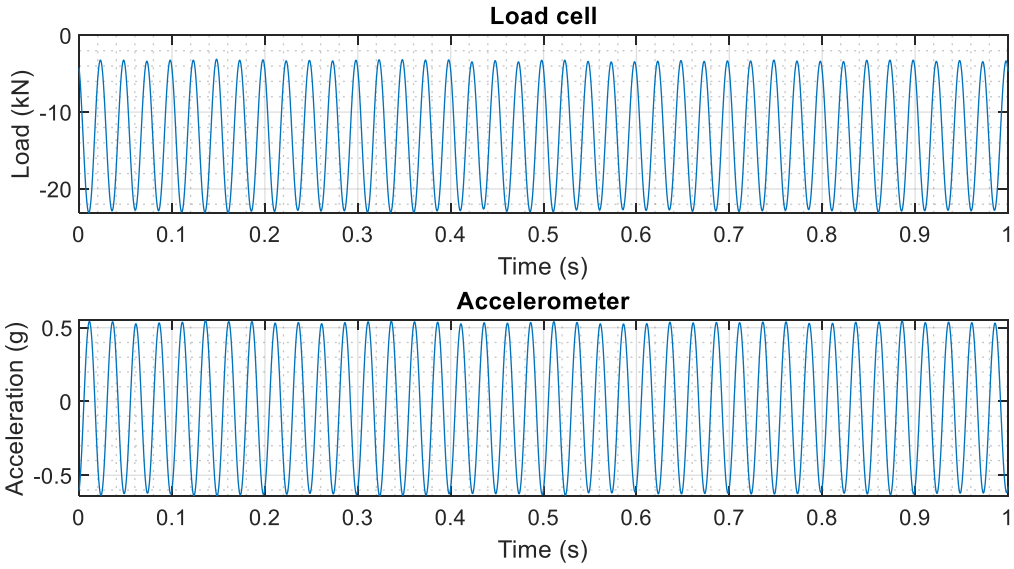

Figure 9-78 Pile 6. 166-day HF cyclic - Snapshot about 52.5 minutes into shaking

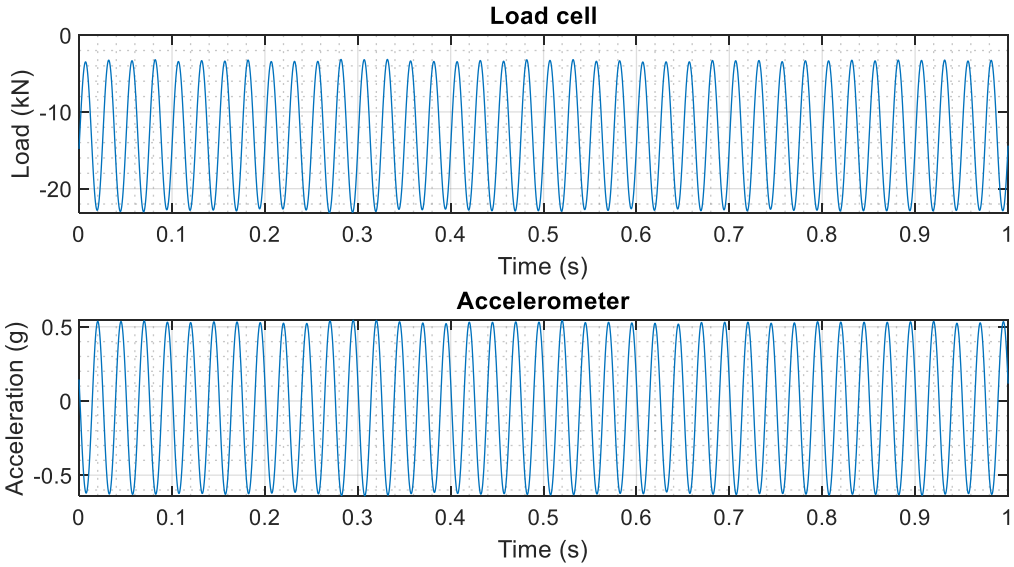

Figure 9-79 Pile 6. 166-day HF cyclic - Snapshot about 57.5 minutes into shaking

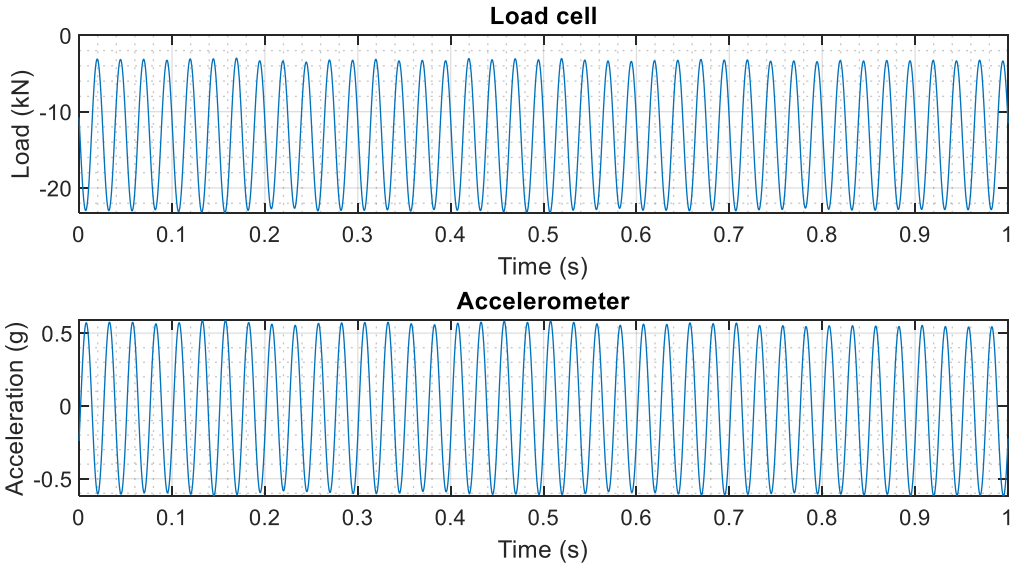

Figure 9-80 Pile 6. 166-day HF cyclic - Snapshot about 62.5 minutes into shaking

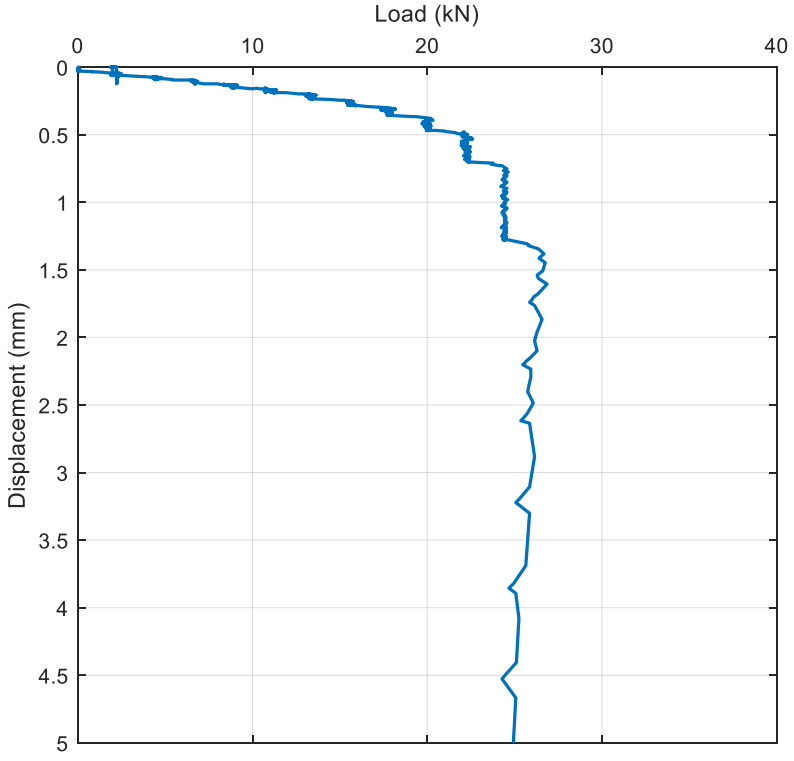

Figure 9-81 Pile 6. 166-day monotonic after HF cyclic

9.3.5 Pile 9 - 168-days after installation

Note: The accelerometer battery depleted during this test.

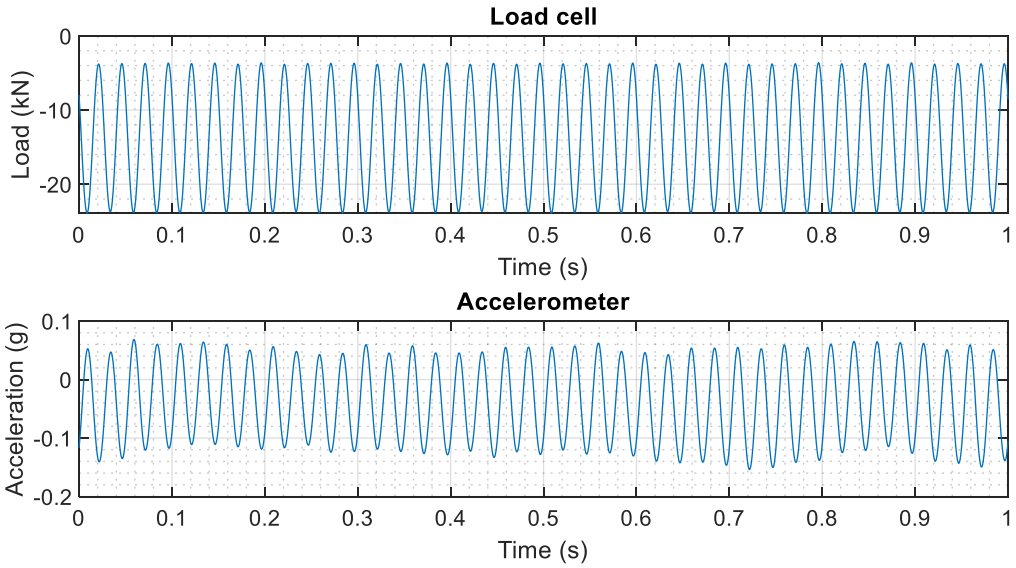

Figure 9-82 Pile 9. 168-day HF cyclic - Snapshot about 2.5 minutes into shaking

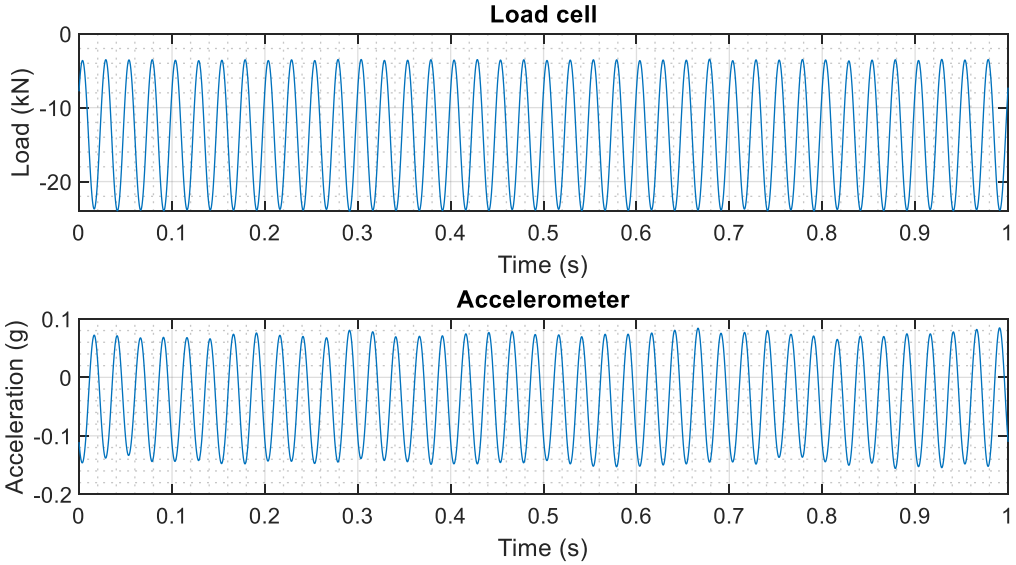

Figure 9-83 Pile 9. 168-day HF cyclic - Snapshot about 7.5 minutes into shaking

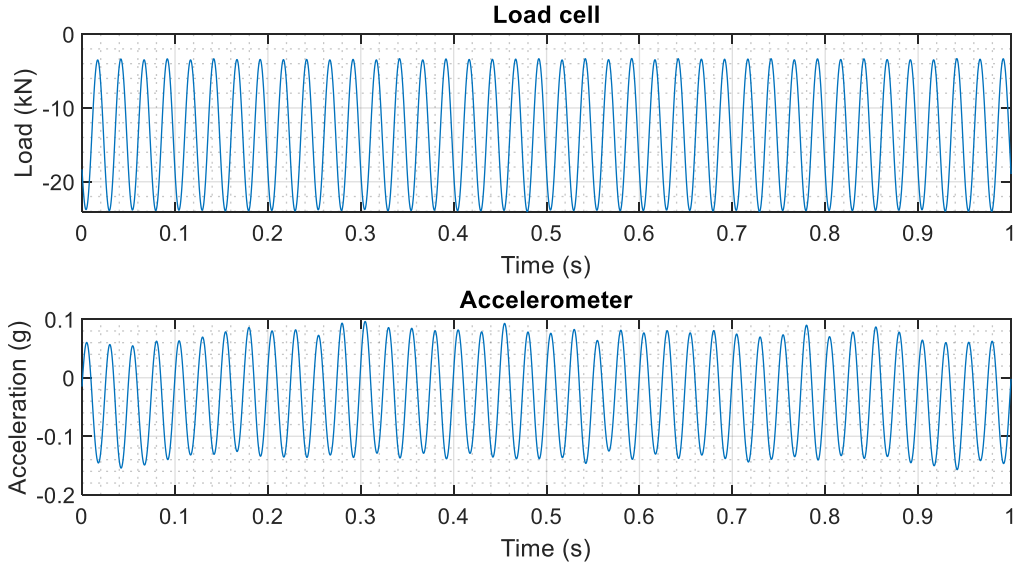

Figure 9-84 Pile 9. 168-day HF cyclic - Snapshot about 12.5 minutes into shaking

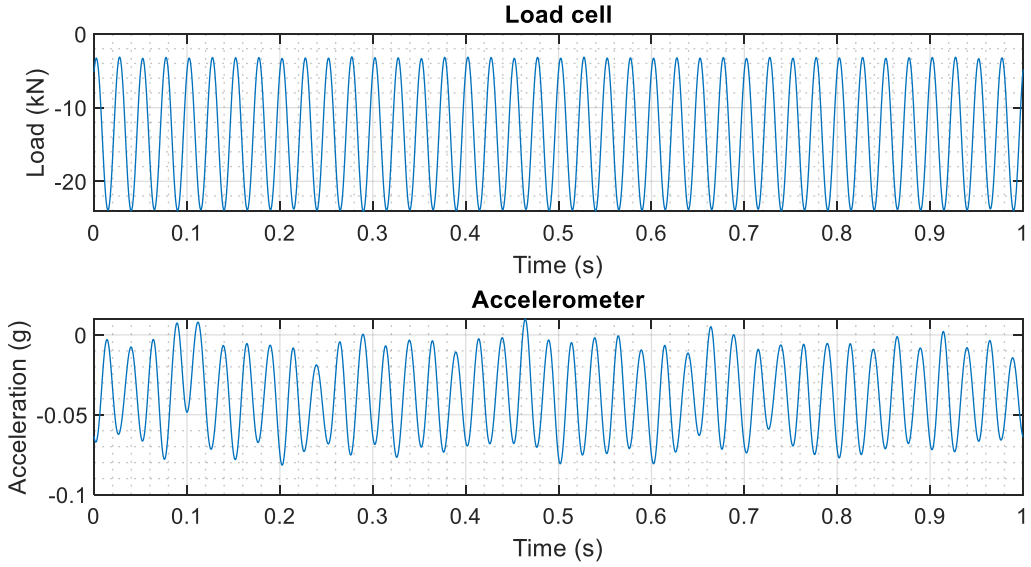

Figure 9-85 Pile 9. 168-day HF cyclic - Snapshot about 17.5 minutes into shaking

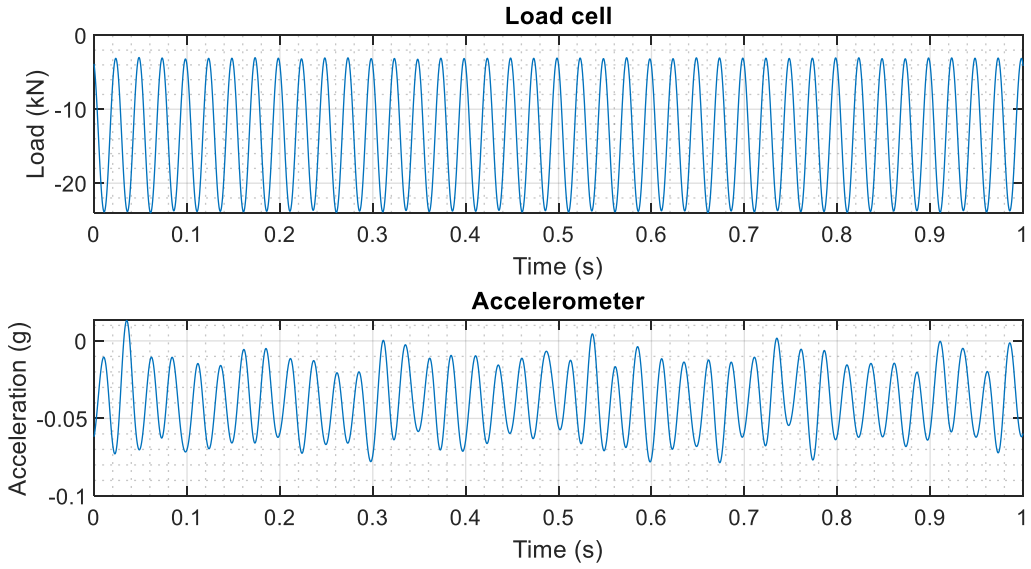

Figure 9-86 Pile 9. 168-day HF cyclic - Snapshot about 22.5 minutes into shaking

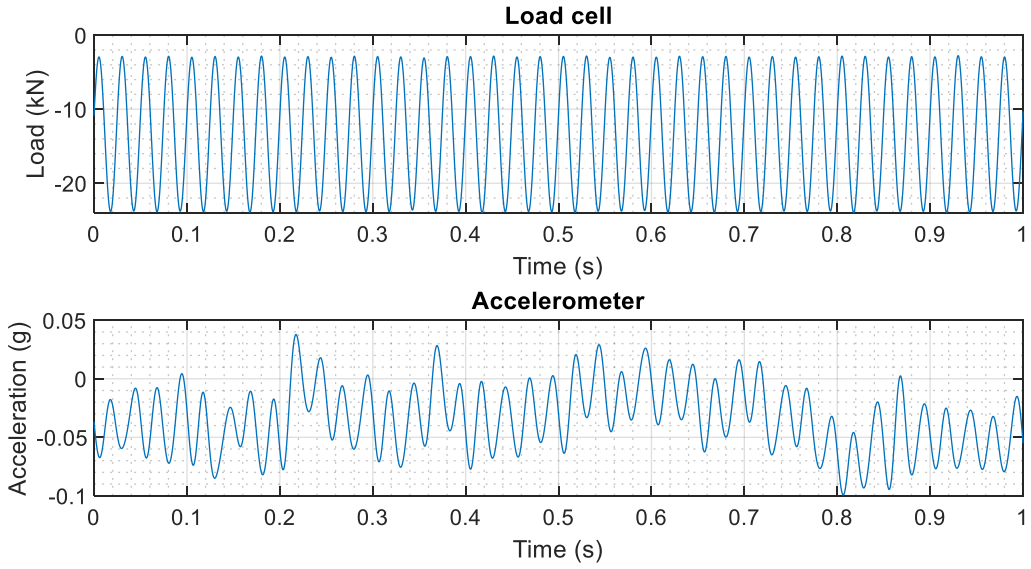

Figure 9-87 Pile 9. 168-day HF cyclic - Snapshot about 27.5 minutes into shaking

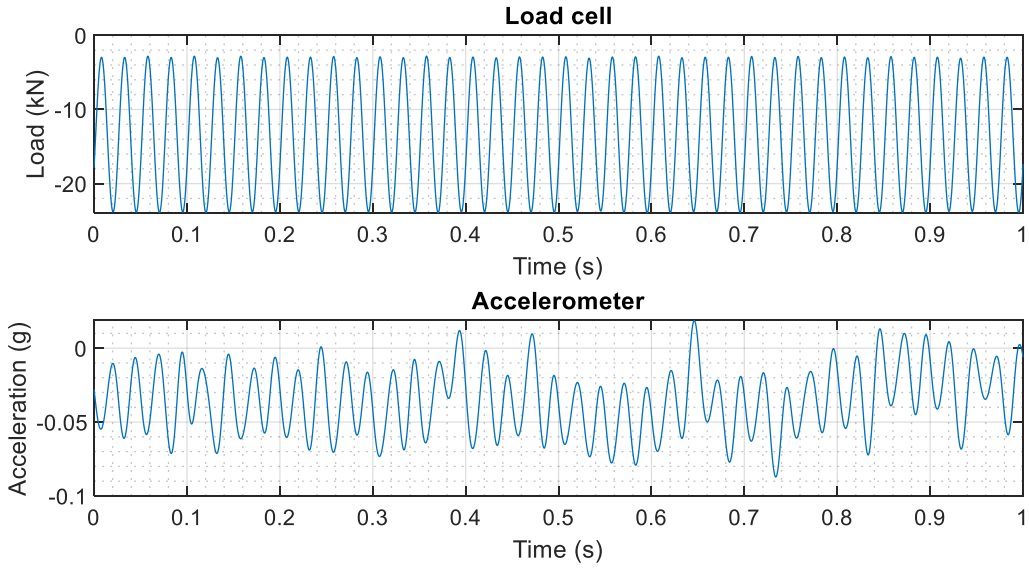

Figure 9-88 Pile 9. 168-day HF cyclic - Snapshot about 32.5 minutes into shaking

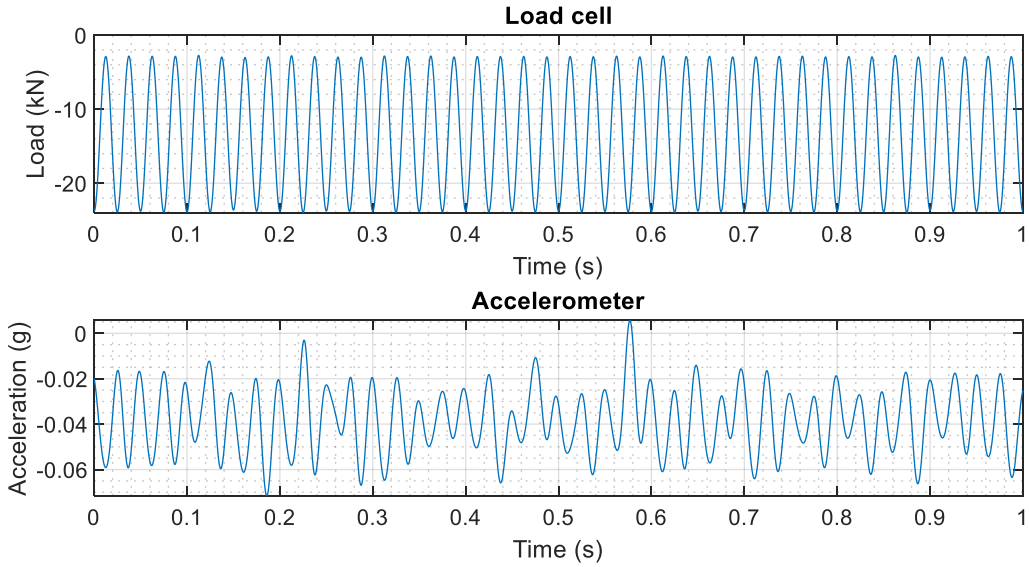

Figure 9-89 Pile 9. 168-day HF cyclic - Snapshot about 37.5 minutes into shaking

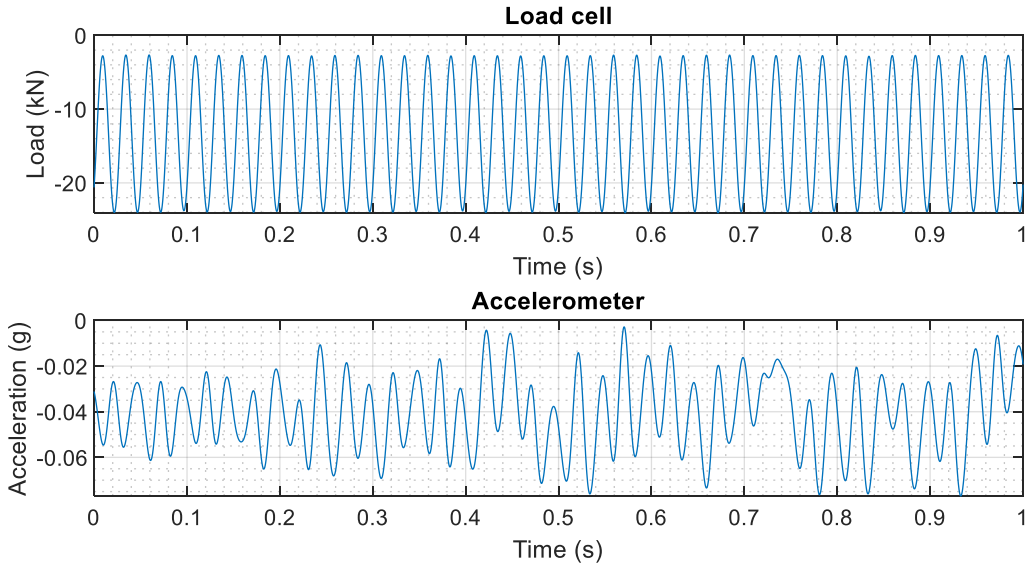

Figure 9-90 Pile 9. 168-day HF cyclic - Snapshot about 42.5 minutes into shaking

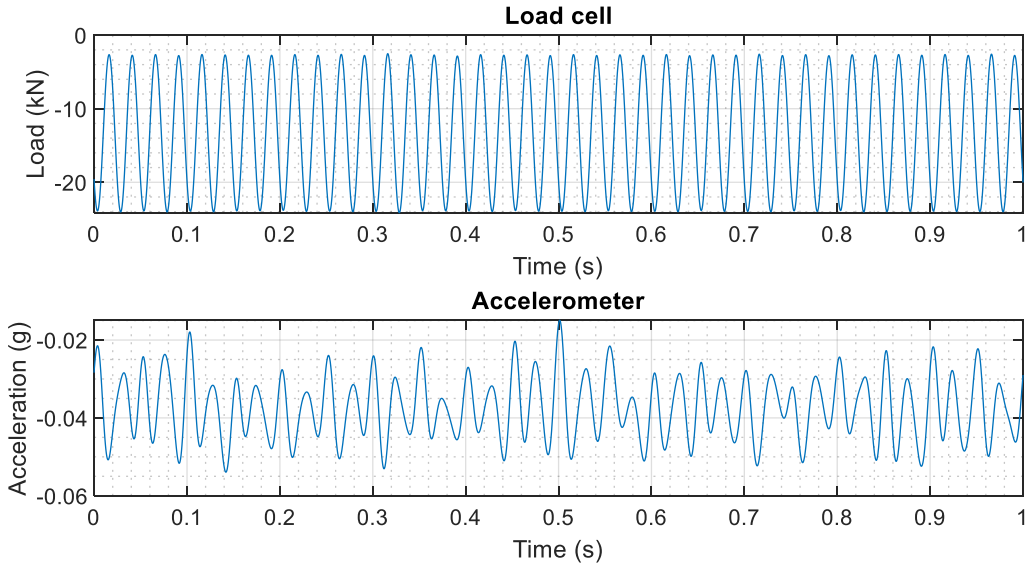

Figure 9-91 Pile 9. 168-day HF cyclic - Snapshot about 47.5 minutes into shaking

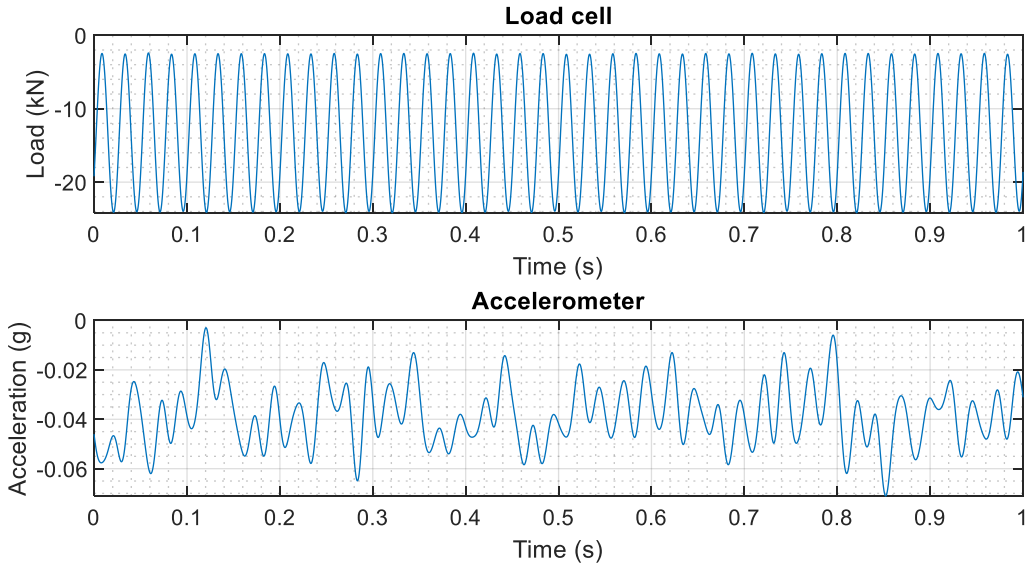

Figure 9-92 Pile 9. 168-day HF cyclic - Snapshot about 52.5 minutes into shaking

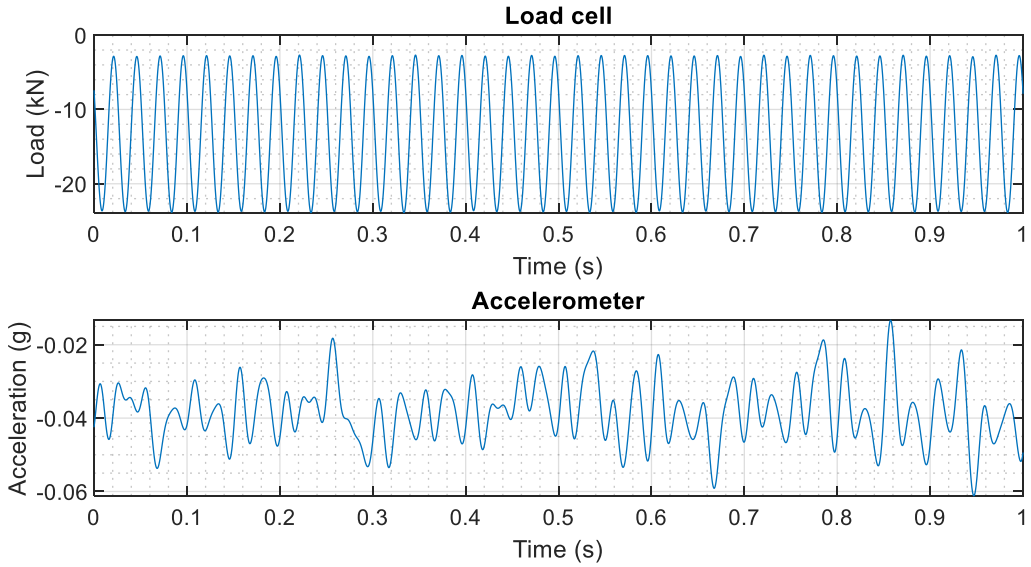

Figure 9-93 Pile 9. 168-day HF cyclic - Snapshot about 57.5 minutes into shaking

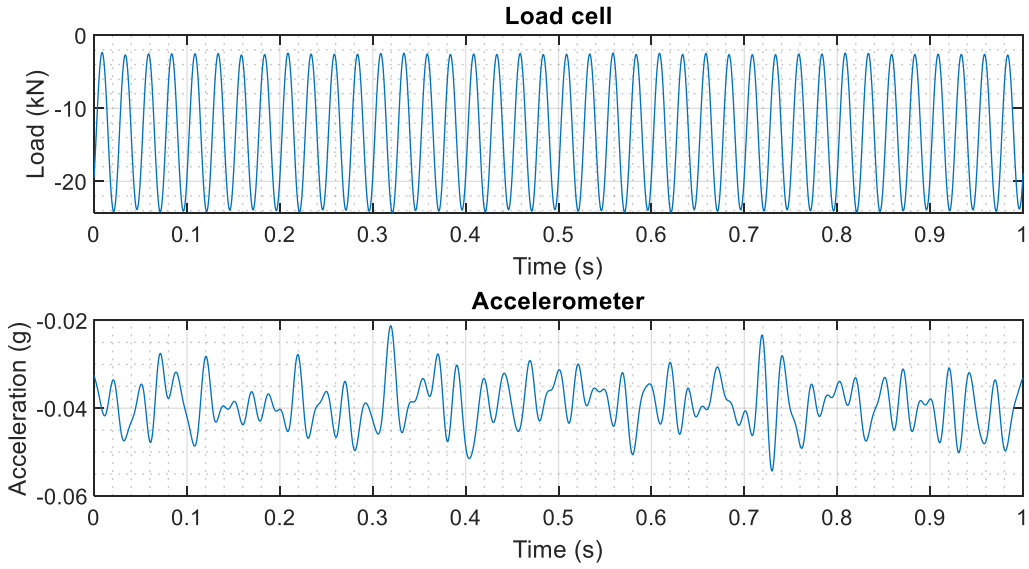

Figure 9-94 Pile 9. 168-day HF cyclic - Snapshot about 62.5 minutes into shaking

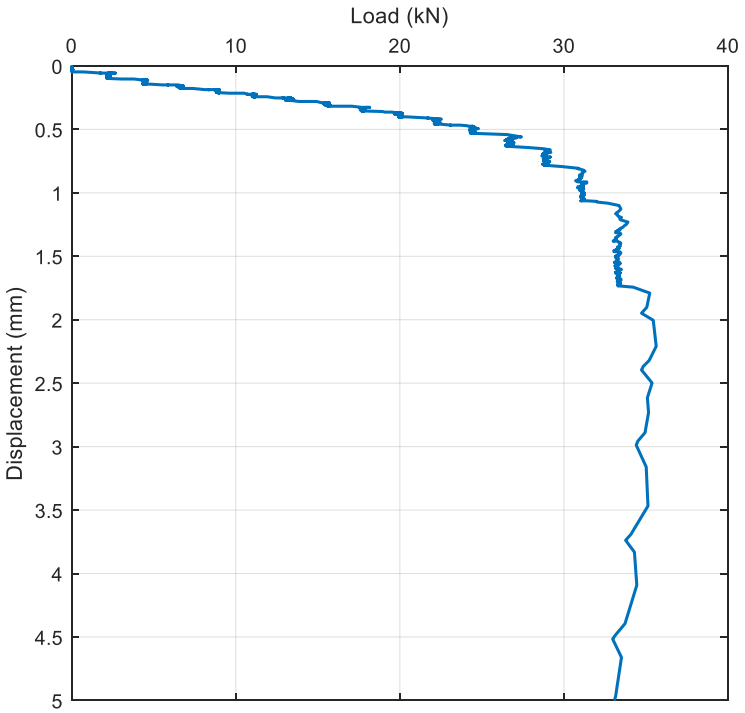

Figure 9-95 Pile 9. 168-day monotonic after HF cyclic

Kontroll- og referanseside/ Review and reference page

Dokumentinformasjon/*Document information*		
Dokumenttittel/*Document title* Model testing of cycle axial loading on piles for jacket foundations		**Dokumentnr./*Document no.*** 18-1076-02-R
Dokumenttype/*Type of document* Rapport / Report	**Oppdragsgiver/*Client*** Bureau of Ocean Energy Managment	**Dato/*Date*** 2019-11-20
Rettigheter til dokumentet iht kontrakt/ *Proprietary rights to the document according to contract* NGI		**Rev.nr.&dato/*Rev.no.&date*** 3 / 2020-08-20
Distribusjon/*Distribution* LIMITED: Distributed to client and available for NGI employees / BEGRENSET: Distribueres til oppdragsgiver og er tilgjengelig for NGIs ansatte		
Emneord/*Keywords* Cyclic, sand, aging, axial, pile , montonic, creep, jacket, wind energy, foundation, BOEM, BSEE		

Stedfesting/***Geographical information***	
Land, fylke/*Country* United States	**Havområde/*Offshore area***
Kommune/*Municipality*	**Feltnavn/*Field name***
Sted/*Location*	**Sted/*Location***
Kartblad/*Map*	**Felt, blokknr./*Field, Block No.***
UTM-koordinater/*UTM-coordinates* **Zone: East: North:**	**Koordinater/*Coordinates*** **Projection, datum: East: North:**

Dokumentkontroll/*Document control*

Kvalitetssikring i henhold til/*Quality assurance according to NS-EN ISO9001*

Rev/ *Rev.*	**Revisjonsgrunnlag/*Reason for revision***	**Egenkontroll av/ *Self review by:***	**Sidemanns-kontroll av/ *Colleague review by:***	**Uavhengig kontroll av/ *Independent review by:***	**Tverrfaglig kontroll av/ *Interdisciplinary review by:***
0	Original document	2019-11-20 ARa			
1	Updated with latest UT tests	2020-05-05 ARa			
2	Updated with completed UT tests	2020-07-09 ARa			
3	Updated with final comments	2020-08-20 ARa			

Dokument godkjent for utsendelse/ *Document approved for release*	**Dato/*Date***	**Prosjektleder/*Project Manager***
	20 August 2020	Amir Rahim

NGI (Norwegian Geotechnical Institute) is a leading international centre for research and consulting within the geosciences. NGI develops optimum solutions for society and offers expertise on the behaviour of soil, rock and snow and their interaction with the natural and built environment.

NGI works within the following sectors: Offshore energy – Building, Construction and Transportation – Natural Hazards – Environmental Engineering.

NGI is a private foundation with office and laboratories in Oslo, a branch office in Trondheim and daughter companies in Houston, Texas, USA and in Perth, Western Australia

www.ngi.no

NGI (Norges Geotekniske Institutt) er et internasjonalt ledende senter for forskning og rådgivning innen ingeniørrelaterte geofag. Vi tilbyr ekspertise om jord, berg og snø og deres påvirkning på miljøet, konstruksjoner og anlegg, og hvordan jord og berg kan benyttes som byggegrunn og byggemateriale.

Vi arbeider i følgende markeder: Offshore energi – Bygg, anlegg og samferdsel – Naturfare – Miljøteknologi.

NGI er en privat næringsdrivende stiftelse med kontor og laboratorier i Oslo, avdelingskontor i Trondheim og datterselskaper i Houston, Texas, USA og i Perth, Western Australia.

www.ngi.no

OSLO
TRONDHEIM
HOUSTON
PERTH

NORWEGIAN GEOTECHNICAL INSTITUTE
NGI.NO/HOUSTON

T +1 281 752 4667
houston@ngi.no

NGI Houston
10615 Shadow Wood Drive, Suite 100
Houston, TX 77043, U.S.A

NGI Oslo
PO Box 3930 Ullevaal Stadion
NO-0806 Oslo, Norway